THE DEVELOPMENT OF A BLASTHOLE STEMMING PERFORMANCE EVALUATION MODEL USING A PURPOSE BUILT TESTING FACILITY

DAWID BOSHOFF

Presented as partial fulfilment of the requirements for the degree

M.Eng (Mining)

IN THE FACULTY OF ENGINEERING, BUILT ENVIRONMENT AND INFORMATION TECHNOLOGY

DEPARTMENT OF MINING ENGINEERING

UNIVERSITY OF PRETORIA

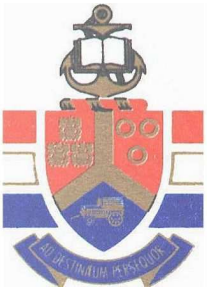

I hereby declare that this dissertation is my own unaided work. It is being submitted for the degree M.Eng (Mining) at the University of Pretoria, Pretoria. It has not been submitted before for any degree or examination in any other University.

Dawid Boshoff
NAME OF AUTHOR

ABSTRACT

THE DEVELOPMENT OF A BLASTHOLE STEMMING PERFORMANCE EVALUATION MODEL USING A PURPOSE BUILT TESTING FACILITY

Supervisor: Prof RJ Thompson

Co-Supervisor: Mr B Prout

Department: Mining Engineering

University: University of Pretoria

Degree: M.Eng (Mining Engineering)

Abstract

The ability of an explosive to break rock is influenced considerably by the extent of confinement in the blasthole and it is believed that confinement is improved by the use of stemming. The aim of this thesis is to present the first and second stages of results in developing a stemming performance testing and evaluation facility for small diameter boreholes. The results showed that different stemming products have differences in terms of their functionality, which can have a major impact on the efficiency of rock breaking. Two test procedures were used, one through the exclusive use of compressed air and the second using a purpose built high pressure test rig with small quantities of explosives.

Both tests were used to identify and evaluate the ability of various stemming products to resist the escape of explosive gas through the collar of a blasthole. Extensive research was conducted to determine the types of stemming products most commonly used in South African underground hard rock mines, and the differences in design between the various products are discussed. The first stage of tests using compressed air only did not prove adequate to predict with certainty the pressure behaviour in the borehole of a particular product under high pressure conditions.

The purpose built high pressure test rig proved to be a very effective tool to test stemming products under high pressure conditions. The test rig will enable manufacturers of stemming products to optimise stemming design and enable end users to test stemming products under laboratory conditions. Well designed stemming products will improve the rock breaking ability of explosives and decrease energy loss through the collar of the blasthole. With less energy loss through the collar of the blasthole, support and hanging wall damage is reduced, resulting in reduced quantities of explosives needed to provide required fragmentation.

Table of contents

List of figures

List of tables

1 BACKGROUND

An explosive primarily provides the energy needed for rock breakage. Energy supplied by an explosive at the beginning of the fragmentation process is absorbed by the rock in initiating fractures and fragmentation. In the blast design, efforts are made to increase the portion of energy spent on mechanical work of rock breakage. The idea of the fragmentation process is not to dissipate the explosive energy in excessive size reduction of the rock or to release the energy into the rock strata and environment as vibration and noise. The performance of an explosive is considerably influenced by the extent of confinement in the blasthole. The increase of confinement leads to more cost-effective rock-removal and fragmentation (Persson et al,1994). An available stemming material is often used to enhance confinement of the explosive in the blasthole. The exact mechanism involved in confinement is poorly understood. Those factors, that govern the performance and type of stemming material, are not well documented in existing literature (Cancec et al,2001).

The aim of the document was to present the first and second phase of the work in developing a stemming performance testing, modelling system and evaluation facility. The first phase involved the assessment of the available field of knowledge in relation to explosives in rock breaking, and more specifically, the interaction of stemming material with the explosive and the surrounding rock mass during the blasting process. The first phase tests were conducted at low pressure utilising compressed air. The second phase tests were conducted at high pressures and utilised high pressure hydraulic equipment.

The purpose of embarking on high as well as low pressure test was to establish if there is any correlation between the performance of the different stemming materials at low and high pressure. It was also done to investigate the possibility of extrapolation to pressures similar to that of commercial explosives.

2 PROBLEM DEFINITION

2.1 Introduction

Previously the effect of stemming in blasting was not fully understood and there was no system that could effectively measure the performance of stemming in a blasthole. The systems that have been developed so far can measure some of the parameters that affect the performance of stemming but do not take all the important parameters into consideration.

2.2 Overall project objectives

Develop a stemming performance testing, modelling system and evaluation facility.
Investigate the relationship between low pressure compressed air tests and high pressure balistide tests
Conduct comparative tests on the performance of various stemming materials.

The first stage of the work involves an assessment of the field of knowledge pertaining to explosives in rock-breaking, but more specifically, the interaction of stemming material with the activated explosive column and the surrounding rock mass.

3 LITERATURE STUDY

3.1 Introduction

The purpose of the literature study was to provide a comprehensive insight into the existing literature regarding this research field. For clarity, relevant terms are defined below.

3.2 Definitions and terms of the study

Airblast: A compression wave that travels through the atmosphere in a manner similar to the p-type body wave that travels through the earth (i.e., back and forth movement along the line of advance of the wave, Leet, 1960). Airborne shockwaves result from the detonation of an explosive but can also be caused by rock movement or release of expanding gases into the air (Stig O Olofsson, 2002).

Blast: The action of breaking and displacing rock by means of explosives.

Blasthole: Physical hole drilled in rock strata with the purpose of containing the explosive until the blast is initiated.

Chapman-Jouguet plane (CJ-plane): The CJ-plane is an imaginary plane behind the reaction zone and ahead of the detonated products that are at high pressure and temperature. (Brinkmann, 1990)

Collar: The top of a borehole or blast hole

Confinement: The containment of an explosive in a borehole by a non-combustible material.

Deflagration: “The rapid combustion sometimes accompanied by flame, sparks or spattering of burning particles. A deflagration, although classed as an explosion generally implies the burning of a substance with self contained oxygen so that the reaction zone advances into the nonreacted material at a velocity lower than the sonic velocity of the explosive”. (Chapter 8, Study Notes, PRX 310, Rock Breaking).

Detonation: “An exothermic chemical reaction that propagates with such rapidity that the rate of advance of the reaction zone into the non-reacted material exceeds the sonic velocity of explosive. The rate at which the chemical reaction proceeds is known as the “Velocity of Detonation”. When this rate of advance attains such a value that it will continue without diminution through the explosive, it is termed the stable detonation velocity. When the detonation velocity is equal to or greater than the stable detonation velocity of the explosive, the reaction is termed a high order detonation. When it is lower, the reaction is termed a low order detonation”. (Chapter 8, Study Notes, PRX 310, Rock Breaking)

Explosive: “A substance that undergoes decomposition or combustion with great rapidity, evolving much heat and producing a large volume of gas. The reaction products fill a much greater volume than that occupied by the original material and exert an enormous pressure, which can be used for blasting and for propelling”.(Encyclopaedia of Columbia University Press, 2005)

Flyrock: Undesirable throw of rock from the blast (Olofsson, 2002).

Fumes: The toxic oxides of nitrogen produced by detonation.

Ground vibration: Shock wave emitted from a blast transmitted through the surrounding ground.

Powder factor: The ratio of weight of explosive in kilograms to the tons of material blasted.

Primer: Cap sensitive cartridge of high explosive used to initiate blasting agents.

Shock wave: “Is a wave formed of a zone of extremely high pressure within a material, which propagates through the material at a speed in excess of the speed of sound. A shock wave is caused by the sudden, violent disturbance of a material, such as that created by a powerful explosion or by the detonation of an explosive. A shock wave decays rapidly with increasing distance from its point of origin, gradually changing into an ordinary sound wave”. (Encyclopaedia of Columbia University Press, 2005)

Stemming: Stemming may be defined as the filling of part or all of the collar region of a vertical or horizontal blast hole with an inert (non explosive) material used to

confine the explosive energy propagating from the explosive gases generated by the explosion and reducing the unwanted effects of airblast and flyrock. Stemming may be used to separate explosives in a blast hole to create decked charges.

Velocity of detonation (VoD): "The velocity of detonation of an explosion is the rate at which the detonation or combustion wave travels through the explosive product. The speed or how fast the chemical reaction occurs or the rate of the reaction. Velocity of Explosion (VOE) refers to both high and low explosives. The reaction speed is measured in meters/second". (Encyclopaedia of Columbia University Press, 2005).

3.3 The necessity of stemming

In the case of the detonation of an explosive, a chemical reaction releases large quantities of energy. This energy is released in the form of shock and gas pressure. The pressure interacts with the medium in which the explosive is confined. This is followed by a pressure wave that radiates from the point of detonation. The sole purpose of this pressure wave is to generate maximum rock fragmentation. Brinkman (1990) stated that approximately 50% of the explosive energy is lost if unrestricted venting is allowed to occur through the blasthole collar, but lacks experimental proof. A brief description of the behaviour of explosives during detonation is provided in paragraph 3.3.1.

In most literature reference is made to the heave effect of explosives and the role stemming plays in the moving of materials. In the underground environment the contrary is most often required as rock should be kept close to the working face in order to reduce secondary effects.

3.3.1 Chemistry and physics of explosives

This is a brief overview of important features of detonation which control how the explosive delivers its energy.

Different types of explosives behave (detonate) and release energy. Commercial explosives tend to behave non-ideal, in that they do not reach the Chapman-Jouget detonation velocity. The amount of energy released by an explosive is dependent on how far it approaches the ideal behaviour when detonating. The overall performance of an explosive in rock blasting or any other application is dependent on how much thermal energy is released. The thermal energy in the chemical reaction that occurs when the material detonates determines how much useful mechanical work the reaction products can do as they expand. The sudden release of energy and reaction products at high pressure occurs by means of a rapid chemical reaction in the explosive. This explosive is contained in a drill hole in the rock and results in the propagation of compression waves in the explosive and in the surrounding rock material.

Explosives may contain the same chemical energy but their field performance may differ. This is due to differences in:

- detonation velocities
- the ratio between shock and heave energy
- the expansion work done before the rock breaks and the gaseous products that are ventilated through the cracks that formed

3.3.1.1Ideal and non-ideal detonation

Chapman and Jouget first developed ideal detonation over a century ago (Brinkmann, 1990). The important components of this ideal detonation are shown in figure 3.1 below.

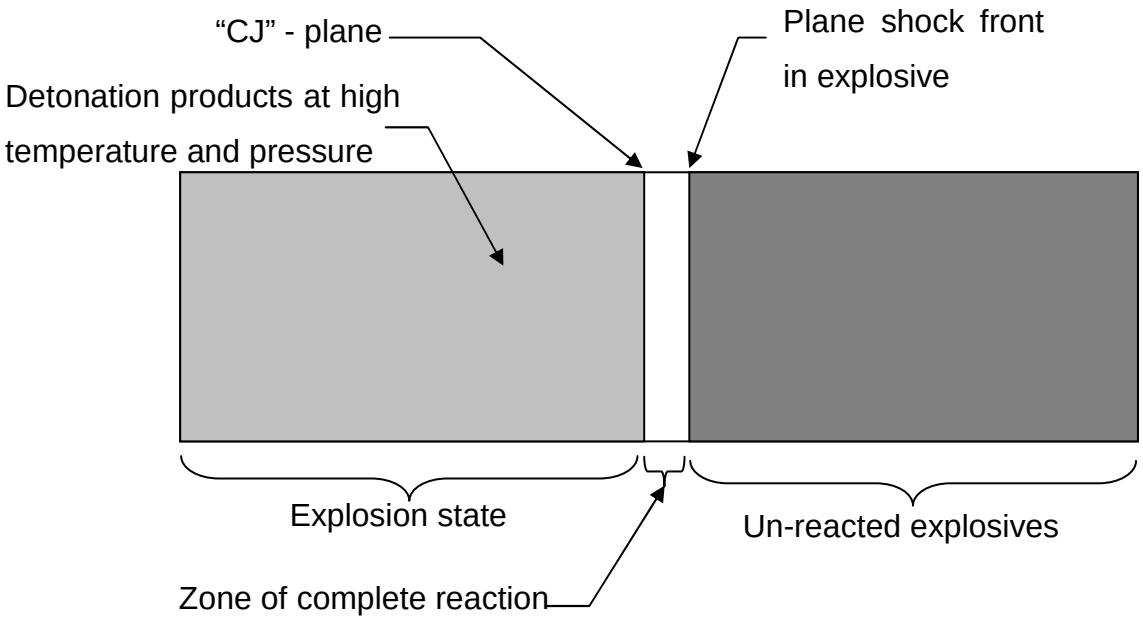

Figure 3.1 Section view of an idealized explosive charge showing an ideal detonation process (Brinkman, 1990).

In this case the chemical reaction is completed immediately behind the shock front. Such detonations propagate with the well-defined Chapman-Jouget detonation velocity. A plane shock wave travels through the explosive, which heats and cause a chemical reaction that supports the shock wave. The reaction zone is thin and bounded at the rear by the Chapman-Jouget (CJ) plane. Thus, all the potential energy contained in the explosive is liberated almost instantly in the short reaction zone. Behind the CJ-plane are the stable detonation products which are mainly gases at high temperatures and extreme pressures. This is termed the explosion state where it is envisaged that the detonation products occupy the same volume as the explosive.

The above state never actually occurs in most commercial explosives owing to lateral expansion at and immediately behind the CJ-plane (zone) during real detonation, therefore the detonation is non-ideal (Brinkman, 1990). The factors that affect the degree of non-ideal behaviour include the physical properties of the

confinement medium, charge diameter, coupling ratio and the size of explosive ingredients as well as their intimacy of contact.

Figure 3.2 illustrates the non-ideal detonation process. In this case the shock front is curved due to reduced pressure and reaction rates near the edge of the explosion.

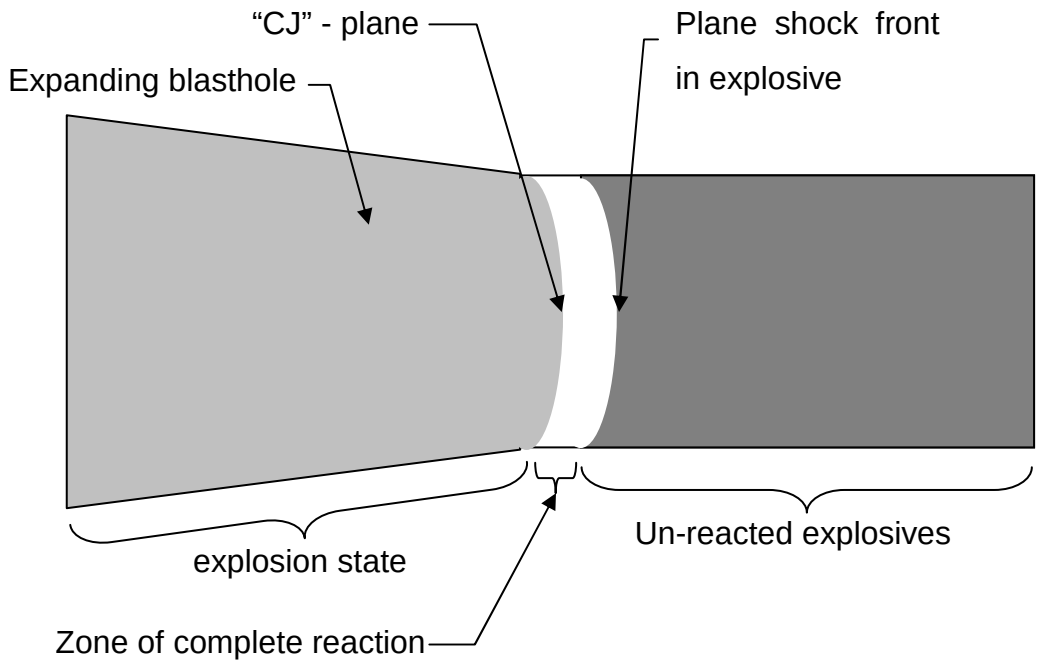

Figure 3.2 : Features of a non-ideal detonation process (adapted from Brinkman, 1990).

The primary reaction zone represents the volume where the reaction energy supports the shock wave, and is bounded at the rear by the CJ-plane (Brinkman, 1990). The greater the amount of energy released in this zone the more ideal the explosive and the greater the resulting velocity of detonation. Any reaction behind the CJ surface does not support the shock front but contributes in the breakage of the rock.

3.3.1.2 Detonation and borehole pressure

The detonation pressure (ideal) can be estimated with the formula (Persson *et al*, 1994):

$$P_{cj} = \frac{\rho D^2}{4} \qquad \text{Equation 3.1}$$

where

ρ is the density of the explosive

D is the ideal velocity of detonation

Commercial explosives often behave in a non-ideal way due to a long reaction zone, which influences the velocity of detonation.

The pressure of detonation products in the explosion state i.e. the borehole pressure of a fully coupled hole (i.e. no air gaps between the charges) hole can be estimated through (Persson *et al,* 1994):

$$P_b = \frac{P_{cj}}{2} \qquad \text{Equation 3.2}$$

3.4 Strength of explosives

The strength of an explosive is not entirely related to the chemical energy theoretically available in the explosive composition but some other factors also come into play. These include detonation properties, the rates of the chemical reactions, the shock wave propagation and the strength characteristics of the rock material to be blasted. Although such factors need to be considered when one

determines the amount of energy released by an explosive, the energy released can be calculated by adding heat of formation at constant volume of the reaction products and subtracting the heat of formation at constant volume of the explosive. As an example a CHNO explosive, i.e., an explosive containing the atoms of carbon, hydrogen, nitrogen, and oxygen, gives as its main reaction products carbon dioxide, oxygen and nitrogen. The chemical reaction formula of such an explosive, allowing small deviations from oxygen balance by allowing small amounts of CO, H_2 or O_2, is as shown below (Persson et al 1994):

$$C_xH_yN_zO_w \rightarrow xCO_2 + \frac{y}{2}H_2O + \frac{z}{2}N_2 + (\frac{w}{2} - x - \frac{y}{4})O_2 \quad \text{Equation} \quad 3.3$$

where

$C_xH_yN_zO_w$ represents the chemical composition of several compounds including cyanic acid, isocyanic acid and fulminic acid

CO_2 is carbon dioxcide

H_2O is the chemical composition of water

N_2 is the chemical composition of nitrogen

O_2 is the chemical composition of oxcygen

With x, y, z and w constant real numbers

3.5 Explosive rock interaction

The effect of stemming, in terms of retaining the gas pressure in the blast hole, can be understood through a discussion of the explosive-rock-interaction during detonation. Although this subject is not completely understood, this discussion may shed some light on the purpose of stemming in retaining the gas pressure for a time, long enough to do the work on the rock. It has been shown that the gas energy is the prime mover of the fragmented material (Armstrong et al, 1993).

Sarma (1995) also found that the confinement to the explosive gases is one of the factors affecting the interaction of the rock and the explosive. The explosive-rock interaction consists of the following phases (Armstrong et al, 1993).

Phase 1: The primer (or booster) is initiated and the generated pressure wave forces the oxidant and the fuel of the explosive together to begin the chemical reaction.

Phase 2: Immediately the chemical reaction begins (and also as the primer is initiated) and a shock wave is transmitted in three dimensions from the point of initiation. This shock wave causes cracks to propagate into the surrounding medium.

Phase 3: At the onset of the chemical reaction, gaseous products of the reaction are formed at extremely high temperatures and pressures behind the reaction front.

Phase 4: The explosive energy absorbed by the rock mass accelerates the rock mass resulting in its movement. The figure below (figure 3.3) graphically illustrates the explosive rock interaction (from Lownds, 1995)

Position A on the curve represents the explosive pressure and volume at initiation, position B represents the equilibrium state (where the pressure of the explosion gases in the borehole cavity is matched by the stress in the surrounding rock) and position C represents the point at which the gases escape into the atmosphere. The line OB represents the response of the blasthole wall to the explosive loading and is dependent on the stiffness of the rock. The energy delivered up to this point is termed shock energy and is represented by zone 1 (Area OABD). Position D on figure 3.3 represents the volume of explosion gases at the equilibrium state and

position E represents the volume of explosion gases at the time of venting into the atmosphere.

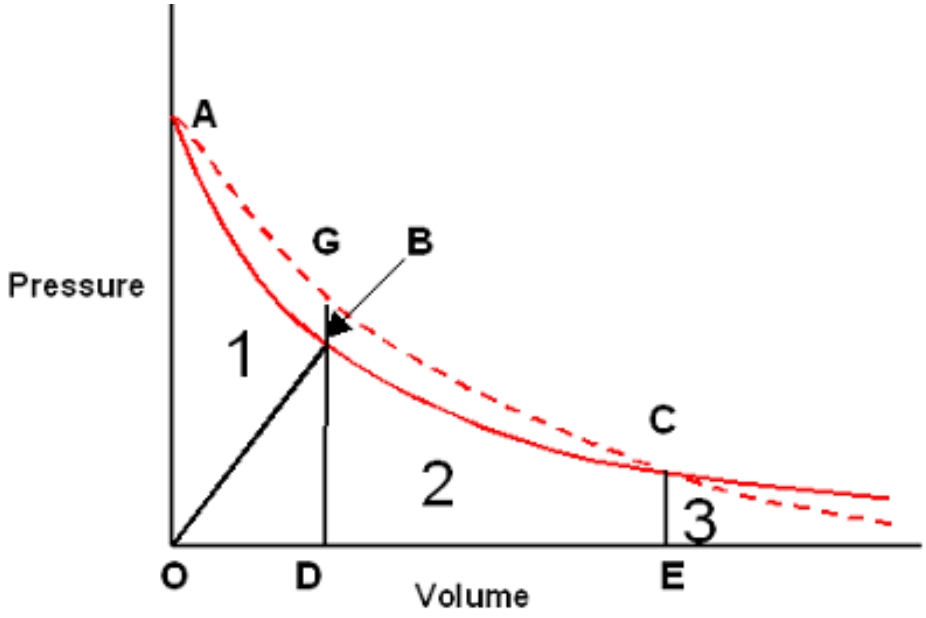

Figure 3.3: Partition of explosive energy released during blasting (Lownds, 1995).

The energy delivered up to this point is described as heave energy and is represented by zone 2 (Area DBCE). Any further gas expansion that occurs after atmosphere venting, is wasted energy and is represented by zone 3. The effective energy released by the explosive is the combined area of zone 1 and 2.

The confinement of the explosive charge ensures that the energy generated by the explosive is utilized in rock fragmentation and therefore minimises the energy dissipated in the generation of airblast, flyrock and excessive overbreak. If the explosive gases are allowed to escape to the atmosphere, useful energy will be lost. Therefore, containment of the gases in the borehole is an important phase of optimising the energy released by the explosive.

Improved confinement will result in a reduction in explosive gas venting. This reduction will cause an increase in the borehole pressure and is represented in

figure 3.3 by the dotted line. The larger area under the graph (AOECG) would imply more shock and heave energy are available to break rock.

Jensen et al. (2000) used Arbitrary Lagrangian Eulerian (ALE) computational techniques in a study to model the explosive or rock interaction during pre-splitting. They found that the pressure in the borehole fluctuates for several cycles during detonation until an equilibrium pressure is reached. This pressure fluctuation results in a fluctuation of borehole stress and expansion, and may contribute to the damage of the rock mass. Jensen et al. (2000) concluded that these observations could also be used to investigate the ejection of stemming material but needs further investigation.

3.6 Benefits of stemming

Explosives yield large quantities of energy generated by a chemical reaction. Useful work is available by means of expansive force within the great volume of energetic gas evolving from the explosive during the reaction. If the blasthole is not well confined with the adequate stemming material, the release of this large amount of energy will result in the generation of flyrock, airblast, and excessive ground vibrations (Otuonye, 1981).

The main purpose of stemming is to retain the energy long enough to do the work that it is intended for. The retention of energy results in more work being done to the rock, reduction in the velocity (the range) of flyrock hence, enhancing safety, reduction in ground vibrations minimizing drilling and reduction explosive costs.

Armstrong L.W. et al (1993) carried out a study to determine the effect of confinement on the fragmentation size inter alia. Two tests were carried out; with one test controlled the rate of release of gases and the second test used stemming materials with known degrees of confinement.

The experiments were carried out using concrete blocks (0.5m x 0.5m x 0.65m), of the desired strength, and were loaded with 5g of plastic PETN based explosive in a 10mm diameter borehole, with a depth of 225mm, 100mm from one face of the block. The remaining three sides of the concrete block were paved with 12mm thick tiles to act as fly plates to prevent spalling of the sides of the concrete. Figure 3.4 schematically illustrates the experimental setup. The figure shows different equipment used for the experiment. The experiment was conducted done to test various parameters in blasting, with the effect of confinement being one of them.

In the case of controlling the rate of release of gases, a heavy duty steel plate was bolted on top of the concrete block and a hole drilled in the plate aligned with the centre of the blasthole. As the flow rate of gas through an orifice, is proportional to the cross-sectional area of the orifice a change in gas release rate could be achieved. In this series of tests, no stemming was used.

In this experiment they found that the fragmentation size decreased as the product gases are confined in the blasthole for longer periods of time. That is, as the gas pressure is confined more effectively within the blasthole finer fragments are produced. This is illustrated by table 3.1, which shows the variation of fragmentation size with the degree of confinement. This has been graphically represented in figure 3.5.

The experiment was repeated using stemming materials. The concrete blocks were set up as discussed above, and different types of stemming materials, with known degrees of confinement, were used. Measuring the fragmentation size assessed the effect of these different levels of confinement on fragmentation. The results obtained are shown in table 3.2.

The tests carried out by Armstrong *et al* (1993) reveal that confinement can improve fragmentation, as illustrated by the decrease in fragmentation size as

confinement increases. Although the experiment was carried out in the laboratory, it is representative of the effects of confinement or stemming in mining conditions.

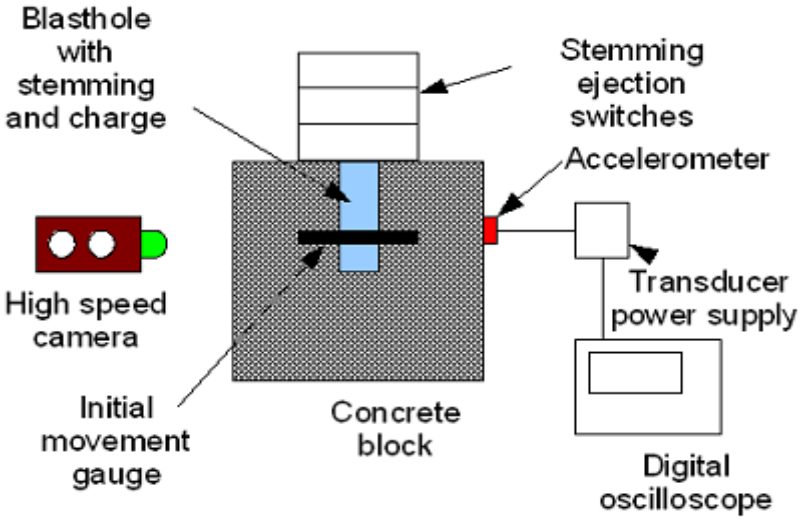

Figure 3.4: Typical blast chamber experimental layout (Armstrong *et al*, 1993)

Table 3.1: Steel plate experimental results (Armstrong et al, 1993)

Hole diameter (mm)	Degree of confinement (%)	*Fragmentation size (mm)*
0	100	*54*
1	99	*62*
7	50	*74*
10	*0*	*117*

Confidence in the results could be increased by increasing the number of tests.

A study conducted by Otounye (1981) revealed that airblast levels can be reduced by 98% and ground vibrations levels lowered by 36% if adequate stemming lengths are adopted. The benefit of stemming is not to entirely stop the leakage of gas, but also to form a mechanical barrier to the force of explosion. This results in better decomposition of the explosive and the production of less fumes in lower concentrations, as well as a reduction in noxious gases and dust (Otounye, 1981).

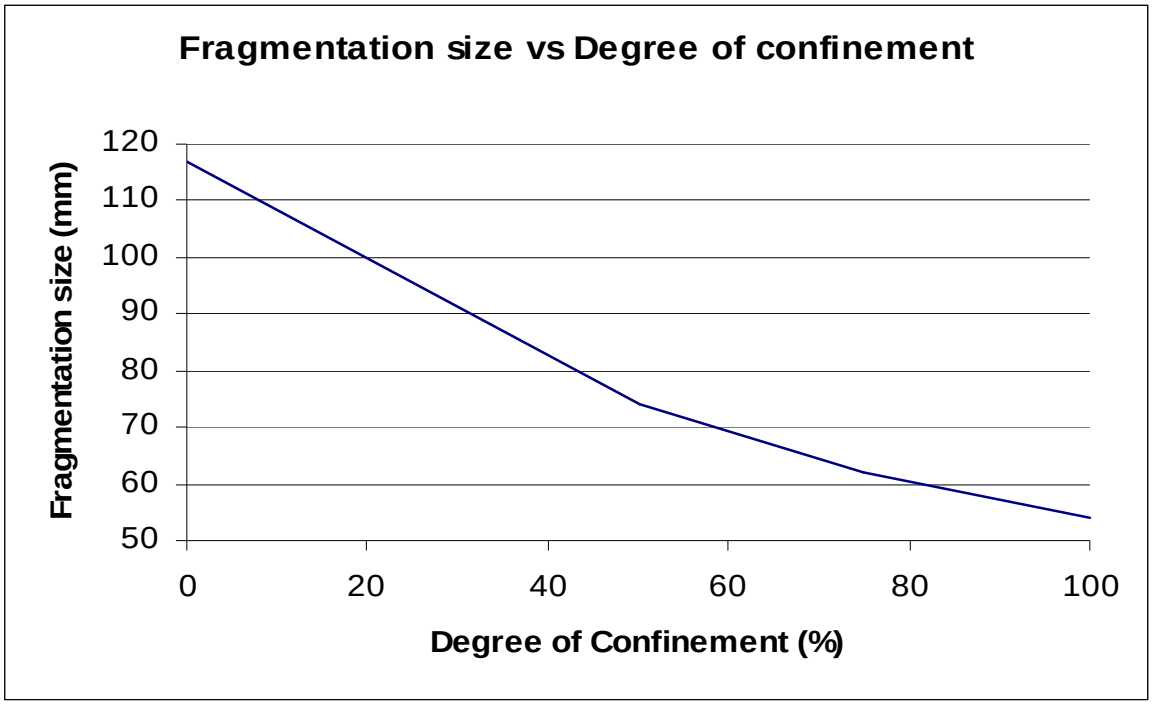

Figure 3.5: Fragmentation versus degree of confinement (Armstrong *et al,* 1993)

Table 3.2: Stemming material laboratory results (Armstrong et al, 1993)

Stemming material	Block strength (MPa)	Confinement (log pressure) (kPa)	Mean fragment size (mm)
Nil	20	2.04	93
Sandstone	20	2.08	44
Limestone	20	2.66	51
Cement	20	4.30	51
Nil	40	2.04	11
Sandstone	40	2.08	53
Limestone	40	2.66	54
Cement	40	4.30	62

Down-stream benefits like better diggability, higher crusher input, lower crusher amperage and an increase in productivity are realized.

3.7 Stemming performance parameters

Kershavarz (2005) developed “A simple approach for determining detonation velocity of high explosive at any loading density”, Mohammed Hossein Kershavarz (2005) stipulates that detonation velocity and pressure are two performance parameters that may be used to determining the effectiveness of different explosives. The effectiveness of stemming has also been found to relate to parameters, in which stemming can increase the VOD (Velocity of detonation) as well as the gas pressure in the blast hole of a given explosive. Otuonye (1994) found that stemming could be used to maximize the effectiveness of an explosive at the face and minimize the magnitude of elastic waves that propagate down the entry of an underground mine.

The majority of analyses and studies that have been conducted on explosives, but more specifically on stemming design are limited to the surface mining environment. Specific aspects pertinent to surface mines are not necessarily important considerations for to the underground mining environment for example; the effects of flyrock and airblast are important considerations for surface mining, whereas the effect of blasting on increasing the probability of a methane or dust explosion is a far more important pertinent issue to the underground mining environment. Hence, the relevant literature pertaining to these two mining environments, is discussed separately.

3.7.1 Stemming in surface mining

3.7.1.1The effect of confinement on detonation velocity

Kershavarz (2005) discussed an approach in analysing the effect of specific parameters on the velocity of detonation (VOD) of an explosive.

According to Kershavarz (2005), the detonation velocity of an explosive depends on the following three principal parameters:

The composition of explosive and its oxygen balance.

1. The heat content of an explosive.
2. The loading density of the blasthole.

However, confinement as one of the principal parameters that can affect the detonation velocity of an explosive, was not considered.

Contrarily, Esen (2003) evaluated the importance of confinement on the velocity of detonation of an explosive. Esen (2003) found that “confinement is clearly of the essence in the application of explosives to mining in general, and of rock in particular”; and added that the nature of confinement would affect the detonation process.

Esen further commented that the effect of confinement is to slow the pressure and temperature decrease behind the detonation front down. The purpose of this is to increase the reaction rates. Increase in confinement has therefore the same effect as an increase in charge diameter (Leiper and Hackett, 1987; Presson et al, 1993; Esen and Bilgin, 1998; Bilgin and Esen, 1999 and 200; Deng et al, 1999).

As confinement increases the lateral expansion near the primary zone is subdued. This causes the pressure and temperature to be maintained at greater levels, and thereby increases the extent of the combustion of the primary reaction zone (Esen, 2003). This explains why commercial explosives can detonate with a significantly higher detonation velocity in confinement than in air (Louw et al, 1993).

Esen (2003) tested nine different commercial explosives at confinements ranging in uniaxial compressive strength from 15.3 MPa to 108.0 MPa and a dynamic

Young's Modulus ranging from 9.1 GPa to 91.7 GPa. The blastholes for this experiment varied between 32mm and 241 mm.

Based on the tests mentioned above Esen developed the following empirical model:

$$D_{confined} = D_{unconfined} + a \times \left[\frac{D_{CJ} - D_{unconfined}}{D_{CJ}} \times \frac{K}{1 + b \times K} \right] \qquad \text{Equation 3.4}$$

where

$$K = \frac{E_d}{1 + \upsilon_d}$$

$D_{confined}$ = confined velocity of detonation in m/s;

$D_{unconfined}$ = unconfined velocity of detonation in m/s;

D_{CJ} = velocity of the CJ-plane; K the rock stiffness (GPa);

E_d = dynamic Young's Modulus (GPa);

υ_d = dynamic Poisson's ratio;

a and b constants equal to 112.819 and 0.132 respectively

In this empirical model, the rock is the only medium of confinement and stemming has not been considered. Esen (2003) suggested that this model could be adapted to include stemming as part of confinement but the technical details thereof were not included in this study.

A non-linear regression analysis has shown that the effect of confinement is a function explosive and rock properties (Esen, 2003). Esen (2003) concluded that for a given explosive and charge diameter, as confinement increases, detonation velocity increases. It was further suggested that if a detonation model can be coupled with confinement inputs it could provide a better platform for the selection of explosives and blast designs.

A study was conducted on a Chilean mine in Doña Inés de Collahuasi, to improve the fragmentation of a very competent rock type, called Ignimbrita. The findings of the study were presented at a conference on explosives and blasting by Cancec *et al* in Montville Ohio (2001) (annual conference of explosive and blasting technique). To evaluate the best stemming alternative a comparison was made between soil, gravel and stemtite. Stemtite is a cone shaped device, manufactured with high impact polyethylene, with compression strength of 103. 42 MPa. The purpose of this device is to seal the blasthole collar, once blasting has occurred. The device is as shown in figure 3.6 below.

Figure 3.6: Stemtite cone-shaped blasting plug (from Cancec et al, 2001)

A number of parameters were analysed after each blast as well as the performance of the different stemming material. One of these parameters was the velocity of detonation measured in the blasthole.

According to Cancec *et al*, (2001) the analysis of the blasting velocity indicated a better work of the explosive at the level of stemming for holes stemmed with the stemtite device. Cancec *et al*, (2001) provided figures 3.7 and 3.8 to prove that the detonation pressure, for blastholes stemmed with soil, diminishes quickly at the stemming level and when compared with stemtite, the detonation pressure increases when it reaches the stemming level. It was concluded that the gas pressure is retained inside the hole for longer and would therefore do more rock-breaking work.

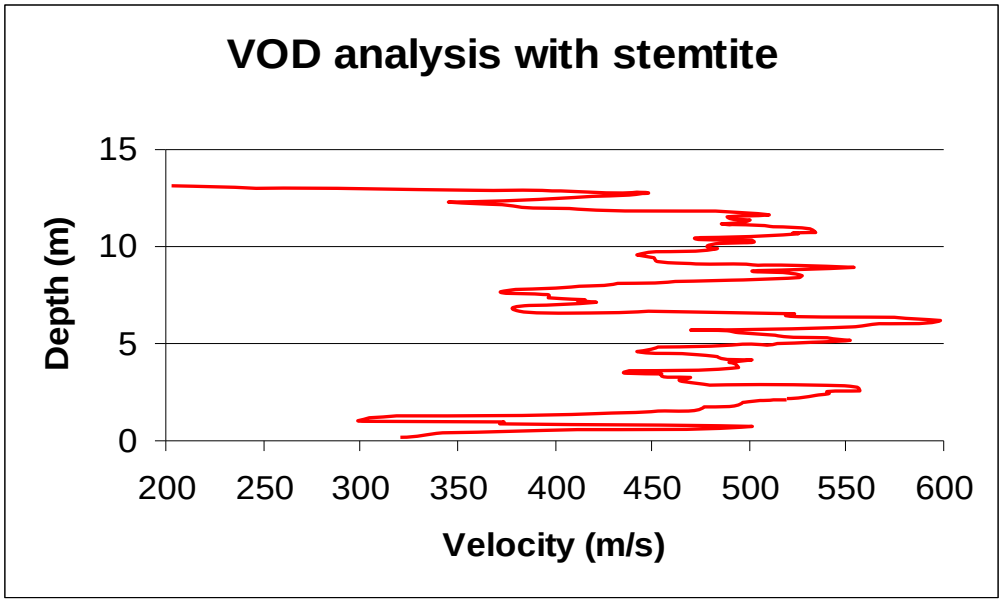

Figure 3.7: VOD (velocity of detonation) behaviour in boreholes loaded with ANFO (ammonium nitrate fuel oil) and stemmed with stemtite (After Cancec, 2001)

The assumptions made by Cancec (2001) are debatable. Considering the graphs 3.7 and 3.8 it can be said that the VOD of the blasts varied considerably as it progressed up the hole. Cancec's study did not clearly show if the two set-ups, represented in the graphs, were exactly similar and if the rock consisted of fairly homogeneous material throughout or not.

Hence it is difficult to determine if the variation is not possibly due to the variation in rock properties. Another factor to consider is that the explosive type used in the experiment, ANFO, is a non-consistent explosive and could also cause variations in the observed VOD of a blast.

Cancec (2001) concluded that the standard deviation from the mean VOD in both graphs is significant. Hence it is difficult to determine whether the changes in the VOD behaviour of the two set-ups are due to the different stemming types or due to these afore-mentioned factors.

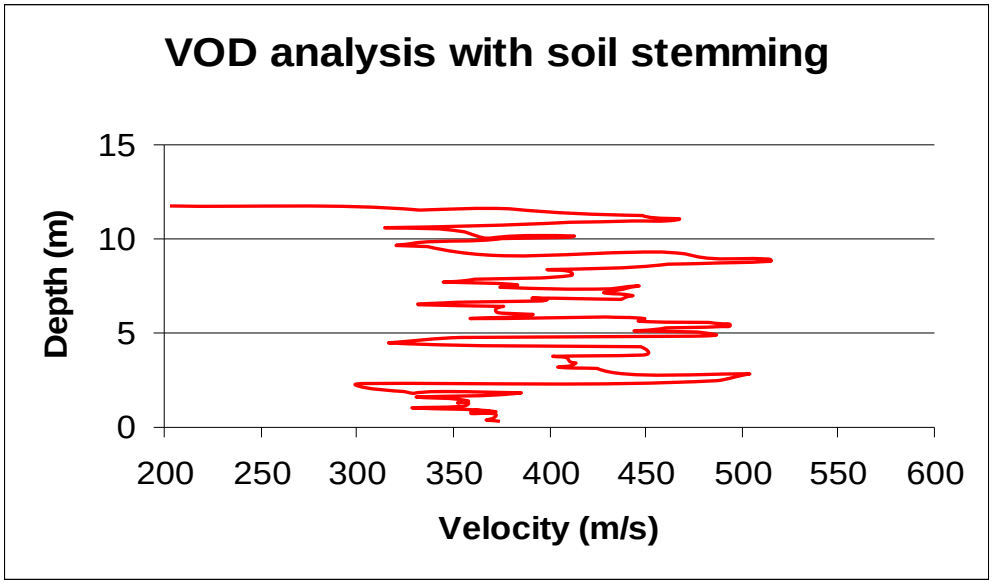

Figure 3.8: VOD behaviour in boreholes loaded with ANFO and stemmed with soil (After Cancec, 2001)

3.7.1.2The effect of confinement on gas pressure

Recently developed theories on rock breakage, stress the role that gas pressure plays in providing the energy necessary for rock breaking (Cook et al, 1996). The detonation of an explosive generates two different pressures. Firstly, the shock front ahead of the detonation zone creates a detonation pressure. Secondly, gas pressure is produced by the rapid expansion of gases caused by a chemical reaction in the borehole. Rock fragmentation is primarily caused by this gas pressure (Ash, 1973; Taylor, 1952; Cook et al, 1996)

Otuonye (1981) highlighted the importance of confinement on the gas pressure effects and on rock. Gas pressure exerts a uniformly distributed force in all directions and will therefore, also apply the same pressure on the stemming of a blasthole as on the sidewalls of a blasthole. Otuonye (1981) found that the gas pressure in a blasthole decreased rapidly from its peak value due to a loss of heat. Increase of volume was observed resulting, mainly from the compaction of

stemming material and the cracking and crushing of the rock. The one controllable component that influences this rapid gas pressure decrease is the compaction or ejection of the stemming material (Otuonye, 1981).

The available energy to break rock can accurately determined using the equation for work done by an adiabatic expansion process as follows (Otuonye, 1981):

$$E = \frac{V_f}{V_I} \times PdV \qquad \text{Equation 3.5}$$

where

V_i is the initial volume of the gas.

V_f is the final volume of the gas

P is the pressure of the explosive gas in Pascal

dV is the change in volume during the explosion

The two different conditions that can be used in the evaluation process of the above integra are: (i) detonation state conditions; and (ii) the explosive state conditions.

The equation shows that the amount of energy available for the breaking of rock is directly related to the final specific volume of gas in the blast hole. The final specific volume in turn is directly related to the compaction or ejection of the stemming material and is therefore a controllable measure.

The pressure in the blasthole at the initial conditions P_i can be calculated with the following equation:

$$P_i = \frac{nRT_i}{V_i \times e_i} \qquad \text{Equation} \quad 3.6$$

where

R is the gas law constant and R = 8.314 J/mol x K

n is the number of moles of the gas

e_i is the covolume of gas in cubic meters

and T relates to Q and C_v by the following relationship:

$$T_i = \frac{Q}{C_v} + T \qquad \text{Equation} \quad 3.7$$

with

Q the heat of the explosion

T the absolute temperature

C_v heat capacity at constant volume

The effect of stemming confinement (i.e. gas energy retention) on fragmentation and movement in blasting was investigated by Armstrong et al (1993) through a series of laboratory scale tests. In these tests concrete blocks of different strengths were used as the model material in the study. Armstrong et al (1993) successfully separated the gas and shock energy by containing the explosive in a steel sleeve and qualitatively examined the crack patterns generated. It was concluded that gas energy was the “primary mover” of the fragmented material in the blasting applications. This confirms results from similar investigations (Cook et al, 1996).

The laboratory tests indicated an increase in fragment size and a decrease in movement of the blasted material as the rate of gas energy release, during the blast, increased. Armstrong et al (1993) observed that the level of gas retention

(i.e. confinement) has a significant, if not controlling effect on fragmentation and movement of the blasted material.

3.7.1.3The effect of stemming on the stress wave

Cowan et al (1986) compared the characteristics of sampled blast wave data required to determine the type of stemming that would reduce the wave amplitude of a sampled blast hence the reduction in the damage of the walls and back area from blasting in an underground mine. Cowan et al (1986) an experimental analysis of the energy waves produced by stemmed and non-stemmed blasts was done (Cowan, Otuonye, Ligon,1986) . In this study a system analysis technique called the Data Dependent Systems (DDS) methodology was used to determine the frequency characteristics for a single, non-reproducible blast wave signature. The DDS statistically minimised the noise in the autospectrum and produced a single accurate, non-reproducible blast wave signature.

The mean squared values of the velocity signatures which are in itself a time domain characteristic, is given by the equation below:

$$\bar{v^2} = \left(\frac{1}{T}\right)\int_0^T \{v(A)\}^2 \, d_t \qquad \text{Equation 3.8}$$

where

$\bar{v^2}$ is the velocity mean squared value

v (A) is the velocity signature and

T is the final time

The velocity mean squared value is an indicator of the kinetic energy of roof particles. The energy of the roof particles, according to Cowan et al (1986), is an

indicator of the wave energy lost to the outside of the blast hole. The results from a study conducted by Cowan et al (1986) indicated that non-stemmed blasts produce larger amplitudes at higher frequencies than limestone-stemmed blasts. This implies that larger amplitudes and higher frequencies can cause damage to the walls of a tunnel and jeopardize the structural integrity of the tunnel. This is indicated in figures 3.9 and 3.10 from Cowan et al (1986). The higher frequencies indicate that more wave energy was radiated to the outside of the blasthole and therefore less energy inside the blasthole to break rock. ([uE]/Hz).

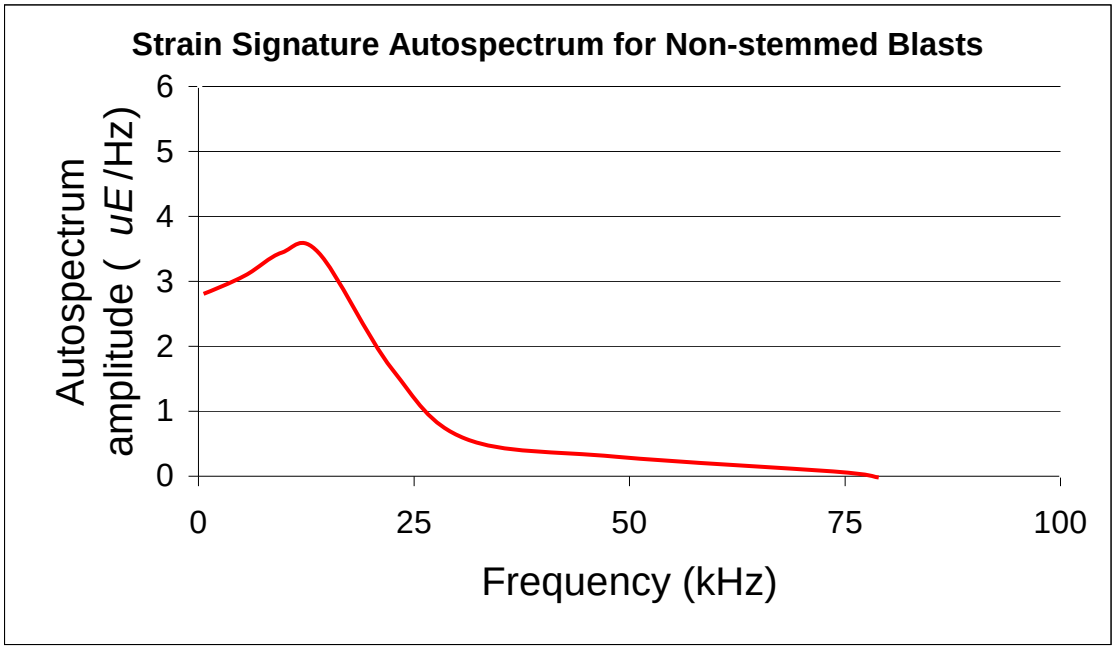

Figure 3.9: Strain signature auto spectrum for non-stemmed blasts (Cowan et al, 1986)

Cowan et.al. concluded that blastholes stemmed with small sized limestone and with coarse basalt produced the lowest energy waves for the stemming types studied. It was further concluded that most of the waves from stemmed blasts contained less energy than non-stemmed blasts.

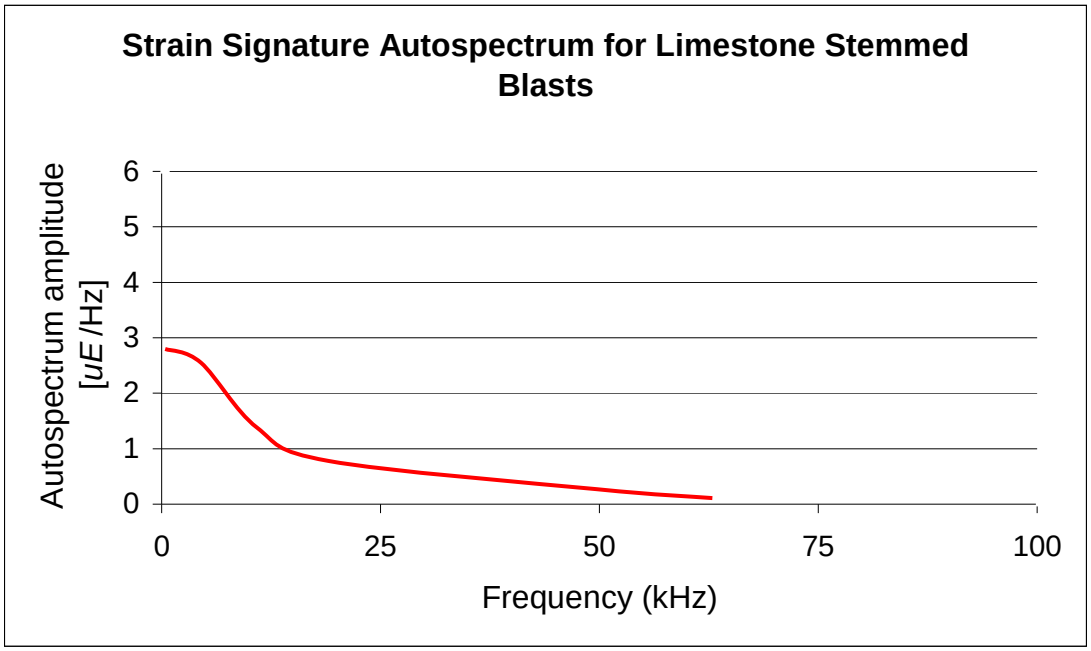

Figure 3.10: Strain signature autospectrum for limestone stemmed blasts (Cowan et al, 1986)

These tests were limited to a small variety of stemming material types and the author identified the need for further research to include a wider range of stemming types to provide more conclusive results.

3.7.2 Stemming in underground mining

3.7.2.1Stemming ejection

It is largely unknown what types of stemming material and the amount of stemming is desirable in underground metal and non-metal mine blasting required to ensure good or improved fragmentation while containing hot gases.

Enforcing the use of permissible explosives and explosive procedures has solved the problems related to blasting practices in fiery mines. However, methane also

occurs in some non-coal mines, particular oil shale, trona, salt, potash, copper, limestone and uranium mines. Blasting procedures at such mines take place with conventional explosives and blasting agents rather than permissible explosives for both practical and economic reasons.

Kopp (1987), made a number of recommendations for blasting underground with personnel present in the mine. Essential among these was the use of stemming to retain the hot gases and flames of the explosive in the borehole until expansion of the burden adequately cooled the gases to avoid methane ignition.

Early laboratory test by Snelling (1912) demonstrated that high explosives were more efficient for containing explosive gases when used in conjunction with stemming for than without. The effects of stemming on the efficiency of low explosive gas to contain gas are less convincing. Later tests conducted in hard rock by the Agnew et al. (1942) also indicated an increase in explosive efficiency with the use of stemming. However, these results were vague and not scientifically conclusive.

Kopp (1987), examined the effectiveness of changes in the lengths of stemming by measuring the rate of stemming ejection in relation to burden movement in an underground mining set-up. It was theorized that, with properly stemmed blasts, the stemming should be contained in the blasthole until burden movement has occurred. Kopp made use of high-speed photography to evaluate the stemming ejection times and compared the results with burden movement. The primary experimental method chosen by Kopp (1987) for studying stemming behavior was high-speed photography. The field experiments were filmed with two cameras, a 16-mm rotating prism camera capable of speeds up to 11 000 frames per second and 16-mm registering pin camera with filming speeds up to 500 frames per second.

In the field tests, both high-energy and relatively low-energy explosives were used. The low-energy explosive was chosen to produce similar effects as ANFO (ammonium nitrate fuel oil), which is an explosive extensively used in the South African underground mining environment (Explosives Today,1987). Both these explosives consisted of 31.75mm cartridges. The volume of the different explosive charges was the same. The blastholes were 38mm and varied in length from 813mm to 1830mm. The stemming material consisted of crushed limestone in two different sizes. The stemming was added after the explosive and filled the hole to the collar. A comparison was made between three different lengths of stemming. The lengths were 508mm, 813mm and 1422mm.

Kopp (1987) conducted the tests with Sandia's "shorted length indication by frequency of electrical resonance" (SLIFER) detonation velocity detection system in each hole. This system measures the rate of crushing or ionising of a coaxial cable buried in the blasthole. This is done by electronically measuring, the length remaining intact as a function of time as the detonation front proceeds up the explosive column. The stemming material is also crushed or compacted, and this rate can be measured with the SLIFER system.

Kopp found that with stemming lengths of 508mm or more, the stemming material was completely contained or took at least 8.8ms for stemming ejection to occur. Table 3.3 indicates the ejection times observed by Kopp (1987).

Table 3.3: Observed ejection times of 508mm stemming material.

Stemming type*	Explosive type	Ejection time (ms)
Fine drill cuttings	High-energy explosives	13
	Low-energy explosives	32
Coarse drill cuttings	High-energy explosives	8.8
	Low-energy explosives	retained
Note: *Stemming materials of 813mm, 1270mm and 1524mm were retained.		

When stemming has been retained, it has achieved its function in terms of confining the hot gases. However, when stemming is ejected, further analysis is required to determine if an adequate length of stemming has been used.

A simple physical model has been suggested by Kopp(1987) to predict the time required to eject stemming. This model depends only on the inertia of the stemming material. The frictional forces that resist movement have been omitted.

The acceleration, of the stemming is given by:

$$a = \frac{F}{M} \qquad \text{Equation 3.9}$$

where F is the force exerted on the stemming by explosive gases, and M is the mass of the stemming. The equation of motion is therefore:

$$S = V_0 t + \frac{1}{2} a t^2 \qquad \text{Equation 3.10}$$

where S is the distance travelled by the stemming, V_0 is the initial velocity of the stemming and t is time in seconds. If the two equations above are combined with $V_0 = 0$ it gives:

$$t = \sqrt{\frac{2SM}{F}} \qquad \text{Equation 3.11}$$

The force, F, can be estimated from the borehole pressure by using first principles of physics:

$$F = PA \qquad \text{Equation 3.12}$$

With A and P being the cross sectional area of the stemming and borehole pressure respectively then the mass of stemming is given by:

$$M = \rho_s A \lambda \qquad \text{Equation 3.13}$$

with l the length of the stemming and ρ_s the density of the stemming material. Substitution of equation (d) and (e) into (c) gives the following relation for ejection time:

$$t = \sqrt{\frac{2S\rho_s\lambda}{P}} \qquad \text{Equation 3.14}$$

Kopp(1987) used the above equation to predict the ejection times for the different blasts in his field tests. Table 3.4 compares the results from the field tests conducted with the results from the calculations done with the above mentioned equations.

Table 3.4: Calculated and observed stemming ejection times (form Kopp, 1987)

Hole diameter (mm)	Stemming length (mm)	Ejection time (ms)		First stemming movement	% Error
		Calculated	Observed		
38	508	0.5	3.4	13	96
38	508	0.5	4.6	9	94
38	508	0.6	6.1	32	98
47.6	610	0.5	2.2	4	88
47.6	610	0.5	2.0	4	88
47.6	610	0.5	2.4	4	88
153	2743	2.1	10	Retained	NA

Table 3.4 gives a clear indication of the applicability of Kopp's calculations when compared to the field test results. The author is convinced that the formulas do not accurately represent the actual conditions of the tests. The conservative results from the calculations confirm this statement. This method should only be used to

obtain an estimate of the minimum stemming ejection time. Improved estimates will require the inclusion of frictional forces to the calculations.

Kopp (1987) also found that a length of stemming to charge diameter ratio of 26 or more prevented premature ejection of stemming and venting of the gases.

The tests mentioned in the previous chapter, where holes had a stemming length to charge diameter ratio of 16, explosive gases would have cooled below the ignition temperature of methane in the time required for stemming ejection. However venting of gases through fractures occurred before stemming ejection and the temperature of the vented gas was estimated by Kopp (1987) to be above the methane ignition temperature. The ignition temperature of methane is 1178℃ Kopp(1987) concluded that for these specific conditions, the stemming lengths of 16 charge diameters could have resulted in methane ignition.

These tests are highlighting the need for further research with more sophisticated instrumentation. It should be noted that the ejection times were three times obtained or greater than those predicted by a simple inertia model.

3.8 Types and sizes of materials

Literature shows that stemming material varies in size and type of material (Otounye 1981). The properties of stemming material have been found to have an effect on the confining capabilities of the stemming material. These properties include the size, angularity, cohesion and the compaction characteristics of the stemming material (Otounye 1981).

The contents of stemming materials used range from soil, crushed limestone/ basalt aggregate to concrete stemming material and stemtite. The most important

parameter that has been used to determine the effectiveness of stemming material is its shear strength that it forms with the blasthole walls. Adequate confinement requires the use of stemming material with strength equal to the ultimate strength of the rock to be used (Otounye 1981). Otounye (1981) found that when crushed stone was used as a stemming material it resulted in better fragmentation and control than drill cuttings. Through numerous lab tests Stimpson et al (2000) found that the addition of cement to loose dry stemming material increased the bond strength of stemming material. This is shown in figure 3.11. An increase in the shear strength causes an increase in axial displacement at failure.

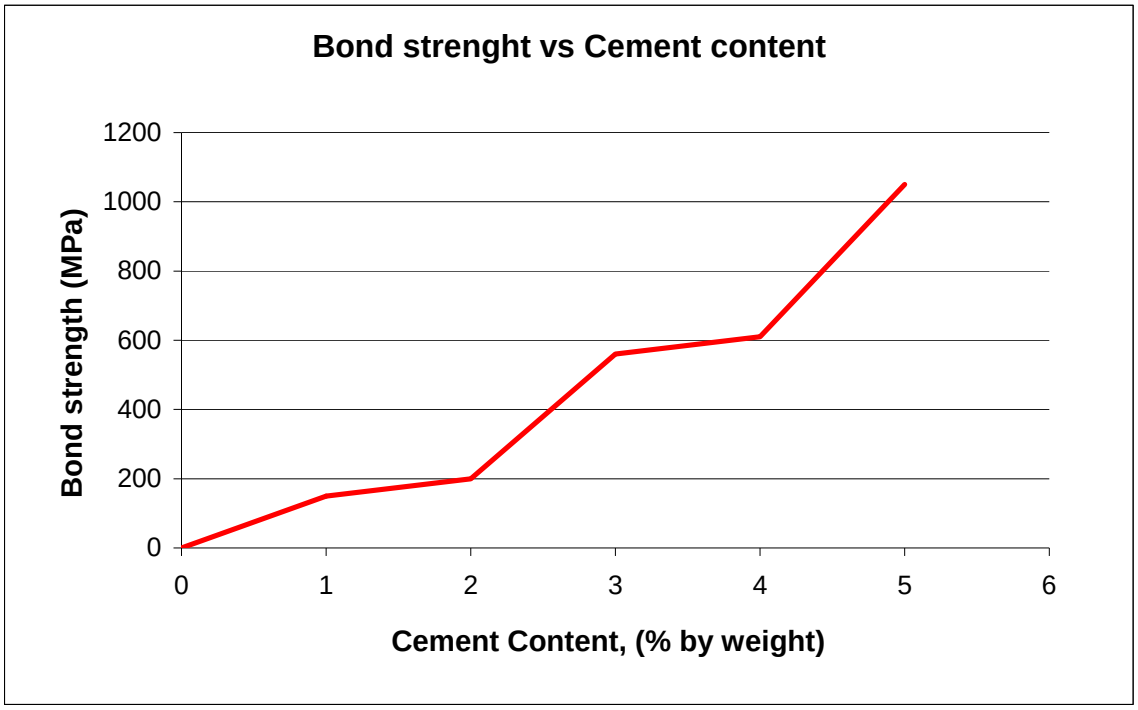

Figure 3.11: The influence of cement content in the increasing cemented aggregate bond strength above un-cemented bond strength (Stimpson *et al*, 2000)

Generally ideal coarse material for stemming material is considered to have an average size between 5 and 7cm. Finer material has been found to have a very low shearing strength and is easily ejected during use. Although coarse material is the most efficient as a stemming material, a wide distribution of particle sizes is

desirable for a good stemming material to improve the interlocking effect and reduce the void ratio.

Otounye (1981) tested different types and sizes of stemming material that included the following; Ottawa sand, river sand, crushed gravel and limestone aggregate. Results showed that limestone aggregates were more effective in providing explosive gas confinement. This was due to the fact that limestone took less time to compact than other materials used in the experiment of the same size. An efficient stemming material compacts quickly when subjected to high explosive pressures after detonation. A material that compacts slowly would not be desirable because of the tendency of gaseous products to leak through the interstices of the stemming material.

Armstrong et al (1993) tested sand and limestone stemming properties using a test rig. The test rig was designed to quantify the relative forces required to eject different stemming materials from blasthole. The rig consists of a concrete tube with an internal diameter of 10mm, which is fitted at its base with a porous brass frit. A 600 KPa air supply is attached to the frit and is used to pressurize the system. A pressure tap is installed directly below the porous frit to measure the pressure applied to the sample. The schematic detail of the rig is shown in figure 3.12

The test rig was used to rank the stemming materials according to their ejection resistance against supplied pressure. The authors acknowledge the test's limitations as the force applied to the stemming material in the ejection rig is of many orders of magnitude lower than that which would be experienced from the detonation of an explosive. Furthermore the test rig does not take into consideration any other parameters that may affect the ejection of material, such as stemming length.

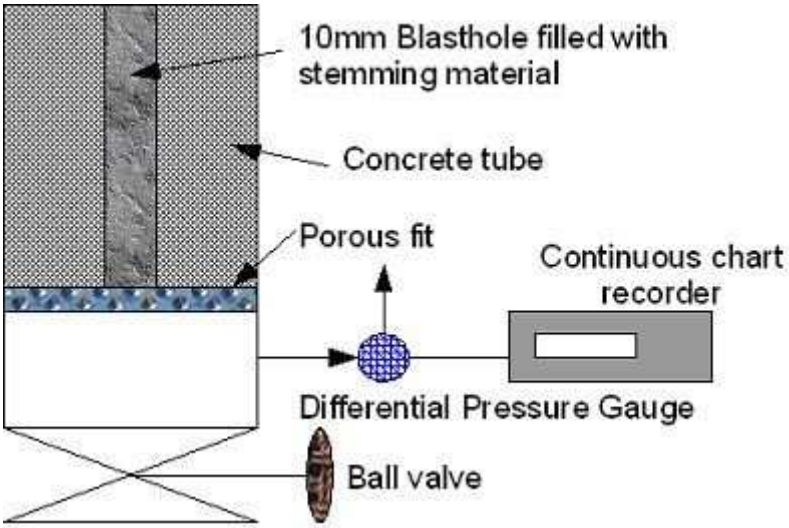

Figure 3.12: Schematic diagram of ejection rig (from Armstrong et al. 1993)

Nonetheless, the test can be used to test a relative resistance of the stemming material in a blasthole.

The performance of stemming is also a function of the shape of individual particles. For stemming material particles to interlock, the particles have to have a certain shape. The indices used in the quantitative description of shape are the roundness and sphericity (Krumbein and Sloss, 1963). The angularity or roundness of a particle is given by:

$$\sum_{t=1}^{N} \frac{r_t}{R} / N \qquad \text{Equation 3.15}$$

where

r = the radius of the corner

R= radius of the maximum circle inscribed by the particle.

N= number of corners in the particle.

Particles with a low roundness factor and high sphericity factor have the ability to interlock with each other and tend to form a bridge or wedge action with themselves and the walls of the blasthole (Otounye, 1981).

The water content of a stemming material can also affect its performance. The high moisture content in plastic materials such as clay, tends to act as a lubricant. This promotes slippage and reduction of the shear strength between the walls of the blasthole and the stemming material itself. It is apparent that high water content will not only reduce the effectiveness of the packing and interlocking action of particles, but also interferes with the wedging action of the particles (Otounye, 1981).

Armstrong et al (1993) found that the addition of small quantities of water increased the resistivity of sand and crushed limestone. Table 3.5 shows the variation of resistivity (change in ejection pressure) with moisture content.

Table 3.5: Stemming ejection rig test (Armstrong et al, 1993)

Material	Size(mm)	Moisture content (Wt%)	Ejection pressure (kPa)
Sand	0.8	0	30
		2	110
		3	110
		7	120
		17	120
Limestone	0.6	0	350
	0.8	0	40
		3	500
	1.5	0	30
		3	500

In general the proper selection of the type of stemming material with the right size distribution and right shape of particles will optimise the rock fragmentation, reduce flyrock and ground vibration therefore increase productivity. In most cases crushed limestone aggregate has been found to be the most effective stemming material (Armstrong et al,1993).

3.9 Stemming length

The length of stemming in any given blast hole is affected by various parameters. Confinement of the charge ensures that energy generated by the explosive is used in the fragmentation of rock. Too short stemming results in the loss of confinement and therefore excessive airblast, flyrock in the contrary stemming that is too long results in the formation of boulders, poor fragmentation and significant overbreak (Otounye, 1981). Different methods have been used in the estimation of stemming length, but none seems to provide a scientific analysis in these estimations. Stemming length has been related to overburden and the diameter of the blasthole, without the consideration of other parameters that may affect in the effectiveness of stemming material. Rules of thumb have been used in the estimation of stemming height for example where stemming has been said to be 1 to 1.2 times the burden and in other cases it has been said to be a third of the length of blasthole. There is no clear method that is used in the estimation of stemming length. Parameters that considered to effect stemming length include the following:

3.9.1 Rock strength

Hagan and Kennedy (1976) found that the optimum stemming length is dependant upon the properties of rock. The strength of any given rock will determine how much stemming is required in terms of length. As a generalisation hard rocks

require a shorter length of stemming compared to soft rocks, in order to avoid a blocky collar area after blasting. Figure 3.13 shows the relation between the lengths of stemming to the type of rock, where, A, represent rock factor (see table 3.6)

3.9.2 Velocity of detonation (VOD)

The VOD has an influence on the optimum length of stemming. Explosives with lower detonation velocity will need a longer length of stemming relative to explosives with higher VOD. It has been established that large quantities of stemming are desirable to increase the confinement of slow burning explosives. Experimental work only included sub-sonic impulse sources due to the inherent nature of supersonic sources to destroy the elements that are in close proximity at detonation. This inherent nature was taken to be a treat to the requirements for research to be reproducible.

3.9.3 Strength and density of the explosive

As the strength and density of the explosive increases, so does the length of stemming required. Figure 3.13 shows how stemming length varies according the type of explosive and the type of rock used.

3.9.4 Position of the primer

The amount of stemming required is also dependent on the position of the primer. If the primer is positioned at the collar (collar priming), the length of stemming will be greater compared to bottom priming.

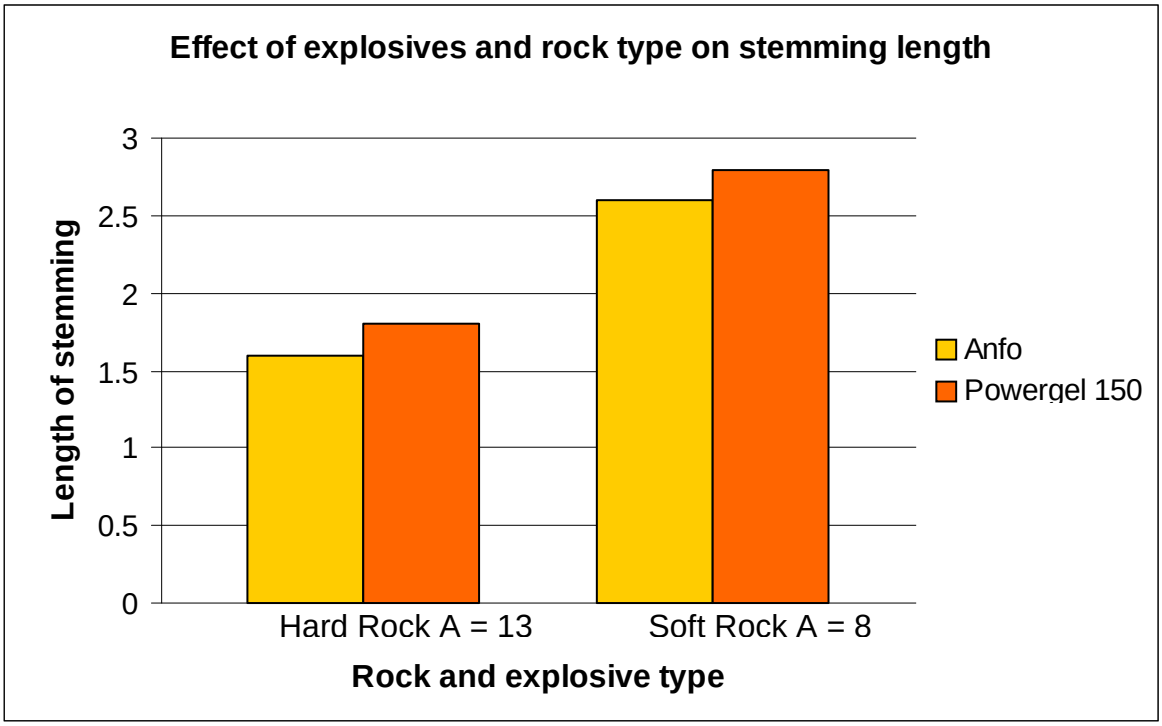

Figure 3.13: Effect of explosives and rock types on stemming length. [Note: Rock factors - Hard rock A = 13; Soft rock A = 8 (Explosives today, June 1987)]

In the AEL bulletin, Explosive Today (1987) a formula was proposed for stemming length estimation. The formula is given below:

$$T = Z \times \frac{12}{A} \times (W \times \frac{E}{100})^{1/3} \qquad \text{Equation 3.16}$$

where

T is the stemming length (m)

Z is the flyrock factor

(Note: where occurrence of flyrock is not problematic use Z = 1 close to exposed civil structures such as roads, bridges, power lines use Z = 1.2, close to buildings and public thoroughfares use Z = 1.5)

A = rock factor (see table 3.8.1)

W = Mass of explosives in 8 hole diameter (kg)

E = relative weight strength of explosives.

Table 3.6: Estimation of rock factor (Explosive Today, June 1987).

Blasting category (UCS)	Typical rock type	Rock factor (A)
Hard (+200MPa)	Andesite, dolerite, granite, ironstone, silcrete	12-14
Medium (100-200MPa)	Dolomite, hornfels, quartzite, serpentine, schist	10-11
Soft (50-100MPa)	Sandstone, calcrete, limestone, shale	8-9
Very soft (-50MPa)	Coal	6

The determination of optimal stemming length requires various parameters to be taken into consideration and the choice of the stemming length has significant influence on blast results, particularly relating to fragmentation and flyrock.

The estimation of the correct stemming length in relation to overburden and hole diameter alone would not yield accurate results. It is therefore important to also consider explosive type and rock characteristics. These are omitted in equation 12 and therefore the limitations of this equation should be noted.

4 CONCEPTUAL MODEL

4.1 Introduction

The behaviour and performance of stemming materials is based on the basic principal of resistance to movement (friction). In chapter 3.6.2.1 the studies done by Kopp (1987) were discussed. Kopp (1987) used the equations of motion to estimate the time it takes to eject stemming. The correlation between the calculated ejection times and the measured ejection times were very low. It was concluded that the use of frictional force calculations should increase the accuracy of the estimated times. Thermodynamic principals have the potential to accurately describe the pressure changes in a blasthole. The following paragraphs will introduce the reader to the principals of friction and thermodynamics and its applicasion to the analysis of stemming materials.

4.2 The laws of friction

Friction force in mechanics is a force that opposes the relative motion or tendency for such motion of two surfaces in contact. It is not however, a fundamental force, as it originates from the electromagnetic forces and exchange force between atoms. The texture of both surfaces influences friction. The factor that will theoretically have the biggest influence on the effectiveness of a particular stemming product is the amount of contact force between the stemming plug and the inside of the blasthole. The higher the contact force, the more friction increases and therefore the resistance to movement increases.

Furthermore if a particular stemming material has been designed to stick to the inner walls of a blasthole, then the amount of friction is not directly proportional to the normal force on the contact surface any longer. The stickiness or stickiness factor of that particular stemming material becomes the property that influences the pressure a certain stemming material can take.

There are three types of frictional forces:

1 Static friction is the friction acting on a body when the body is not in motion, but when a force is acting on it. Static friction is the same as the force being applied. Static friction acts because the body tends to move when a force is applied on it.

2 Limiting friction is the friction applied on a body just before it starts moving. Limiting friction is generally the highest resistive force of the tree.

3 Kinetic friction is the friction which acts on the body when the body is moving. Kinetic friction is usually smaller resistive force than limiting friction.

The work that stemming does during a blast will start just after the blast has been initiated. It will continue to do work until either the rock starts moving or the stemming plug is ejected. The time period that must be analysed would therefore, starts at the beginning static friction begins and ends when the limiting friction phase is over.

The classical approximation of the force of friction known as Coulomb friction is named after Charles-Augustin de Coulomb and is expressed as:

$$F_f = \rho R \qquad \text{Equation 4.1}$$

where

ρ is the coefficient of friction

R is the reaction force normal to the contact surface

F_f is the maximum possible force exerted by friction

This law mathematically follows from the fact that contacting surfaces have atomically close contacts only over extremely small fractions of their overall surface area, and this contact area is proportional to load until saturation takes place. Saturation will occur when all areas are in atomic contact, thus no further increase of friction force takes place.

The static frictional force is given by:

$$F_s = \rho_s R \qquad \text{Equation 4.2}$$

where

ρ_s is the coefficient of static friction

R is the reaction force normal to the contact surface

F_s is the force exerted by static friction

The limiting frictional force is given by:

$$F_{max} = \rho_{max} R \qquad \text{Equation 4.3}$$

where

ρ_{max} is the coefficient of limiting friction

R is the reaction force normal to the contact surface

F_{max} is the force exerted by limiting friction

The kinetic frictional force is given by:

$$F_k = \rho_k R \qquad \text{Equation 4.4}$$

where

ρ_k is the coefficient of limiting friction

R is the reaction force normal to the contact surface

F_k is the force exerted by limiting friction

The coefficient of friction is a dimensionless scalar value which describes the ratio of the force of friction between two bodies and the force pressing them together. It

is important to note that the coefficient of friction is an empirical measurement and cannot be found through calculations, Kinetic friction and static friction are distinct concepts. For kinetic friction, the force of friction does not vary with the area of contact between the two objects, i.e. kinetic friction does not depend on the size of the contact area.

Certain approximations exist that simplify that friction calculations without causing gross inaccuracies. These approximations are:

Friction is independent of:

- surface area
- speed (except when v=0), and
- temperature

Friction is dependent on the nature of the surfaces in contact, and;

The frictional force is directly proportional to the normal force between the two surfaces in contact, except in the case where the stickiness factor has an influence.

The friction that is analysed here is dry friction, which is the resistive force between two clean, dry solid surfaces.

4.2.1 Stemming and friction

Each type of stemming material should have a specific coefficient of limiting friction. Its effectiveness would be determined by the value of this coefficient coupled with a factor that resembles the maximum normal force as a result of borehole pressure at the time of limiting friction. It is again emphasised that the coefficient of friction cannot be calculated for a particular material unless empirical tests results are available that can be used to determine these coefficients.

4.3 Rationale for pressure tests

4.3.1 Gas pressure and Adiabatic work

In a report by (Britton et al., 1984), a methodology was presented for the calculation of borehole pressure generated by an explosive. It was concluded that thermodynamics permits equilibrium explosive gas pressure calculations for initial and final state conditions to be ascertained while neglecting the rate of change (as may be seen in the detonation state parameters). The ideal gas law (equation 4.5) can be used to gain a better understanding in the behaviour of the explosive gasses in a borehole. The ideal gas law is given by:

$$PV = nRT. \qquad \text{Equation 4.5}$$

where:

P is the absolute pressure

V is the volume

T is the absolute temperature

R is the universal gas constant and is equal to: 8.3145 J/mol K and

n is the number of moles for the gas

Explosives generate detonation pressures that range from (19000atm) GPa for Ammonium Nitrate Fuel Oil based explosives to (50 000atm) GPa for emulsion based explosives. The ideal gas law however is accurate at relatively high temperatures and at a low pressure. Because explosives generate such high detonation pressure, the ideal gas law can be adjusted to accommodate calculations that require accuracy at high pressures. This adjustment can be made by the inclusion of a factor. Britton et al. (1984) has suggested the inclusion of a compressibility factor (Z). This factor can be applied to define explosive gas detonation pressure using thermodynamic state functions and establish processes for obtaining heat release and gas temperatures.

The ideal gas law will then change to the format below:

$$PV = ZnRT \qquad \text{Equation 4.6}$$

The specific volume of an ideal gas is given by RT/P. The compressibility factor aims to accommodate for the difference between the specific volume of the ideal gas and the actual specific volume of the explosive gasses. Z relates to the specific volumes as follows:

$$Z = \frac{\rho_{actual}}{\rho_{ideal}} \qquad \text{Equation 4.7}$$

For an ideal gas, Z would be equal to one where as for real gasses, Z may be greater or less than one. This would then indicate the deviation of explosive gas behaviour from normal gas behaviour (Britton et al. 1984).

The Z factor for any gas is almost equal if they are in the same state with the same reduced temperature and reduced pressure. Reduced temperature and reduced pressure can be calculated with the following equations:

$$T_r = T = T_c \qquad \text{Equation 4.8}$$

where:

T_r is the reduced temperature

T is the temperature of the gas, and

T_c is the critical temperature

$$P_r = P = P_c \qquad \text{Equation 4.9}$$

where:

P_r is the reduced pressure

P is the pressure of the gas, and

P_c is the critical pressure

Note: absolute temperatures and pressures are used during these calculations.

The following paragraphs discuss the relationship between pressure and work. This will provide credence to the popular notion that the primary doer of work in rock blasting is the explosive generated gas pressure. This analysis together with the friction analysis will form the foundation of the principles and theories investigated during this study.

4.3.1.1Adiabatic work versus breakage

Previous work displayed a high correlation between breakage versus calculated borehole pressure (figure 4.1) (Britton, 1983; Warden, 1983). It was also shown that the relationship between shock energy and breakage was nearly constant. Further research examining a work relationship would verify these results. The work integral in a borehole may be given by (Cook, 1996):

$$W = \int_{P_i V_i}^{P_f V_f} P dV \qquad \text{Equation 4.10}$$

where:

W is the work

V_f is the final volume

V_i is the initial volume

P is the borehole pressure

It is assumed that a uniform distribution of the explosive gas exists before any venting or movement occurs. This assumption is intrinsically flawed as addressed by Otuonye (1981) that, even with decoupled holes, there is a springing effect that occurs. Equation 4.9 is a function of specific volume and the equation therefore requires that all the parameters are a function of specific volume. The equation can be modified to accommodate the expansion of the explosive into decoupled holes. The reaction will therefore resemble that of confined gases exerting a force on the burden side of the borehole in an irreversible manner. If this adjustment is made the work of the explosive can be defined by:

$$W = P_1 V_1 \frac{n}{n-1}(P_3 - P_1) \qquad \text{Equation 4.11}$$

where:

P_1 is the pressure at venting

V_1 is the volume of gas

C_p=C_v which is the ratio of the specific heats

P_3 is the explosion pressure, and

n is efficiency

Britton and Gozon (1984) plotted a derivative curve using data points given in table 4.1 breakage versus the theoretical plot of adiabatic work was plotted. Figure 4.1 indicates the graphical correlation between these two parameters.

Table 4.1: Work comparison data (Britton and Gozon (1984))

Decoupling ratio (D/R)	Pressure (P) (MPa)	Breakage (B) (kg)	Adiabatic Work (W) (J)	Volume (V) ($10^{à 9}m^3$)
1.0	2214	0.698	1.5227	811
1.5	779	0.576	2.8576	1824
2.0	323	0.510	4.3201	3243
2.5	191	0.479	6.0960	5067
3.0	141	0.375	8.2590	7296

The benefit such strong correlation is that equations for adiabatic work can be used to determine the breakage of the rock, with a high level of confidence and further extensive tests to determine the amount of fragmentation, would be deemed unnecessary. Breakage (B) represent the average size of particles measured in weight (kg).

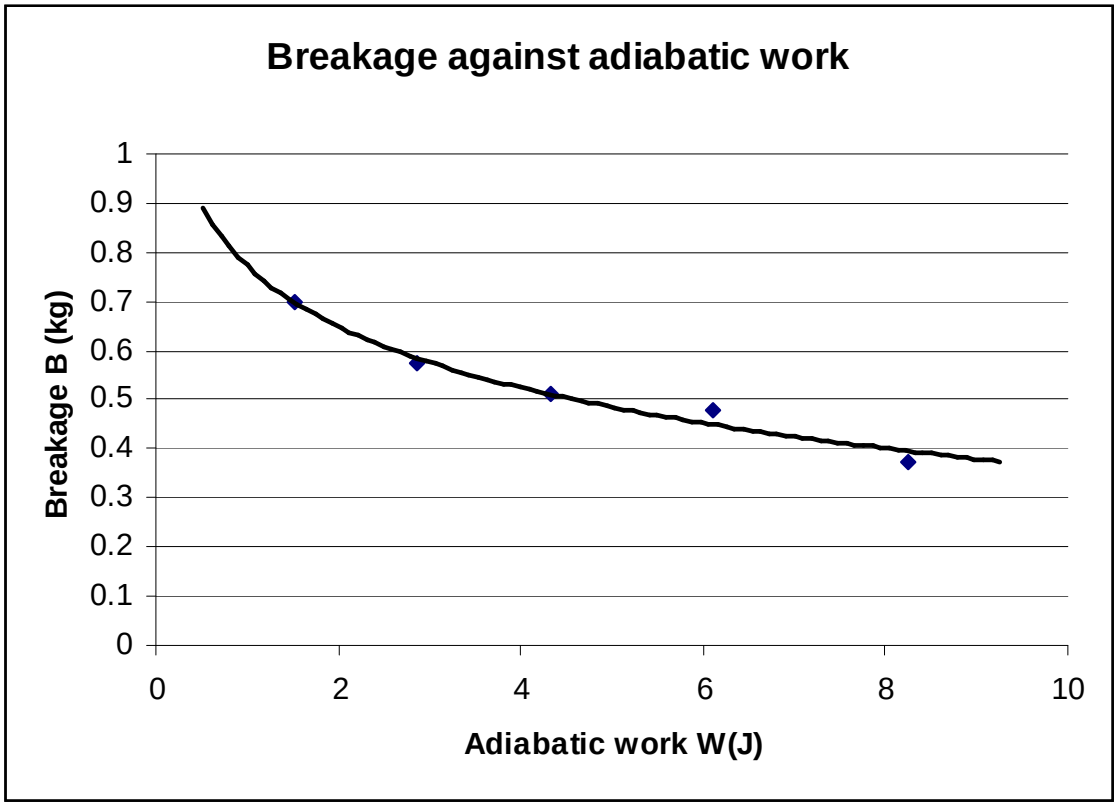

Figure 4.1: Adiabatic work against breakage (Britton and Gozon (1984))

Using regression analysis on the data points, a logarithmic equation yields the most accurate fit of the data. If the Pearson correlation coefficient is applied to this model a value of R^2 = 0.9749 is obtained. Because of the analysis of variance identity, a value of $0 \leq R^2 \leq 1$ should be obtained. However a large value of R^2 does not necessarily imply that the regression model accurate. Adding a variable to the model will always increase R^2 regardless whether or not the additional variable is statistically significant. However if the adjusted Pearson correlation coefficient is

applied, $R^2_{adjusted}$,then it gives a better reflection of the proportion of variability explained by the regression model. This is because the adjusted R^2 takes the number of regressed variables into account. $R^2_{adjusted}$ = 0.9666. This means that this model describes the behaviour of the data to a 97% level of confidence. The equation that the trend line yielded is:

$$B = -0.1787Ln(W) + 0.7725$$ Equation 4.12

Even with the relatively high level of confidence it is still difficult to predict the ability of the equation to describe the data at the extremities. Analyses of rock breaking behaviour might shed some light on the topic. Figure 4.2 gives a graphical comparison between the size of a particle compared to the amount of energy it takes to achieve that particle size. Upon analyses of rock behaviour when broken to a particle size smaller than $10^{-1}\mu m$. Britton et al predicts a slope of m = -1.0 (see figure 4.2). The slope in figure 4.1 relates inversely to the slope in figure 4.2. This suggests that the slope of the curve in figure 4.1 at in increased level of adiabatic work could relate to the particle size and therefore breakage according to the same slope. If the two data points that represents the highest adiabatic work in figure 4.1 is linked with a linear line the slope seem to relate more to the inverse of slope B in figure 4.2 than the slope Britton et al suggests. This could suggest that the graph in figure 4.1 could be look more like figure 4.3. The red dotted line is parallel to the slope between the two data points that represents the highest adiabatic work. The same argument can be followed to question the ability of equation 4.11 to accurately describe the behaviour of the rock at low energies. (Britton and Gozon (1984))

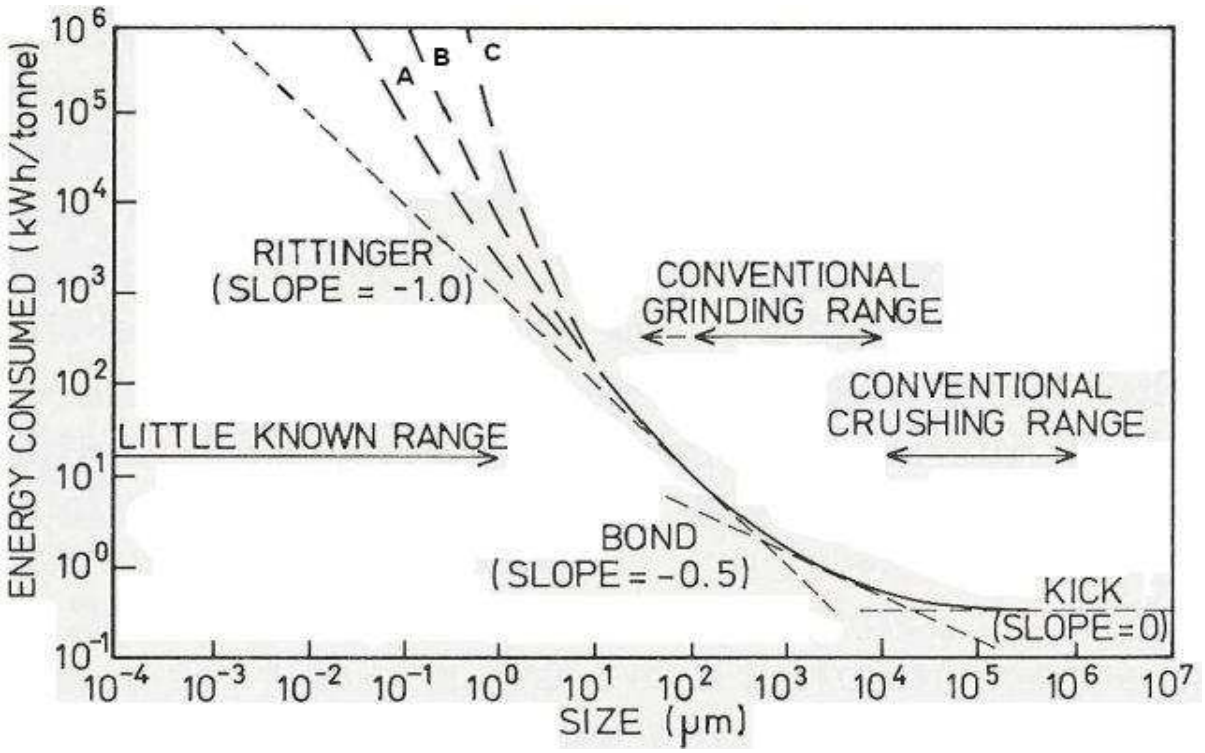

Figure 4.2: Energy consumed against particle size (Britton and Gozon (1984))

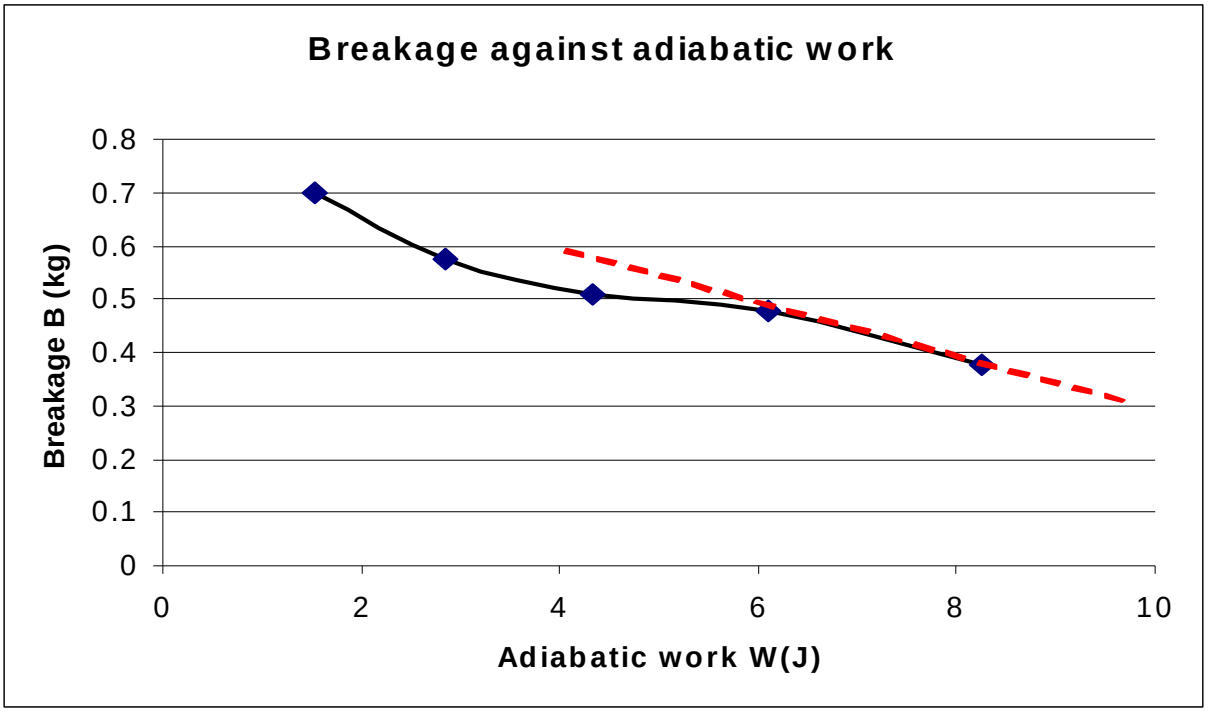

Figure 4.3: Breakage against Adiabatic work. Slope adjusted for high work conditions

Figure 4.3 describes the behaviour of particle size at low energy consumption levels with a slope the approach m = 0. This should relate inversely to the slope of the graph in figure 4.3 at low levels of work. The slope that Britton et al. suggests in figure 4.3 does in fact relates closely to what can be expected at the lower extremities of adiabatic work. This suggests that equation 4.12 should describe the behaviour of adiabatic work against breakage with reasonable accuracy (Britton and Gozon (1984)).

We therefore accepts equation 4.12 as a accurate estimation tool of rock fragmentation or breakage at the lower levels of adiabatic work but questions its ability to accurately describe the behaviour of fragmentation for higher levels of adiabatic work.

4.3.1.2Gas pressure versus adiabatic work

The pressure of the mixture of the gasses in a borehole directly after initiation can be calculated using Kay's rule, the reduced temperatures as well as the number of moles of the product gases. The relationships between temperature, volume and pressure at explosive conditions can be described by particular equations of state. These relationships can be assigned to the different structural parameters for the different atomic or molecular types present in explosive gas mixtures. These equations of state also describe the interaction among the different molecules as well as the influence the different molecular dimensions have on the final state. The first part of Kay’s rule is illustrated in the equation:

$$PV = ZnRT \qquad \textit{Equation 4.13}$$

where

Z is the compressibility factor.

Explosives are mixtures of molecules and the resultant gasses have to be calculated. The second part of the model describes these mixtures:

$(P_c)_{mix} = \sum X_i (P_c)_i$ for pressure and $(T_c)_{mix} = \sum X_i (T_c)_i$ for temperature

Equation 4.14 Equation 4.15

These equations define the final state of the gas in terms of the initial state conditions. The calculations depend on the assumption of thermodynamics versus kinetic governance, as well as the initial state conditions selected. The disadvantage of using these equations however, is that it neglects the detonation state conditions. If a stable explosive mixture undergoes a rapid temperature increase it is usually difficult to describe the conditions accurately with basic thermodynamic principals. However, working with reaction formulas for the chemical reactions seems to provide real benefits. Mass and heat capacity determine temperature, and pressure is a function of that temperature, the number of gaseous moles present in the mixture, and the volume occupied by the gaseous product.

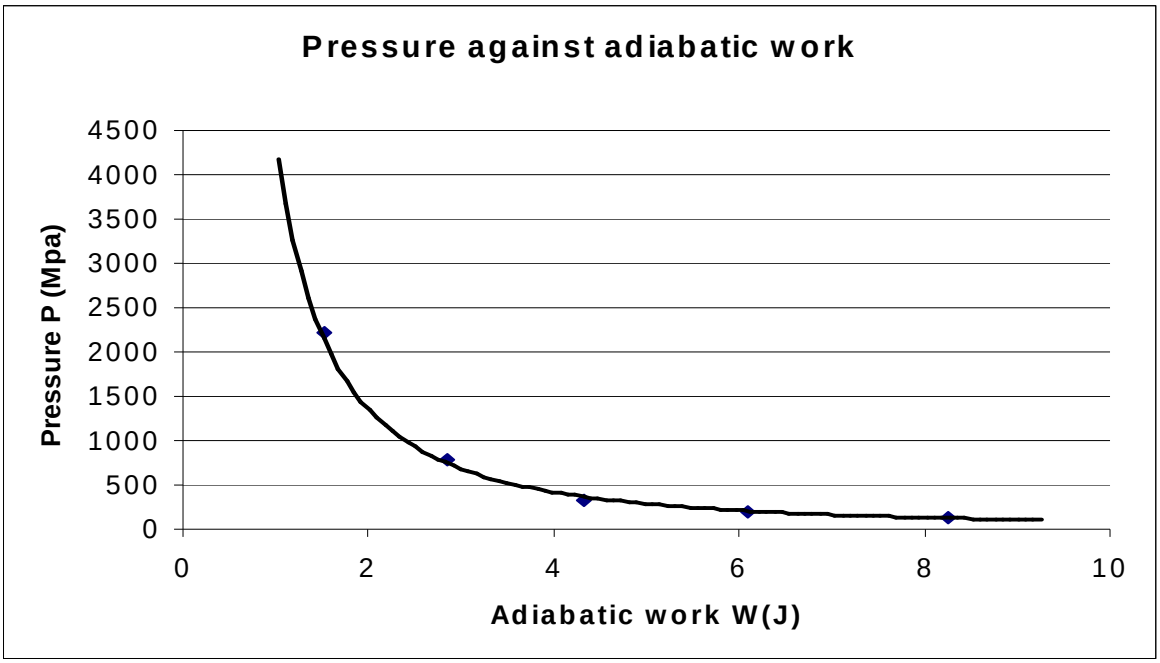

Figure 4.4:Adiabatic work against pressure (Graph published by Britton and Gozon (1984) in the International Journal of Mining Engineering of 1984)

As shown by figure 4.4 adiabatic pressure responds well to calculated pressure. Using regression analysis on the data points, a Power function seems to yield the most accurate fit of the data. The model yield a Pearson correlation coefficient of R^2 = 0.9911.As stated in a previous paragraph a value of $0 \leq R^2 \leq 1$ should be obtained. However a good regression model are not necessarily implied by a large value of R^2. The adjusted Pearson correlation coefficient is applied, $R^2_{adjusted}$. It gives a better reflection of the proportion of variability explained by the regression model. $R^2_{adjusted}$ = 0.9881. This means that this model describes the behaviour of the data to a 99% level of confidence. The equation that the trend line yielded is:

$$P = 4345.3W^{-1.6847} \qquad \text{Equation 4.16}$$

With a 99% level of confidence it can be concluded that the model describes the behaviour of borehole pressure at various levels of adiabatic work well. It is once again difficult to predict the equation's ability to describe the behaviour of the model at the extremities.

The models discussed in the previous paragraphs provide researcher with a number of tools to analyse the behaviour of a stemming material in the borehole. The inference is that work produced by an explosive tends to be a result of explosive generated gas pressure rather than the more constant shock energy. The breakage and adiabatic work respond to calculated borehole pressure relationships with very high correlation. This indicates the primary mechanism for rock breakage is explosive generated gas pressure. Thermodynamic calculations permits equilibrium explosive gas pressure to be calculated from the initial state and final state conditions without consideration of rates to achievement of intermediate states. Procedures for calculating equilibrium explosive gas pressures with the use of thermodynamic state functions and a readily definable process to define the explosive gas pressure by the inclusion of the compressibility factor, Z. The rationale for performing pressure tests in a controlled environment has to

carefully analysed and discussed in the previous paragraphs. It has been proved by various researchers (Brinkman, 1990; Britton et al, 1984; Britton and Gozon, 1984) that the primary mover of rock in a blasthole is the gas generated energy. The focus for this research will therefore be on the analysis of the behaviour of the gas pressure in the borehole. An analysis of the influence gas pressure alone on the behaviour of the stemming is difficult to investigate in an environment where a lot of other factors have got the potential to influence the outcome of study. The ideal would be set up a test facility that can detach the influence that the change in other factors besides that of interest will exercise on that particular behaviour.

4.3.2 Underground tests

Underground tests where performed as part of this particular study in order to analyse the influence that other factors beside that of stemming will have on the results and to analyse the potential of a production stope to serve as an accurate testing facility. The underground tests were conducted in a conventional production stope at Townlands shaft, a platinum producing vertical shaft of Anglo Platinum, situated on the outskirts of Rustenburg, South Africa.

This production stope uses conventional drill and blast mining methods. Drilling is conducted with handheld jackhammers. Blastholes are drilled in a horizontal configuration at 80˚ angles. The spacing between holes is 400mm and the hole diameter is 32mm. Figure 4.5 gives a graphical representation of a block of ground being removed in one blast.

4.3.2.1Data recording process

The progress in the stope was monitored over one month, from 04/07/2006 to 01/08/2006. Various variables were measured including, the depth of the holes drilled, the depth of the sockets, and the advance made during the blast.

The means for the top, middle and bottom values has been calculated and analysed. A total average face advance has then been established for each blast, and then compared to the blasts before and after. A sample of the data recording sheet is given in appendix B.

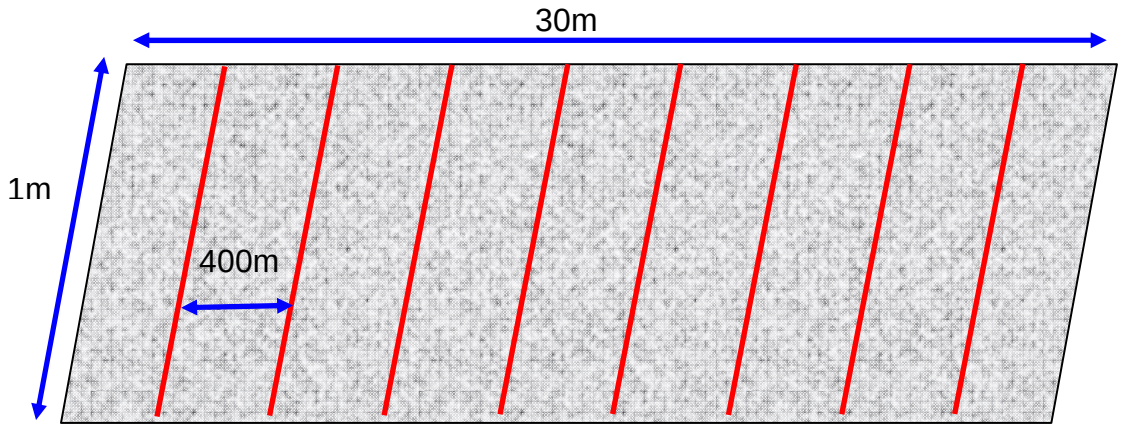

Figure 4.5: Diagrammatic representation of a block of ground being removed in a single blast

4.3.2.2Factors influencing the accuracy of the study

The advance and the socket length are measures that are commonly used to define the efficiency of the blast and these measures have therefore also been used to measure the efficiency and influence of stemming on the blasting performance in studies done by tamping manufacturers. If the researcher uses the advance and the socket length as a measure of stemming performance, he will overlook a number of other factors that will influence the accuracy of the analysis.

These factors include:

- variance in drilling lengths
- deviation from the correct drilling direction

- ineffective sludge removal procedures
- variations in the timing procedures
- poor and ineffective charging-up procedures
- non-homogeneous properties of the rock strata
- geological disturbances

The above mentioned factors all have the potential to influence the outcome of the blast. Some of these factors have a bigger and other a lesser effect but they all have one thing in common, they will influence the outcome of a stemming analysis. If all these factors are not controlled and if there influence on the blast measured and accounted for, it will render the study inconclusive and not representative of the gas pressure in the blasthole.

4.3.2.3Analyses of underground stemming results

The measure of the influence that all of the factors mentioned in the previous paragraphs have on the results of the study is difficult to determine. The following paragraphs will analyse the some of these different factors that was measured in the underground analyses. The objective of the analyses is to determine the influence these factors had on the results of the blasting.

A strong correlation can be seen between the advance and the drilled length in figure 4.5. All these blast holes have been tamped the same way. It is quite clear from the figure that in this underground stope, the drilling discipline has made a big impact on the advance as well as the socket length. It can also be seen that the there is a correlation that seems inversely proportional between the advance and the socket length. All these observed correlations should be statistically tested to determine the measure of the impact. In figure 4.6 the daily advance has been compared with the drilled length as well as the socket length.

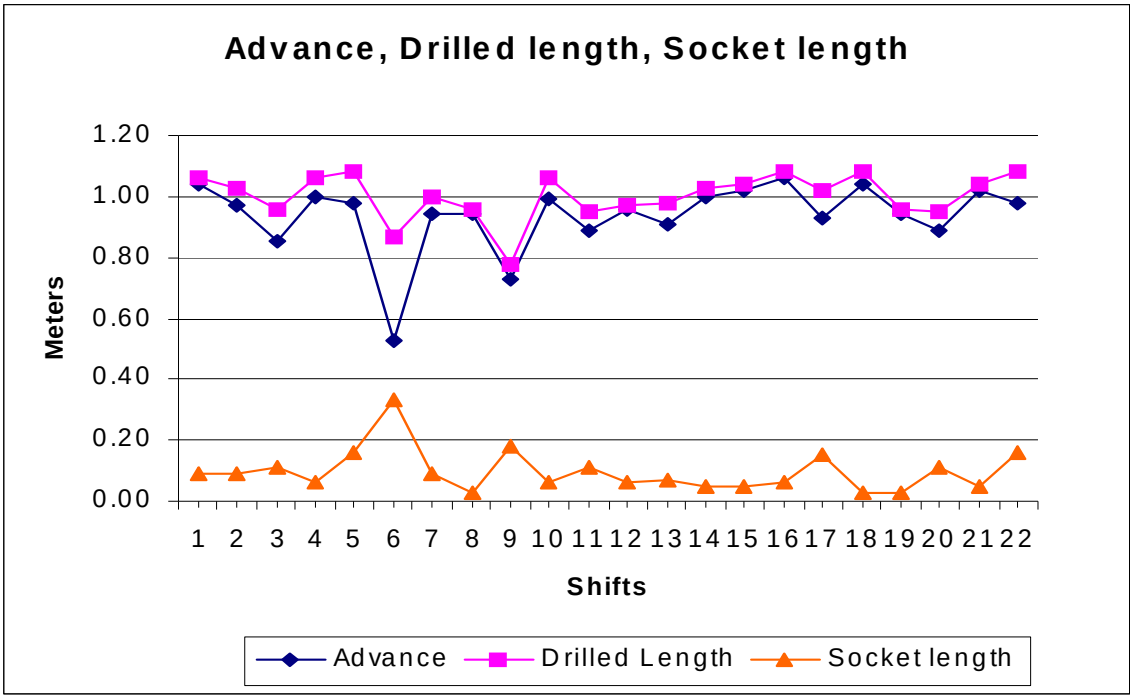

Figure 4.6: The measured average daily advance, drilled length and socket length.

4.3.2.4Drilling consistency

In a stemming performance analysis, drilling consistency is a critical parameter that needs to be kept as constant as possible. The statistical analyses of the drilling consistency should shed some light on the performance of the stemming being analysed. Table 4.2 below compares all the different drilled lengths for the consecutive shifts.

The point estimate of the arithmetic mean of the values in table 4.2 is $\bar{x}$ = 1.01m and the standard deviation is σ = 0.0811. However it would preferable to have an interval in which we would expect to find the true mean drilling length since it is unlikely that μ = 1.00m. This can be accomplished with a confidence interval.

Table 4.2: All the individual drilled lengths for the consecutive blasts in a production stope at Townlands shaft

Drilled lengths (m)									
1.04	1.06	1.11	0.95	1.10	0.96	1.02	0.95	1.02	*0.93*
1.03	1.02	0.83	0.90	0.98	0.95	1.03	0.98	1.05	*1.10*
1.03	1.10	0.97	1.00	1.05	0.75	1.07	1.06	1.11	*0.99*
0.91	1.08	0.95	1.11	1.00	1.03	1.06	1.00	0.87	*0.98*
1.07	1.09	0.80	1.08	0.97	0.98	1.04	1.05	1.06	*1.10*
1.03	0.95	1.05	1.09	1.10	0.92	0.96	1.05	0.99	*1.11*
0.90	*0.98*	*0.90*	*1.03*	*1.10*	*0.95*	*1.06*	*1.05*	*0.80*	

The confidence interval will be as follows:

$$l \leq \mu \leq u \qquad \text{Equation 4.17}$$

This interval is called the 100(1-α) percent confidence interval for the parameter μ.

An assumption must now be made as to the level of confidence that is necessary to yield representative results. A 95% confidence interval should be more than enough in this environment if the influences of all the factors mentioned in chapter 4.2.2 are kept in mind. The quantities l and u are the lower- and upper-confidence limits, respectively, and (1-α) is called the confidence coefficient. The observed interval [l, u] brackets the true value of μ with confidence 100(1-α). This statement has a frequency interpretation; that is, it is not known if the statement is true for this specific sample, but the method used to obtain the interval [l , u] yields the correct statements 100(1-α) of the time.

A 95% confidence interval implies that 1-α = 0.95, so that α = 0.05. Thus $z_{\alpha/2} = z_{0.025} = 1.96$. The lower-confidence limit is:

$$l = \bar{x} - z_{\alpha/2}\sigma / \sqrt{n} \qquad \text{Equation 4.18}$$

$= 1.01 - 1.96(0.0811)/\sqrt{69}$

$= 1.01 - 0.0191$

$= 0.981$

and the upper-confidence limit is

$$u = \bar{x} + z_{\alpha/2}\sigma / \sqrt{n} \qquad \text{Equation 4.19}$$

$= 1.01 + 1.96(0.0811)/\sqrt{69}$

$= 1.01 + 0.0191$

$= 1.0191$

Thus, the 95% two-sided confidence interval is

$$0.9810 \leq \mu \leq 1.0191$$

This is the interval of reasonable values for the mean drilling length (in meters) at 95% confidence. This means that the difference between two drill holes next to each other can, with a confidence of 95%, be up to 4 cm. The result of the drilling inaccuracies can, statistically, cause sockets of up to 4 cm.

4.3.2.5Socket length

As mentioned in a previous paragraph, the socket length and the advance are measures that where used in a number of previous studies to try and determine the effect of stemming on the performance of explosives. There is merit in the

aforementioned analyses to measure overall performance of an explosive, but it lacks the ability to accurately distinguish between and separate the influence the various factors mentioned in the beginning of chapter 4.2.2 had on the energy utilized for moving the rock. Table 4.3 below indicate the socket lengths measured during the underground analyses.

Table 4.3: All the individual socket lengths for the consecutive blasts in a production stope at Townlands shaft.

Socket lengths (m)									
0.09	0.03	0.05	0.48	0.11	0.03	0.03	0.45	0.06	*0.05*
0.06	0.15	0.03	0.15	0.03	0.03	0.00	0.07	0.08	*0.06*
0.20	0.10	0.03	0.12	0.30	0.13	0.04	0.02	0.06	*0.00*
0.07	0.09	0.06	0.09	0.05	0.24	0.09	0.10	0.02	
0.48	0.05	0.03	0.06	0.18	0.01	0.04	0.04	0.17	
0.18	0.06	0.09	0.00	0.09	0.03	0.05	0.05	0.03	
0.08	*0.05*	*0.05*	*0.35*	*0.09*	*0.18*	*0.00*	*0.04*	*0.02*	

The point estimate of the arithmetic mean of the values in table 4.3 above is $\bar{x}$ = 0.0962m (9.62cm) and the standard deviation is σ = 0.1066m (10.66cm). It would be inaccurate to state that on average a measured socket was be 9.6cm. A better representation of the population would be to state a confidence interval about the mean because it is unlikely that μ = 0.0962m. Equation 4.13 will be used to determine the confidence interval. The quantities l and u are the lower- and upper-confidence limits, respectively, and (1- α) is called the confidence coefficient. The observed interval [l, u] brackets the true value of μ with confidence 100(1-α). This statement has a frequency interpretation, but the method used to obtain the interval [l, u] yields the correct statements 100(1-α) of the time.

A 95% confidence interval is acceptable. This implies that $z_{\alpha/2} = z_{0.025} = 1.96$. The lower-confidence limit is:

$$l = \bar{x} - z_{\alpha/2}\sigma/\sqrt{n} \qquad \text{Equation 4.20}$$

$$= 0.0962 - 1.96(0.1066)/\sqrt{66}$$

$$= 0.0962 - 0.0251$$

$$= 0.0711$$

and the upper-confidence limit is

$$u = \bar{x} + z_{\alpha/2}\sigma/\sqrt{n} \qquad \text{Equation 4.21}$$

$$= 0.0962 + 1.96(0.1066)/\sqrt{66}$$

$$= 0.0962 + 0.0251$$

$$= 0.1214$$

Thus, the 95% two-sided confidence interval is

$$0.0711 \leq \mu \leq 0.1214$$

This is the interval of reasonable values for the mean socket length (in meters) at 95% confidence. This means that the difference between the length of the sockets can, with a confidence of 95%, be between 7.1cm and 12.1cm.

4.3.2.6Advance

In any industry an important objective would be to maximize the utilization of the operational expenditure (OPEX). Practically, this would mean that one would like to maximize the profits by maximizing the performance while keeping the OPEX as close to constant as possible. To maximize your profits in an underground stope,

the objective should be to maximize the advance per blast. For each blast the OPEX would be the same, but the profit would be directly equivalent to the advance made by that blast. The objective in the underground stope would then be to maximize the advance. The maximum profit, would be achieved if the advance is equal to the drilled length. An advance as close to the drilled length would be ideal. Table 4.4 below indicate the daily advance that was measured in the production stope.

Table 4.4: All the the daily advance for the consecutive blasts in a production stope at Townlands shaft.

Advance per blast (m)									
1.10	0.90	1.10	0.45	0.88	1.05	0.96	0.40	1.00	*1.00*
1.08	0.90	1.09	1.04	0.92	0.96	1.30	1.08	1.00	*1.00*
0.65	0.90	1.10	0.97	0.40	0.96	0.97	0.99	1.00	*1.18*
1.00	0.88	1.05	0.80	1.00	0.80	0.85	0.90	1.14	
0.45	0.92	0.90	1.00	0.80	0.96	1.10	1.06	0.90	
0.70	0.85	0.88	1.30	0.95	0.92	1.00	1.00	1.10	
0.85	*0.95*	*1.10*	*0.50*	*0.88*	*0.80*	*1.18*	*1.00*	*0.99*	

The point estimate of the arithmetic mean of the values in table 4.10 above is $\overline{x}$ = 0.936m and the standard deviation is σ = 0.186m. To state that the average advance of the blasts is 0.936m. A more accurate indication of the population would to state a confidence interval about the mean. It is unlikely that the population mean μ = 0.936m. The confidence interval will be determined by equation 4.13. The lower- and upper-confidence will be given by l and u respectively. It has been determined previously that a 95% confidence interval is acceptable. This implies that $z_{\alpha/2} = z_{0.025} = 1.96$. That gives a lower-confidence limit is:

$$l = \overline{x} - z_{\alpha/2}\sigma/\sqrt{n} \qquad \text{Equation 4.22}$$

$$= 0.936 - 1.96(0.186)\sqrt{66}$$

$$= 0.936 - 0.044$$

$$= 0.892$$

and the upper-confidence limit is:

$$u = \bar{x} + z_{\alpha/2}\sigma/\sqrt{n}$$

$$= 0.936 + 1.96(0.186)\sqrt{66}$$

$$= 0.936 + 0.044$$

$$= 0.980$$

The 95% two-sided confidence would therefore be:

$$0.892 \leq \mu \leq 0.980$$

Practically this means that the mean advance would be between 89cm and 98cm, 95% of the time.

4.3.2.7Comparative analysis

A comparative analysis between the average advance, average drilled length and the socket length should shed some light on the consistency of some of these parameters. One would expect that the measured socket length would be the difference between the drilled length and the advance. However that is far removed form the truth. Column C table 4.5 is the difference between the average advance (column A) and the average drilled length (column B). Column D, the average socket length should then be the same as column C. It is clear from the table that, that is not true. Column E indicates the difference (in cm) between columns D and C. The last column represents the percentage difference between columns D and C. The last column in table 4.5 indicates the percentage difference

between the socket length and the arithmetic difference between the average drilled length and the advance.

Table 4.5: The average advance, average drilled length and the socket length.

A	B	C	D	E	Percentage difference
Ave Advance (m)	Ave drilled length (m)	B-A (m)	Socket length (cm)	D-C (cm)	
1.04	1.06	0.02	9	7	64%
0.97	1.03	0.06	9	3	20%
0.85	0.96	0.11	11	0	0%
1.00	1.06	0.06	6	0	0%
0.98	1.08	0.10	16	6	23%
0.53	0.87	0.34	34	0	0%
0.94	1.00	0.06	9	3	20%
0.94	0.96	0.02	3	1	20%
0.73	0.78	0.05	18	13	57%
0.99	1.06	0.07	7	0	0%
0.89	0.95	0.06	11	5	29%
0.96	0.97	0.01	6	5	71%
0.91	0.98	0.07	7	0	0%
1.00	1.03	0.03	5	2	25%
1.02	1.04	0.02	5	3	43%
1.06	1.08	0.02	6	4	50%
0.93	1.02	0.09	15	6	25%
1.04	1.08	0.04	4	0	0%
0.94	0.96	0.02	3	1	20%
0.89	0.95	0.06	11	5	29%
1.02	1.04	0.02	5	3	43%
0.98	1.08	0.10	16	6	23%

If the researcher uses only the advance and the socket length as an indication of tamping performance then the assumption will be made that the socket length as merely the difference between the drilled length and the advance. According to this data that assumption will only be true about 30% of the time. This faulty assumption will then cause the researcher to overlook vital information about the data. The information about the data that may be overlooked is:

- drill holes may not be parallel to each other
- drill holes may be off-line
- drill holes may not be of the same length
- drill holes may incline/decline more than accounted for

Figure 4.7 below gives the percentage column of table 4.5 in graphical format. The faulty assumption discussed before assume that the percentages in the table below is equal to zero, which is clearly not the case.

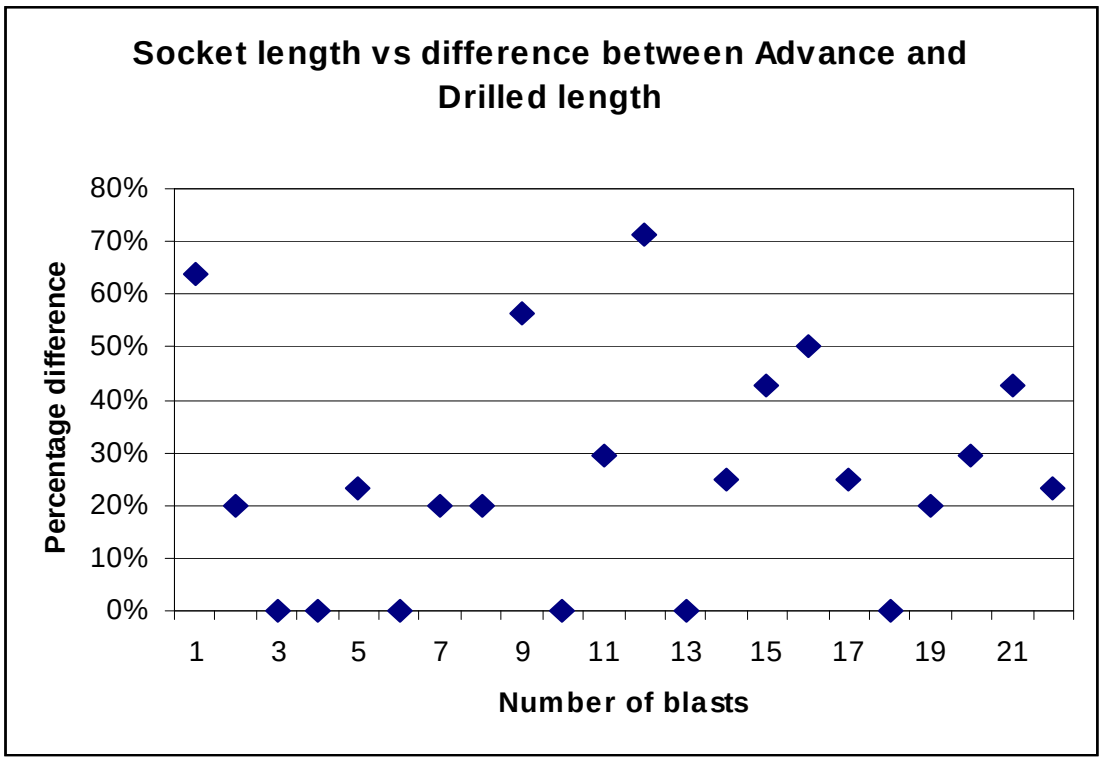

Figure 4.7: Graphical analysis between the socket length versus the difference between the advance and the drilled length.

The error in the drilling of the holes discussed in a previous paragraph is indicated on section by figure 4.7. In the figure the assumed position of the drill hole, indicated in green, is compared to the possible actual position of the drill hole, and indicated in red. The actual maximum advance is also compared to the actual advance.

Figure 4.9 is a graphical representation of the errors in the assumptions in three dimensions. An example of a possible error will now be discussed. Lets assume that the actual drilled hole is off-line from the intended hole by $15°$ in the vertical plane so that
$\delta = 15°$ and off-line by $10°$ in the horizontal plane so that $\theta = 80°$.

The actual maximum advance can then be calculated as follow:
Lets assume "a" assumed length of the drilled hole is 1.2m and "b" the actual length of the drilled hole as 10cm shorter so that b = 1.1m. As discussed earlier we will take, $\delta = 15°$ and $\theta = 80°$.

$c = 1.1 \times \cos 15°$ and
$d = c \times \sin 80°$ then

$$d = 1.1 \times \cos 15° \sin 80°$$
$$= 1.05m$$

this means that "d" the actual maximum advance is then 1.05m. The error is therefore 15cm. This is just an example of what is possible.

Table 4.12 indicates the possibilities of errors in the assumptions. The table indicate different values for θ and δ. These values refer to possible angles measured according to the graphical description given in figure 4.8.

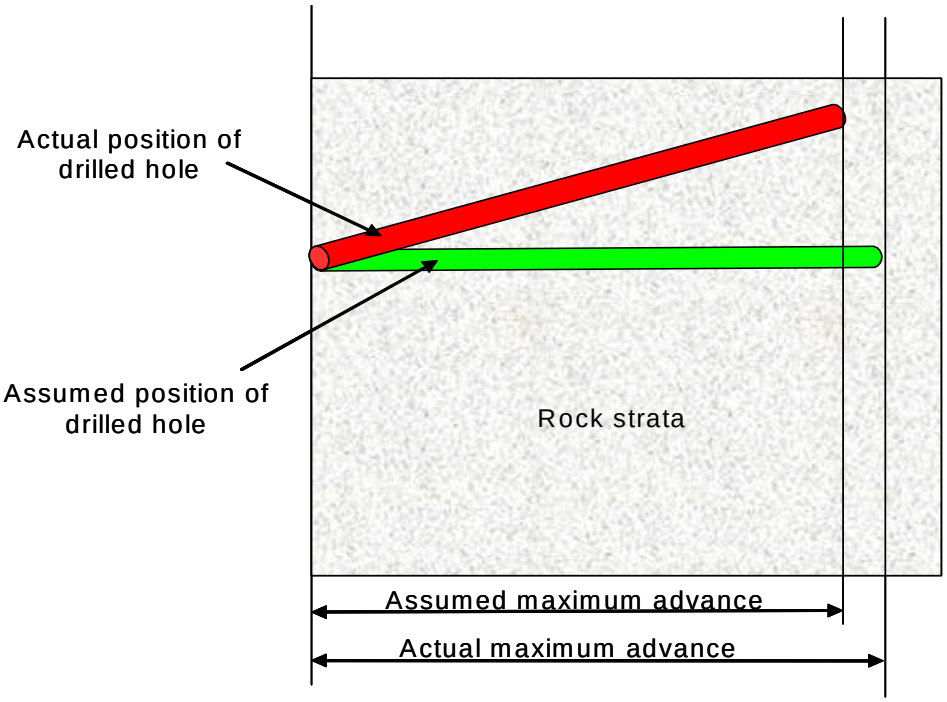

Figure 4.8: Section view of the possible errors that may occur in the assumed maximum advance.

Table 4.6: The possibilities of errors that can be made with the assumptions discussed.

Assumed length of drill hole (m)	Actual length of drill hole (m)	Value of θ (degrees)	Value of δ (degrees)	Assumed maximum advance (m)	Actual maximum advance (m)
1.20	1.20	90.0	0.0	1.20	1.20
1.20	1.15	87.5	2.5	1.20	1.15
1.20	1.10	85.0	5.0	1.20	1.09
1.20	1.05	82.5	7.5	1.20	1.03
1.20	1.00	80.0	10.0	1.20	0.97
1.20	1.00	77.5	12.5	1.20	0.95
1.20	1.00	75.0	15.0	1.20	0.93

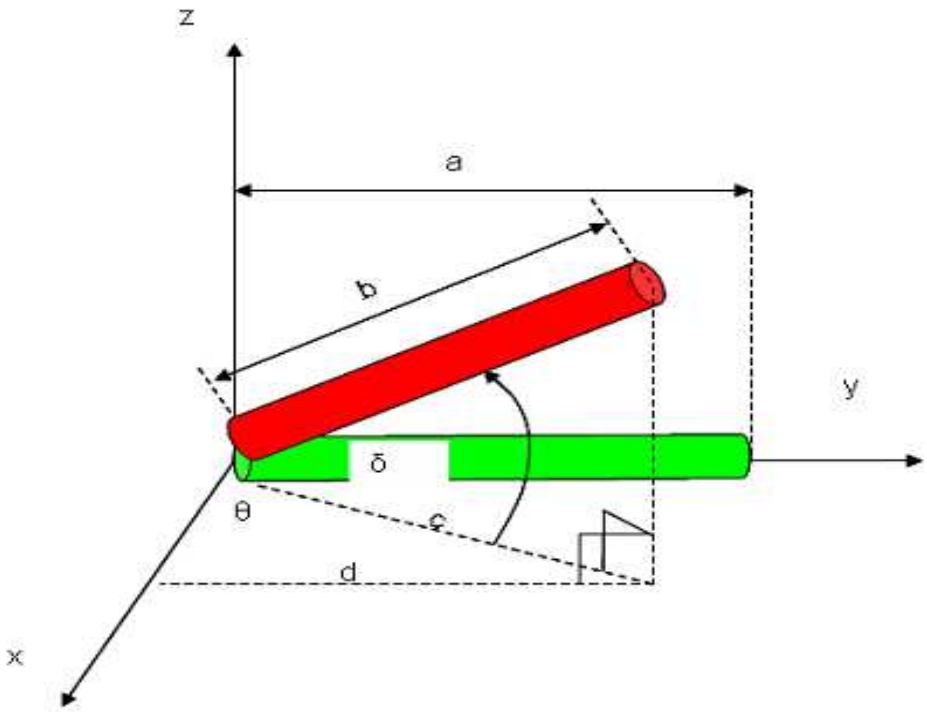

Figure 4.9: A graphical representation of the errors in the assumption in 3 dimensions.

It has been establish that to test the stemming in the underground environment would not yield the desired results. The problem that presents itself now is that the underground environment is where the final product must be implemented and the final tests should be performed in that environment. It will only be possible to establish the influence of stemming materials on the blast, once the influence of all other major factors has been calculated and its influence eliminated from the calculations.

4.4 Variance in Rock Quality Designation

Another factor for consideration is the degree to which the rock strata present homogenetic properties. This can have an influence if two consecutive blasts in the same rock strata have a significant difference in properties. Uniaxial compressive

strength (UCS) and tensile strength (TS) are shown to be broadly dependent on rock type, and strongly dependent on the degree of structural alteration as reflected by the Rock Quality Designation (RQD) (Wilson *et al.* 2005). The variation in the degree of structural alteration in the Bushveld Complex is significant and its influence on the performance of basting agents greatly unknown.

4.5 Conclusion

Traditionally scientific research must be public and reproducible. If the tests are destructive and there is no way that others can reproduce the test conditions, then the findings of such a study would be questionable. This study focuses on the physical behaviour of different stemming materials that are currently available on the market. Hence these products will be compared and analysed in a testing environment where the influence of the stemming material on the blast can be isolated from all other factors. Another requirement will be that the tests are conducted in an environment that is as representative of real conditions as possible.

If all the factors mentioned in chapters 4.2 and 4.3 are taken into consideration it is clear that a scientific analysis will only be possible if the conditions under which the analysis is conducted is repeatable and therefore non-destructive.

5 RESEARCH DESIGN AND METHODOLOGY

5.1 Introduction

This study is motivated by the need to test stemming materials in simulated conditions that cause rock failure, but in an environment that is more controlled and that is non-destructive. In chapter 3.3.2 it was stated that the purpose of stemming is to retain the gas pressure for a time, long enough to do the work on the rock. In previous studies it has been shown that the gas energy is the primary mover of the fragmented material (Armstrong et al, 1993). Sarma (1995) also observed that the confinement of explosive gases is one of the factors that affect the interaction of the rock and the explosive. Hence, as an initial phase this study tested different stemming materials for their ability to retain gas in a borehole. If selected stemming materials can not withstand low air pressures, it could be implied that they would also not be able to withstand higher gas pressures under explosive conditions. However, the contrary is also possible. Due to the kinetics and high pressure and temperature conditions it is difficult to predict this behaviour with accuracy. A way to separate the effect of gas pressure on a particular stemming device was investigated.

The deformation behaviour of different stemming products during the application of a single air pulse compared to the opening of a valve was considered. The main difference between a single pulse and the opening of a valve is the time window required to achieve the required pressure change (zero to the maximum). This could have a major impact on the kinetic behaviour of the stemming products. The effect of the deformation on the normal force and, consequently on the friction against the sidewalls of the borehole, have to be carefully considered.

A test facility was designed that allowed stemming materials to be blown from a borehole with compressed air. Air pressure was applied by opening a valve. A pressure transducer was incorporated in the system to measure change in

pressure. A time window of 10 seconds was electronically analyzed with a pressure transducer.

The testing of the stemming products was conducted over two phases. In the first phase, stemming materials were tested for resistance to air pressure up to 600 kPa. In the second phase, a shock wave of air and explosive gas mixture was applied in a single pressure pulse. This single pulse was applied using small quantities of ballistite. The maximum pressure that was obtained during the second phase was 1260 kPa.

One of the primary objectives of this study is to propose a design of a testing facility that tests stemming materials at controlled pressures but would represent their relative performance under explosive pressures. The pressures at which detonation occurs in underground mining are extremely high and are not taken to be controlled pressures. The concern is whether the small quantities of explosives will give the same or similar kinetic conditions when compared to blasting with ANFO in a borehole underground. The following hypothesis is proposed.

5.2 Proposed hypothesis

For the purpose of the study the pressure classes will be defined as follow:
Low pressure is between 0 and 600kPa
High pressure form 600kPa to 1 200kPa

The proposed hypothesis is then as follow:
H_0: There is no significant difference between the median values of the low and high pressure systems when no stemming was used.

H_1: There is a significant difference between the median values of the low and high pressure systems when no stemming was used.

From an experimental and practical perspective ideally a low pressure testing facility that correlates directly with a high (explosive) pressure result would be the ideal objective.

5.3 Experimental testing – Phase one

5.3.1 Experimental setup

Experiments were conducted at facilities provided by the University of Pretoria, in Pretoria. For simplicity, the experimental setup will be explained in using three separate diagrams (figure 5.1, 5.2 and 5.5). A 5.5t Norite (Granite) block was used for the experimental testing. A 32mm hole was drilled through the block (figure 5.1). The hole in the Norite (Granite) block simulated a blast hole in an underground mine. The diameter of the hole was 32mm with a length of 1m. The dimensions of the block were approximately 1m x 1m. A compressed air pipe was securely connected to the one side of the hole (A). The stemming product to be tested was placed in the other side of the hole (B). Compressed air was fed from the opposite side of the hole (A). Figure 5.1 illustrates the experimental setup diagrammatically.

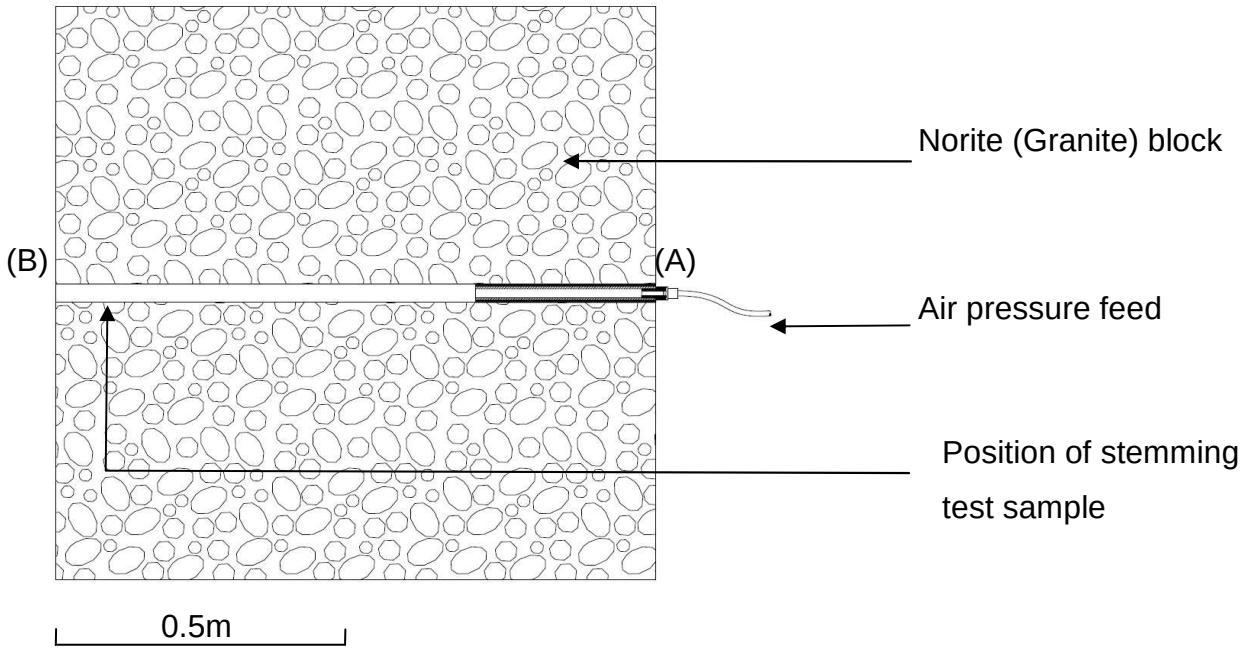

Figure 5.1: Section view of the Norite (Granite) block.

A steel tube was secured with resin into the block (fig 5.2). The outside of the steel tube was modified to increase the roughness of the surface in order to ensure a strong bond between the inside of the block and the steel tube. This tube served as an anchor for the incoming compressed air line. The compressed air line (A^1) was secured to a compressed air coupling. Thread was cut inside the steel tube to accommodate the compressed air coupling. Figure 5.2 graphically displays the connection. The compressed air line A^1 (figure 5.2) was connected to compressed air line A^2 (figure 5.3). (The two figures were separated to simplify the discussion.)

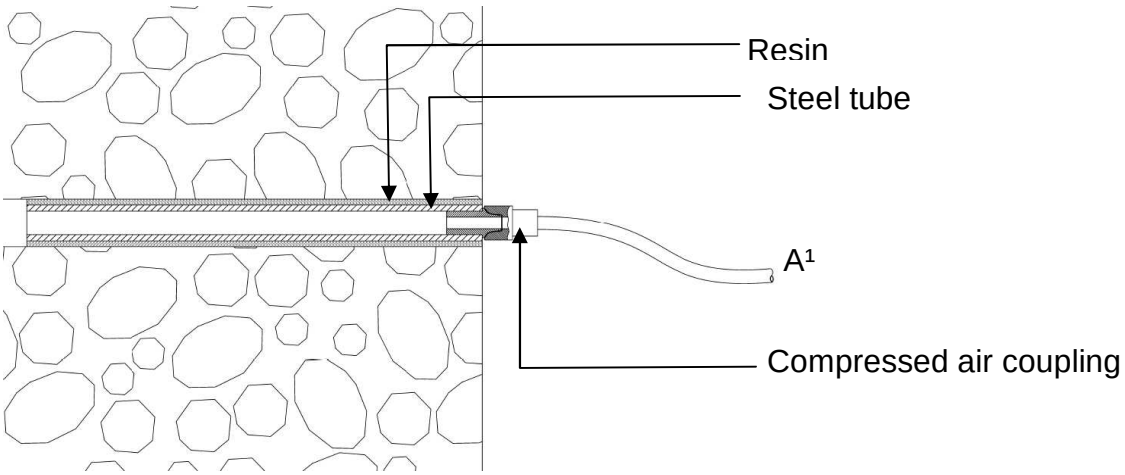

Figure 5.2: Compressed air connection with Norite (Granite) block.

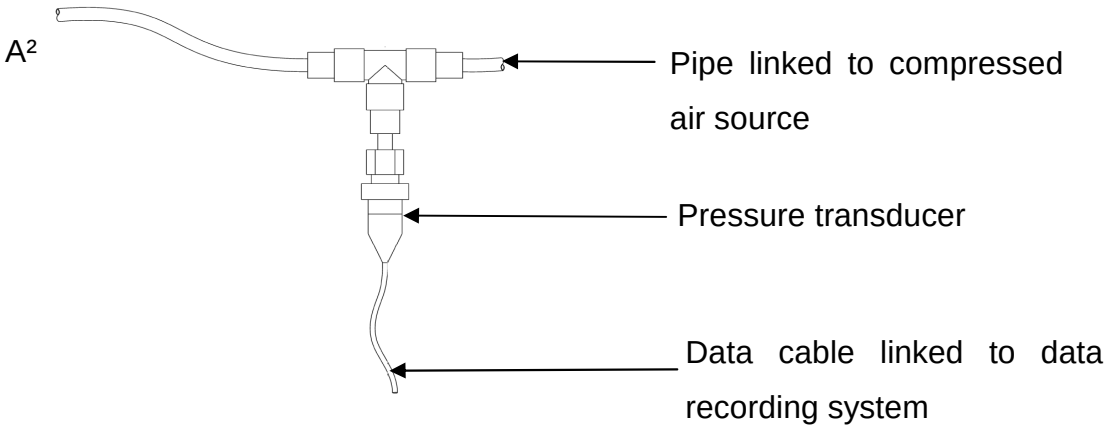

Figure 5.3: Pressure transducer connection

A pressure transducer was connected to the compressed-air line. A gate valve was installed between the pressure transducer and the compressed air source (fig 5.3). The function of the pressure transducer was to measure the change in pressure

versus time. The recording system acted as the power source of the pressure transducer. The data cable of the pressure transducer was connected to the data recording system. Figure 5.3 is a diagrammatic display of the pressure transducer and its connections.

5.3.2 Testing method

The first phase of testing was conducted using compressed air. For each test run, the stemming product to be tested was inserted into the hole in the Norite (Granite) block from the open ended side (figure 5.1, (B)). The stemming products that, according to the instructions, required to be manually secured in the hole were supported from the inside of the hole with a stopping device that prevented the stemming product from entering the hole deeper than required. At the same time, the stopping device, allowed compressed air to pass.

As soon as the stemming product was in the hole at the correct position, the gate valve was opened. The correct position is a third of the blasthole starting at the collar (Brinkman, 1990). The pressure transducer then measured the pressure change inside the pipe. It was assumed that the difference between the pressure in the pipe and the pressure inside the hole was negligible. The data generated by this process was then recorded by the data recording system (explained in section 5.5).

5.4 Experimental testing - Phase two

5.4.1 Experimental setup

Experimental testing for the second phase was conducted in collaboration with AEL (African Explosives Limited). These tests where conducted at Modderfontein in Johannesburg, South Africa.

A purpose built stemming testing device was constructed for the second phase tests. The device was a pressure chamber made from a thick walled steel outlet pipe and reaction chamber. These two components were welded together. A thick

circular support plate was attached to the reaction chamber at the reaction chamber pipe interface (figure 5.4). The support plate ensured a secure connection between the pipe and the reaction chamber. The reaction chamber was also equipped with a safety valve (figure 5.4). A photo of the purpose built stemming testing device is shown in figure 5.5. Six swing-bolts were added to the circumference of the reaction chamber. These bolts kept the door shut during detonation, but allowed access to the reaction chamber during the loading process. An O-ring was placed between the door and the reaction chamber to ensure a tight seal. The door in the closed position and a swing-bolt in the downward position are indicated in figure 5.6. A pressure transducer was attached to the reaction chamber (figure 5.4). The purpose of the pressure transducer was to measure the pressure change in the reaction chamber.

Two detonation contacts were inserted through the outer casing of the reaction chamber and then insulated (figure 5.7). A thick steel plate was placed in position on two slides, attached to the inner walls of the reaction chamber.

A door was fastened to the reaction chamber with a hinge attachment (figure 5.7). Steel legs were welded to the device to ensure stability during detonation. The steel support legs are shown in the figure 5.5. Pressure was generated inside the reaction chamber by detonating ballistite. An electric detonator was attached to the detonation contacts and inserted into the ballistite (figure 5.7). A shot exploder was connected to the outside of the detonator contacts. A photo of the ballistite in the reaction chamber is shown in figure 5.8. Masking tape was used to ensure that the container in which the ballistite is contained was stable before detonation and that the detonator was the middle of the ballistite.

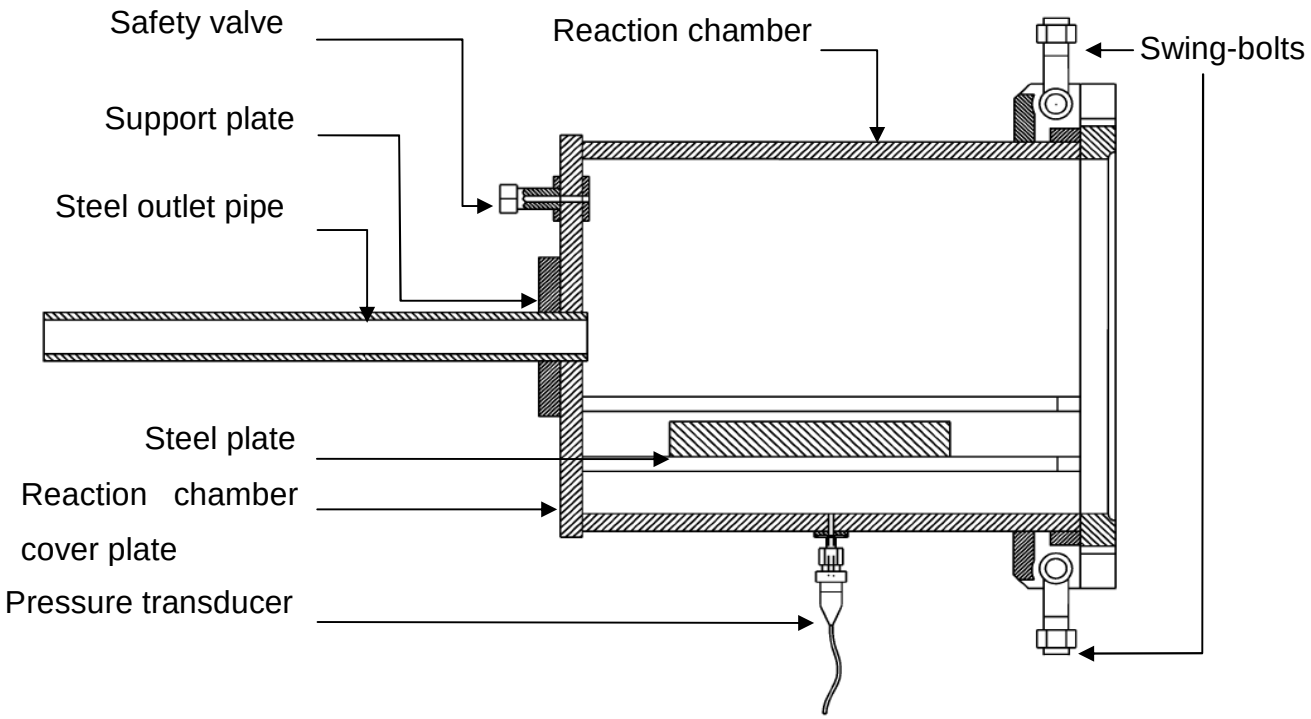

Figure 5.4: Section view of the pressure chamber.

Figure 5.5: Purpose built stemming testing device with support legs.

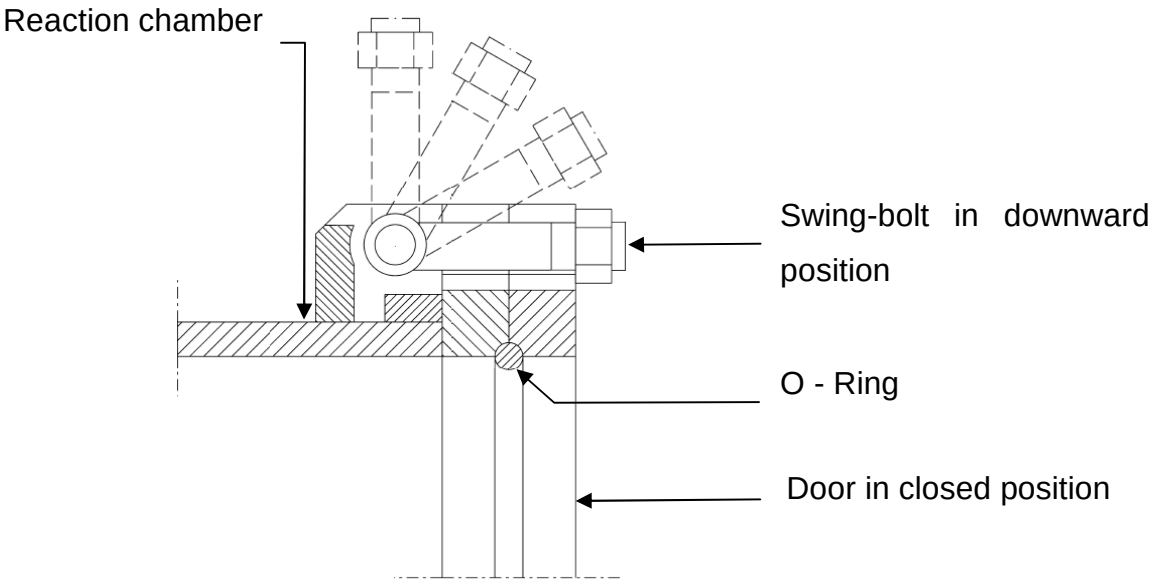

Figure 5.6: Cut out view of the reaction chamber, the door in closed position and one of the swing bolts in the downward position.

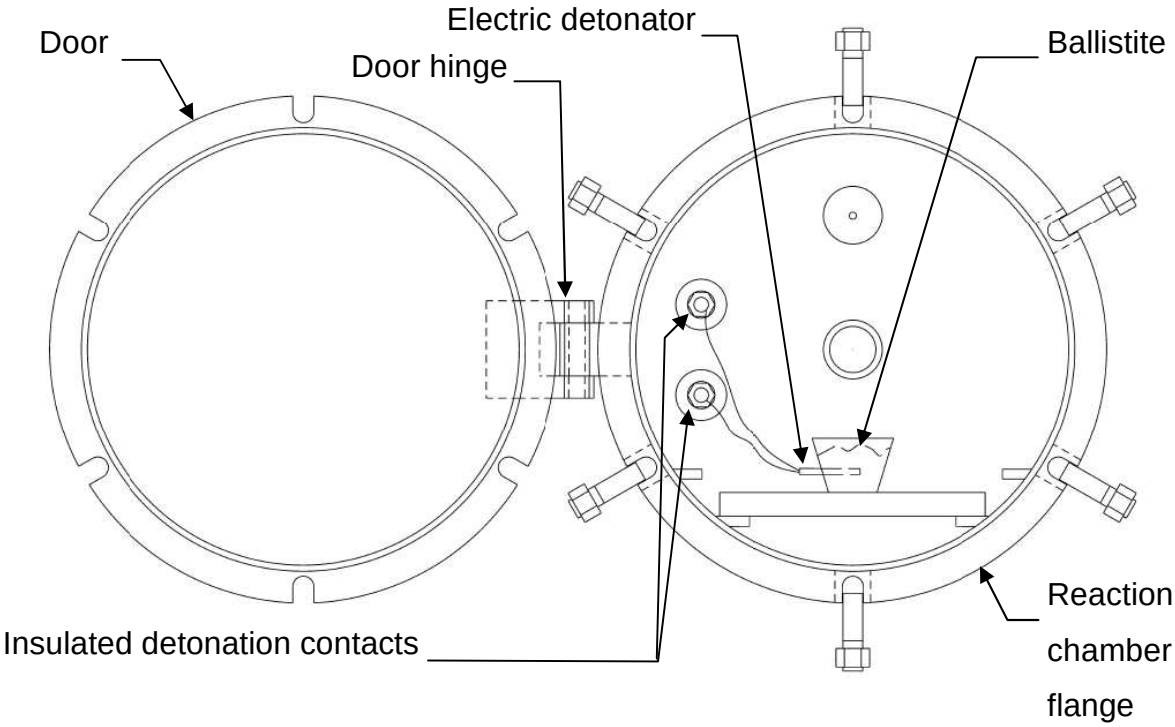

Figure 5.7: Reaction chamber viewed from open end with door in open position.

Figure 5.8: Ballistite in the reaction chamber.

At the end of the steel outlet pipe, a trip switch was added (figure 5.9). The purpose of the trip switch was to determine the exact ejection time. The peak pressure obtained from the transducer was then correlated with the feedback form the trip switch to determine the exact pressure at ejection.

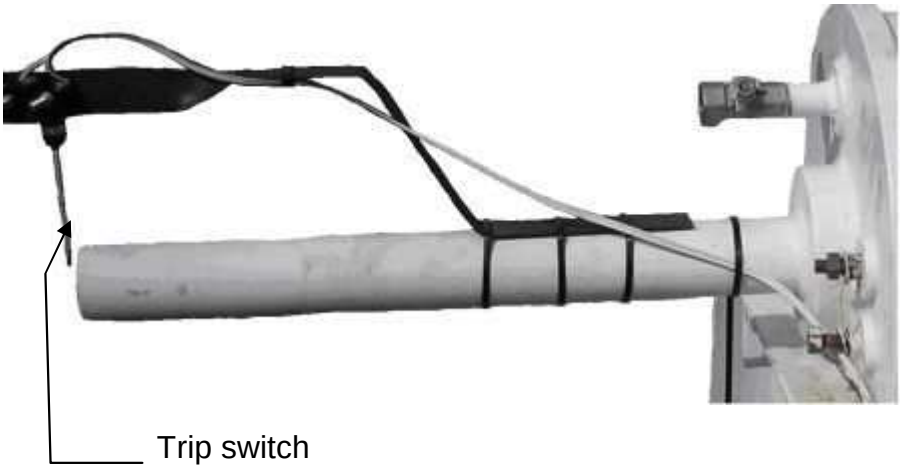

Figure 5.9: Trip switch at the end of the outlet pipe.

5.4.2 Mechanical properties

The reaction chamber is 310mm long with a diameter of 300mm. The enclosed volume of the chamber was 22 litres. The maximum allowable pressures were calculated previously (De la Rey, 2007). The details of the output from the software have been included in Appendix C. The maximum pressures for the main components were as follows:

- Reaction chamber flange = 3000kPa
- Door = 1400kPa
- Reaction chamber cover plate = 4000kPa
- Steel outlet pipe = 11200kPa

5.4.3 Thermo chemical properties

The ambient atmospheric pressure at the test site was 83kPa (South African Weather Service). The test site was situated at an altitude of 1750m and the average temperature was 27ºC (300.15K) (South African Weather Service). The molar volume in the reaction chamber was 30.01 λ/mol and the chamber therefore contained 0.73g-moles of air given that the molecular weight of air at 29 g/mole, the molar quantity of air is equivalent to 21.26 grams.

The molar heat capacity of air at constant pressure (C_p) is 28.42 j/g-mole-K at 300.15K. The variation with temperature (from 27ºC to explosive temperatures) can be presented by the smooth curve (Sonntag et al, 1998), explained by the following equation:

$$C_p = a + bT + cT^2 \qquad \text{Equitation 5.1}$$

Where:

C_p = modular heat capacity at constant pressure(j/g-mole-K)

T = Absolute temperature (K)

a, b & c = constants

For each particular gas the constants a, b and c will be unique. The values for air is a=6.386, b=1.762 and c=-0.2656. These values where obtained by the method of iterations (Sendrei, 2007).

At constant volume and constant pressure the heat capacity can be expressed by the ratio:

$$\frac{C_p}{C_v} = \gamma = 1.4 \qquad \text{Equitation 5.2}$$

Where:

C_v = modular heat capacity at constant volume (j/g-mole-K)

γ = adiabatic exponent

The value of the adiabatic exponent γ of 1.4 is specific to air (Sonntag et al, 1998).

5.4.4 Testing method

As previously discussed, the second phase of testing was conducted using compressed air. For each test run, the stemming product to be tested was inserted into the steel outlet pipe (see figure 5.4) from the open ended side (point (A) figure 5.4). The stemming products that required to be manually secured in the hole were supported from the other side with a purpose made stopping device to prevent the stemming product form entering the hole deeper than required. After the stemming product was in the hole at the correct position, a predetermined amount of ballistite (discussed in a later paragraph) was measured off. The ballistite was poured into a paper container. The paper container was then positioned on the steel plate (figure 5.8). An electric detonator was then inserted into the paper container through the one side (figure 5.8). The two wires of the electric detonator were then connected to the insulated detonator contacts (figure 5.8). The outside of the insulated detonator contacts was connected to lead wires from the shot exploder. The door of the reaction chamber was then closed and the swing-bolts placed in the downward position (figure 5.5). The swing-bolts were then tightened to ensure a secure seal.

The ballistite was then detonated using an electric shot exploder. The pressure transducer measured the pressure change inside the reaction chamber during the detonation process. It was assumed that the pressure distribution in the reaction

chamber was uniform. The data generated by this process was then recorded by the data recording system (explained in section 5.5).

5.4.5 Thermo chemistry of ballistite

Ballistite is a double-base homogeneous propellant. Homogeneous propellants are characterized by the fact that the fuel and the oxidizer belong to the same molecule. Double base propellants are a combination of nitrocellulose (NC) and nitro-glycerine (NG). Nitrocellulose serves as the binder and nitro-glycerine causes it to gel. For the highest specific impulse, the nitro-glycerine content should be about 85%. Since nitro-glycerine is an oily liquid, plasticizers are needed to enhance the mechanical properties.

Ballistite is a quick-burning propellant with a high flame temperature, high energy output and yields no solid residues (Szendrei, 2007). Ballistite was used because of its short burning time and the absence of solid residues. The characteristics of the ballistite that was used in the tests are listed below.

Most ballistite compositions possess similar thermochemical chemical properties, but shapes and dimensions vary. The physical ballistite granules are built up of layers. This is due to the manufacturing process. During detonation, burning proceeds parallel to the layers, so that all surfaces recede parallel to themselves. These layers form the webs of the granular. This allows for the burning time to be estimated. Since the burning process starts from both sides of the web (Szendrei, 2007), the maximum depth of burning until the web has been burnt through is then half of the thickness of the web i.e. 0.0735mm, and the time required for complete burning is 18.4ms. In a loosely packed charge, all grains can be assumed to burn simultaneously (Szendrei, 2007).

There are two sources of pressure inside the reaction chamber:

1 1 The ballistite liberate gases of 0.8 litres per gram. If it is assumed that the stemming product does not move in the first 18.4ms due to the time taken to overcome static friction, the volume of the reaction chamber will stay constant. This would then increase the pressure even in the absence of heating.

2 2. The gases are liberated at a high temperature, while the air was at 27 ºC. After equilibrium between these two temperatures has been reached the resultant mean temperature will be significantly higher than the ambient temperature.

Table 5.1: Properties of the double base propellant ballistite.

Property	Value
Grain diameter	1.23mm
Web thickness	0.147mm
Heat combustion	5192J/g
Adiabatic flame temperature (T_a)	3125K
Gas volume (n)	0.037mol/g
Force (F)	1136J/g
Specific heat ratio	1.215
Bulk density	1620kg/m^3
Burn rate	4 mm/s at 1 MPa

5.4.6 Pressure generation

Burning ballistite propellant was used to generate pressure in the pressure chamber. It is assumed that adiabatic conditions are present and that stemming ejection occurs after all the ballistite has burnt. The peak pressures are calculated as a function of the charge mass. The strength of the vessel determined the maximum charge weight.

It was assumed that the detonation chamber was a ‘closed’ pressure vessel and that the detonation chamber has similar physical properties to closed-vessels used for the measurement of thermo-chemical properties of propellants. The following characteristics of detonation chamber influenced the pressure inside the chamber:

- Low loading density (kg propellant/ litre-volume)
- Contained air has a large influence on the final pressure

- Non-rigidity of the stemming plug in the steel outlet pipe

Calculations were compared for a pressure range from 10 to 1000kPa. The redistribution of combustion energy as the internal energy of the gases in the combustion chamber formed the basis of the calculations.

From experimental observations, it has been established that the behaviour of gasses at low density behaves as an ideal gas. The ideal gas equation of state would therefore, be more than adequate for the calculations. Given the equilibrium temperature T, the peak pressure is (Sonntag et al.,1998):

$$P_{max} = \frac{(n_{bal} + n_{air})RT}{V} \text{ (Pa)} \qquad \text{Equitation 5.3}$$

where:

n_{bal} = molar quantity of gas liberated by the ballistite

n_{air} = molar quantity of the air in the reaction chamber

R = universal gas constant (8.3145 J/mol K)

V = volume of the reaction chamber (m^3)

The peak pressures in the reaction chamber were calculated (Szendrei, 2007) and are listed in table 5.2 according to increasing quantity of ballistite.

The peak pressures indicated in table 5.2 are the maximum pressure of ballistite possible. This is due to the fact that it was assumed that the chemical reaction in the reaction chamber is adiabatic (i.e. no heat loss) and that the stemming plug only starts moving after all the ballistite is completely combusted.

The amount of ballistite used during all the tests was 20g. This was due to the mechanical properties of the critical constraint in the experimental setup. Under ideal conditions an amount of 20g of ballistite could generate a peak pressure of 1330kPa and the maximum pressure that the door of the reaction chamber could handle was calculated to be 1400kPa.

Table 5.2: The calculated peak pressures of ballistite (Szendrei, 2007).

Ballistite (g)	Equilibrium Temp. (K)	Peak pressure (kPa)
1	570	170
2	793	250
3	980	320
4	1140	390
5	1283	460
6	1410	520
8	1622	650
10	1800	770
15	2122	1050
20	2350	1330
30	2653	1870
40	2842	2410
50	2975	2930
60	3070	3460
75	3175	4240
90	3252	5020
120	3349	6580
150	3412	8130
200	3478	10720

5.5 The recording system

The same recording system was used for both phases of the tests. The spider 8 acted as the power source for the pressure transducer. The switch used an independent power source. The output of both the switch and the transducer was fed into the Spider 8 (figure 5.9). The Spider 8 was connected to a personal computer (PC). The data analysis software used for the experiments was Catman express (paragraph 5.6.1).

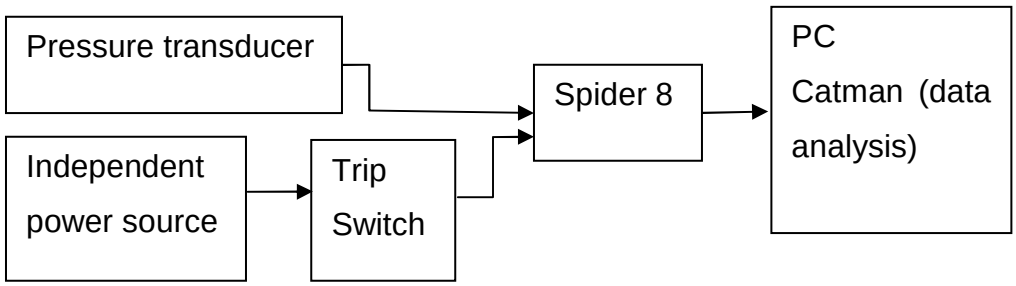

Figure 5.10: Data recording system

Both the Pressure transducer and the switch sent out a weak electric signal to the Spider 8. The Spider 8 is a multi-channel electronic Personal Computer measurement unit for parallel, dynamic measurement data acquisition using a computer. This electric signal was then converted into a digital signal that the Personal Computer recognises and the software then displays this data then either as a graph, or as separate data points. The separate data points were used in the statistical analysis and are discussed in chapter 6.

5.5.1 The pressure transducer

5.5.1.1Internal mechanics

An Absolute Pressure Transducer from HBM (Hottinger Baldwin Messtechnik) was used in this study. This pressure transducer uses a 4-20mA signal and is also known as a pressure transmitter. Since a 4-20mA signal is least affected by electrical noise and resistance in the signal wires, such transducers are best used when a signal must be transmitted long distances.

5.6 The Software package

Catman express software was used to capture the data electronically. The software and licensing was supplied by the University of Pretoria.

5.6.1 The Software structure

Catman Express is a modular program for controlling HBM (Hottinger Baldwin Messtechnik) measuring devices and for acquiring and editing measured values. Figure 5.8 illustrates the basic modules and the command flow of the software.

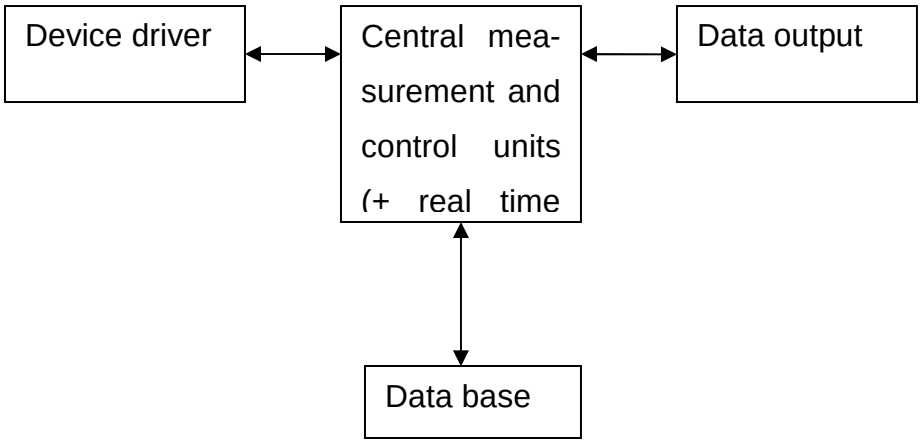

Figure 5.11: The basic Catman modules

5.6.2 Configuration of time channels

When defining a new device, the first line in the I/O channel range is defined as a time channel. The time channel is used as the real time base on the x-axis. The time scale to be used needs to be decided upon, i.e. a scale in either absolute time or relative time. When absolute time is specified, the date and time are read from the PC clock. The precision of this starting value is only as good as the precision of the clock in the PC. However, in contrast to relative time, absolute time is recorded in whole seconds only and does not account for fractions of a second. Furthermore, only one value is retrieved per period. In the event of the triggered measurement, the first value that the device sends is written to instant zero. When relative time is selected, the time resolution can be set in milliseconds, seconds, minutes or hours.

5.6.3 Connections and measurements

The spider uses a 12V supply voltage and it needs a universal power pack for voltages from 110V through 240V. The Spider 8 has a separate analogue to digital converter for each channel and provides synchronous data acquisition without multiplexers or sample-and-hold stages. Sampling rates of up to 9600 values per second can be measured. This capability presents itself ideal for a measurement procedure that must take place in a tenth of a second, which is the case under blasting conditions. The Spider 8 also has the capability to eliminate noise effects from the data by using anti-alias pre-filters as well as programmable

6 DATA ANALYSIS – LOW PRESSURE TESTS

6.1 Introduction

Experiments were conducted with different stemming materials over a course of time. Different stemming materials were analysed for their ability to resist air pressure. To begin with, the stemming selection procedure is discussed. This is followed by an analysis of the characteristics of a “good” stemming material. The test results of the different stemming materials were analysed individually and sorted into categories of similar performance based on the characteristics of a “good” stemming material. The pressure test results for each of the products were also statistically analysed and are presented here at the end of each section.

6.2 Stemming selection

Various generic stemming products where selected for the testing. A telephonic survey was conducted whereby amongst underground hard rock mines in South Africa, utilizing small diameter blast holes. For each mine the individual responsible for the material store was questioned. The following were determined:

- If stemming was a stock item on the materials bill of the mine;
- If stemming was indeed a stock item then the type of stemming was determined and;
- the supplier’s details for the stemming material were also obtained.

The sample included 16 mining houses. It was found that of the 6 most commonly used stemming products are homogeneous gravel capsules, homogeneous clay capsules, Polyutherane foam, heterogeneous gravel capsules and mechanical plugs. The percentage usage distribution of each is displayed in figure 6.1. An example of each of these 6 generic stemming products were chosen for the experimental testing.

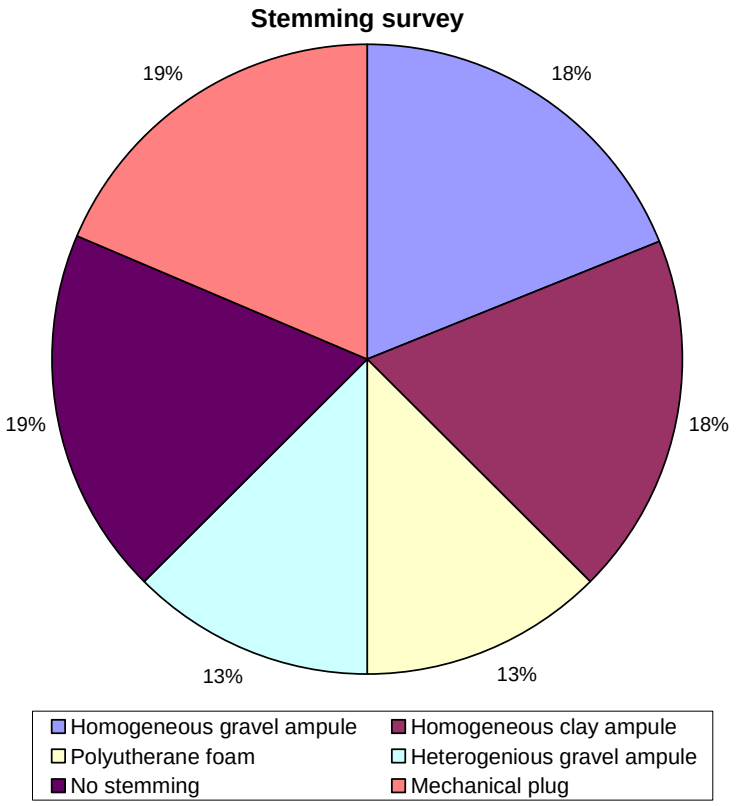

Figure 6.1: The percentage distribution of the stemming products being used by 16 different mining houses in South Africa.

The commodities mined by these mining houses included gold, silver, uranium, antimony, chrome and platinum group elements. The products were assigned to different alphabetical letters section 6.3 below.

6.3 Characteristics of good stemming.

The time pressure curve of a stemming product describes the stemming product's ability to maintain a pressure inside the blasthole. The time required to reach this maximum pressure indicates the products ability to deform the shape of the hole. The products ability to deform can be directly linked to the static friction that the product experiences in the hole. The more effectively and the quicker a product can deform to adapt to the shape of the hole, the quicker the largest possible area can be in touch with the sidewalls of the hole. It can therefore be said that a short

rise time would then be the ideal to obtain optimum pressure rise in the blast hole. The rise time versus the pressure of ideal to not-so-ideal products has been indicated in the time versus pressure curve (figure 6.2). A time versus pressure curve would practically describe the ability of the stemming product to act as an effective seal.

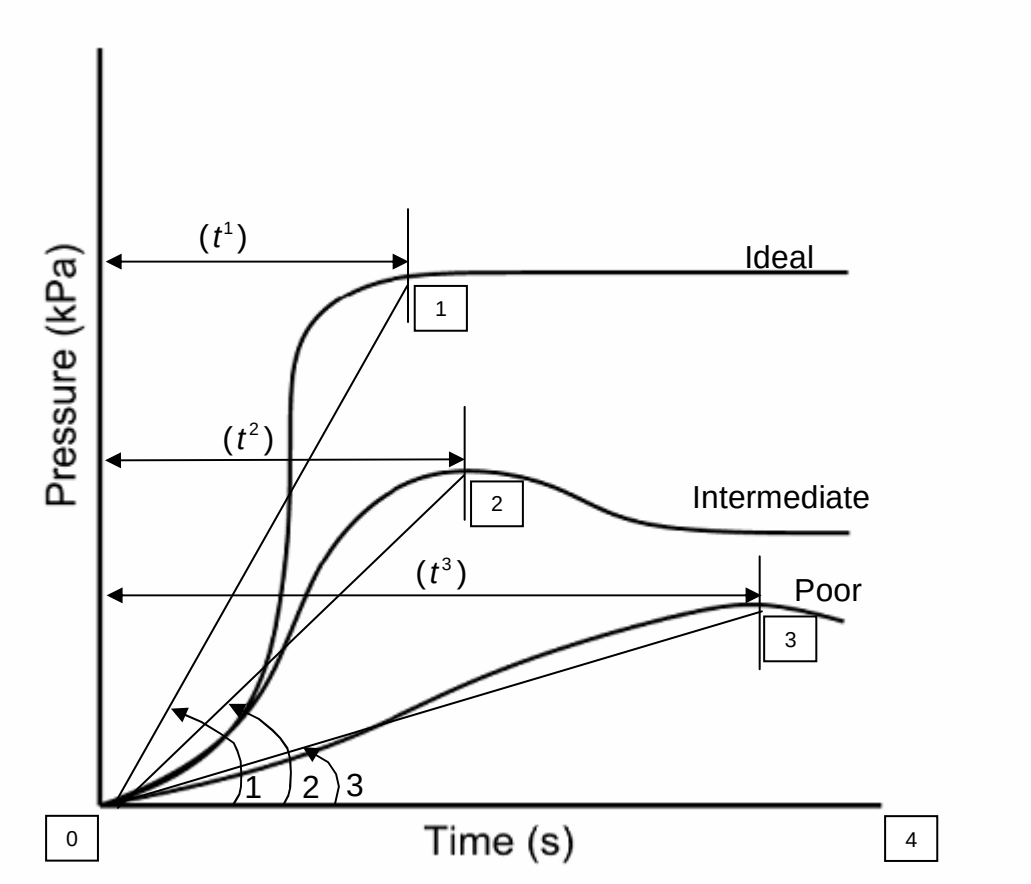

Figure 6.2: Time versus pressure curve

t^1: Rise time for ideal stemming

t^2: Rise time for intermediate stemming

t^3: Rise time for poor stemming

The times indicated on the graph as t^1, t^2 and t^3 are the rise time of and ideal, intermediate and poor stemming respectively. The time t^1 indicates the rise time of an ideal stemming material. The angle between the lines 0-1 and 0-4 indicates the

time-pressure ratio of an ideal stemming material. On the other hand a poor stemming material (t^3) would take a much longer time to reach maximum pressure. The maximum pressure is also much lower than that of the ideal stemming material. An ideal stemming material can then be described as a stemming material that requires the shortest possible rise time to reach the maximum possible pressure.

The more friction in the blasthole, the more likely it is for the graph to approach ideal behaviour as depicted by the line 0-1 in figure 6.2. If there is less friction the pressure over time should approach less ideal condition. As explained in chapter 4, the resistance at this point is called limiting friction.

The pressure force relationship of ideal stemming in figure 6.2 can be explained by a force analysis as follows. The pressure build up in the blasthole can be divided into two phases:

The first is between point 0 and point 1. Here the following applies:

Force exerted by air pressure in blasthole < resistive force from stemming

$$\frac{P}{A} < \mu_{max} R \qquad \text{Equation 6.1}$$

The second is at point 1 as well as after point 1 the following applies:

Pressure in blasthole = resistive force from stemming

$$\frac{P}{A} = \mu_{max} R \qquad \text{Equation 6.2}$$

The pressure-force relationship of intermediate stemming as in figure 6.2 can be explained by a force analysis as follow. The pressure build up in the blasthole can be divided into three phases:

The first is between point 0 and point 2 (figure 6.2). Here the following applies:

Force exerted by air pressure in blasthole < resistive force from stemming

$$\frac{P}{A} < \mu_{max} R \qquad \text{Equation 6.3}$$

The second is at point 2 here the following applies:

Pressure in blasthole = resistive force from stemming

$$\frac{P}{A} = \mu_{max} R \qquad \text{Equation 6.4}$$

The third phase is after point 2 and here the following applies:

Pressure in blasthole > resistive force from stemming

$$\frac{P}{A} > \mu_{max} R \qquad \text{Equation 6.5}$$

The pressure-force of the poor stemming as in figure 6.2 can be explained by a force analysis as follows: The pressure build up in the blasthole only consists of one phase:

From point 0 till the end of the time window (i.e. point 4) the following relationship applies:

Pressure in blasthole > resistive force from stemming

$$\frac{P}{A} > \mu_{max} R \qquad \text{Equation 6.6}$$

6.4 Data correction

Two corrections were applied to the data. Firstly, the starting times of all the test runs did not correlate with each other. The starting times were altered to coincide with one another.

The second correction that was applied to the data was necessary to account for the differences in system pressure. The compressed air system used in this experiment used a pressure vessel that is pumped to a high pressure with a piston

air pump. When air is drawn for the first run the pressure is high (up to 600kPa). For each consecutive test run thereafter, the system pressure will be lower until the pressure drops too low (below 300 kPa). The pump then automatically starts again and pumps the vessel to a high pressure.

To allow for these changes in system pressure, the pressure readings were adapted with a constant value equal to the difference between the mean and that particular test run. The mean value that was used is the pressure of the system after equilibrium has been reached.

6.5 Product A

6.5.1 Product description

This particular product is made up of fine (<0.05mm) clay particles are held together in a cylindrical plastic pouch. The product is manufactured by Minova, South Africa is shown in figure 6.3

6.5.2 Prescribed use

The stemming capsule is to be soaked in clean water for about 10min before insertion. The stemming capsule is then inserted into the hole by hand. Only one capsule is to be inserted per hole. After the stemming capsule pouch is inserted by hand, a loading or charging stick is used to secure the plug as tight as possible. This procedure was followed at all times during the testing procedure.

Figure 6.3: Photo of clay stemming capsule.

6.5.3 Pressure test results

The pressure test results are indicated in figure 6.4. The figure clearly shows that the tests results can be divided into two distinct categories. The first category is the group of test runs that produced an almost vertical rise to the maximum pressure and then held the pressure until the ten seconds testing period was over. During these test runs the stemming capsule was not blown out the hole but managed to maintain the pressure throughout. The maximum pressure that the product held was 332 kPa.

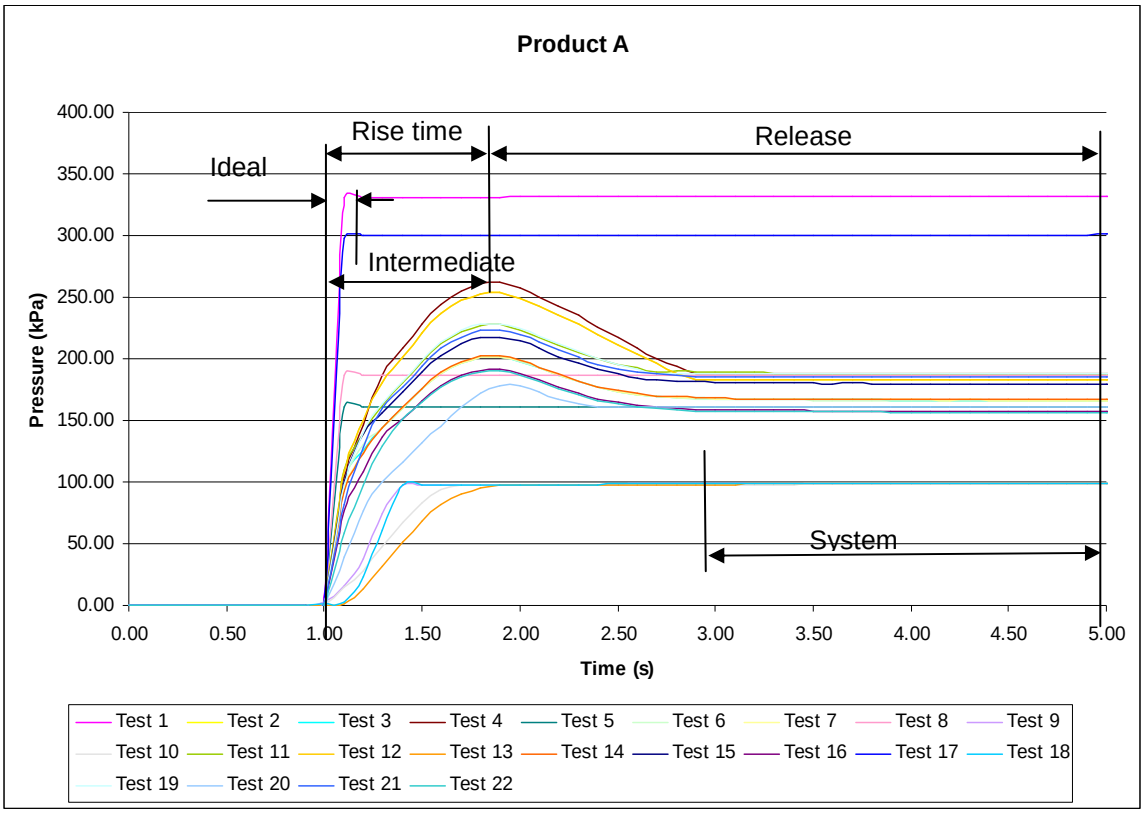

Figure 6.4: Results from pressure tests from product A.

The second distinct category that could be identified was the test runs that had a medium pressure build up followed by ejection. This category includes those test runs that had a slow build up in pressure, reached a maximum and then exhibited a sudden drop in pressure due to the system pressure. Test run 7 of this category was used as an introductory discussion tool in the next section.

6.5.4 Method of analysis

During the physical testing, these test runs behave significantly different to the rest of the test runs. The stemming capsules deformed causing the normal force perpendicular to the sidewalls to increase. This increase in normal force resulted in an increase in friction against the sidewalls of the hole. This increase continued until the force caused by the pressure overcame the frictional force opposing the movement. As soon as this point is reached the stemming capsule starts to move. This movement caused an increase in the volume of the hole. This behaviour is in line with Boyle's law. According to the Boyle gas law: $P \propto \frac{T}{V}$, if T is constant then $P \propto \frac{1}{V}$. This means that if the volume in a closed pressure vessel increases a pressure drop can be expected and visa versa.

Boyle's gas law can be used to investigate the rate of stemming ejection of any particular test run. The data collected during test run 7 of product A will be used to investigate the behaviour of the air in the blasthole.

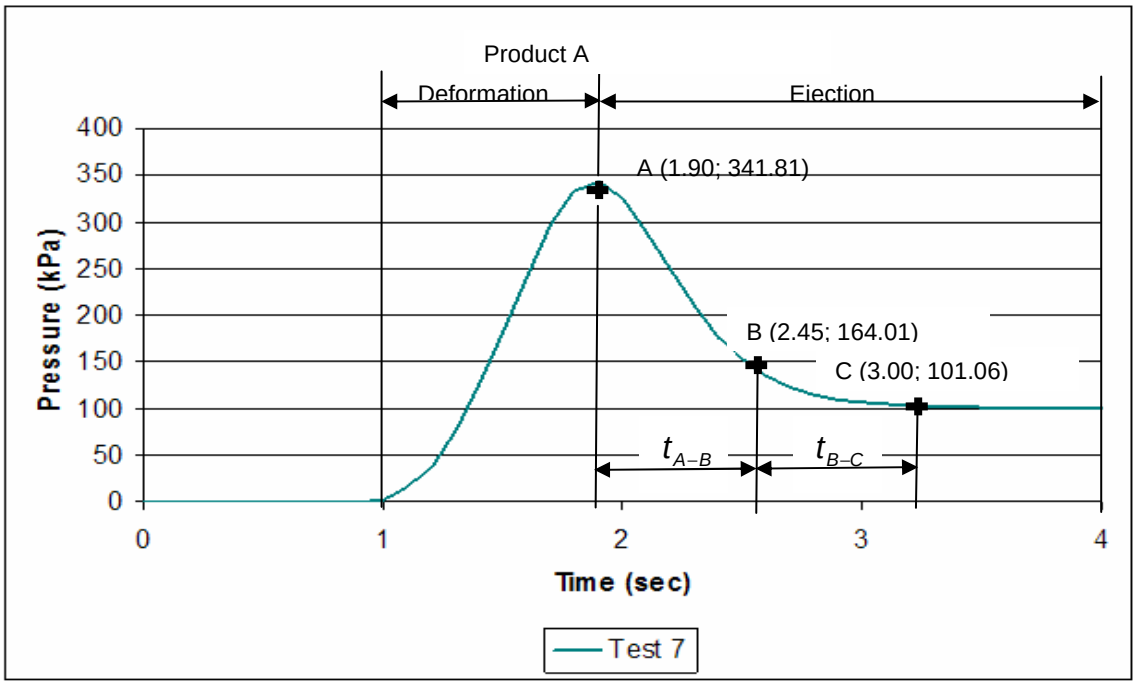

Figure 6.5: Test run 7 of Product B

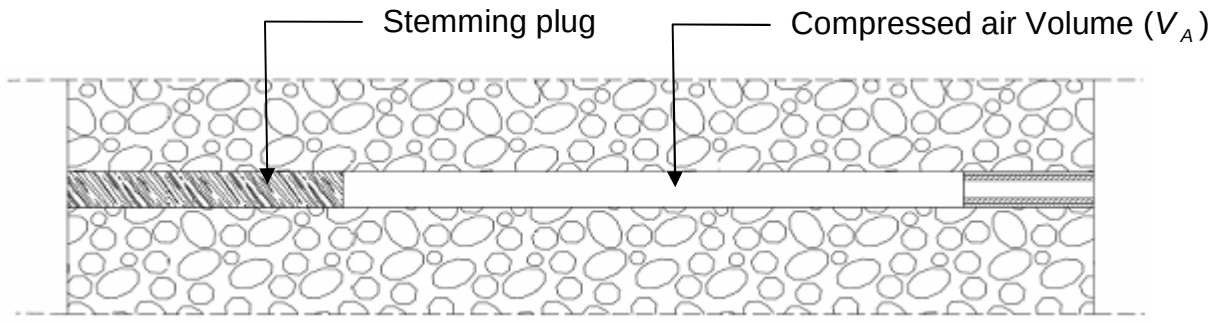

Figure 6.6: Stemming plug just before movement (position A in figure 6.5)

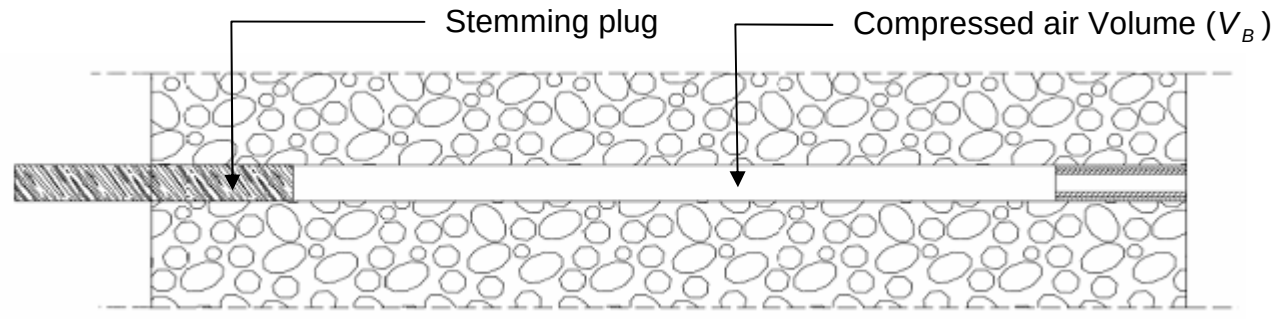

Figure 6.7: Stemming plug in the middle of the ejection phase (position B in figure 6.5)

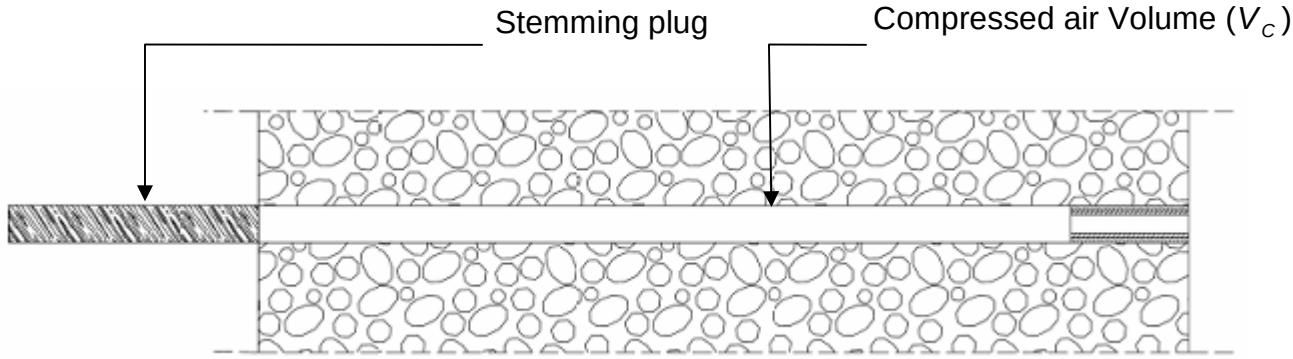

Figure 6.8: Stemming plug just before leaving the blasthole (position C in figure 6.5)

In figure 6.5 $t_{A-B} = t_{B-C}$. If it as assumed that the volume of compressed air in the blasthole only starts to change as soon as the projectile (i.e. the stemming

capsule) starts to eject at which point, point A in figure 6.5 indicates the start of the change in volume.

A section of the Norite (granite) block that includes the blasthole, has been shown in the figures below. Position A, B and C in figure 6.5 above is depicted in figure 6.6, 7 and 8 respectively.

If ejection only starts at point A in figure 6.5 then it can be assumed that any significant changes in the volume of the gas(air) in the blasthole occurs when the projectile (stemming product) starts moving out the hole. The initial volume would therefore be at point A. The final volume would then be the volume at the position where the stemming product is just about to leave the hole. It needs to be determined whether the conditions in the blasthole follow Boyle's gas law. Boyle's law is expressed by the following mathematical equation:

$P_i V_i = P_f V_f$

where:

P_i = Initial Pressure (kPa)

V_i = Initial Volume(m^3)

P_f = Final Pressure (kPa)

V_f = Final Volume (m^3)

The initial and the final pressures can be read off the graph in figure 6.5 above. The initial and final volumes can then be calculated. If it is assumed that the volume of air in the pipe between the transducer and the end of the steel tube in the hole (figure 5.2) stays constant, then the initial volume of air in the blasthole can be taken as:

$$V_i = \frac{\pi d^2}{4} \times (\lambda_{blasthole} - \lambda_{eject}) \qquad \text{Equation 6.7}$$

where:

ΔV = change in volume of the blast hole (m^3)

d = diameter of the blasthole (m)

$\lambda_{blasthole}$ = the length of the blasthole in the Norite block minus the length of the steel tube in the hole (m)

λ_{eject} = the length of stemming that has been ejected (m)

$$V_i = \frac{\pi 0.034^2}{4} \times (0.7 - 0.225) = 404.0 \times 10^{-6} m^3$$

and:

$$V_f = \frac{\pi d^2}{4} \times (\lambda_{blasthole})$$

$$V_f = \frac{\pi 0.034^2}{4} \times (0.7) = 634.5 \times 10^{-6} m^3$$

The validity of the equation can now be tested. The value of the initial pressure and the final pressure can be read of the graph in figure 6.5.

With $P_i = 341.81 kPa$ and $P_f = 101.06 kPa$,

$P_i \times V_i = 341.81 \times 404 \times 10^{-6} = 138.1 \times 10^{-3}$ kJ

Where $P_f \times V_f = 101.06 \times 634.5 \times 10^{-6} = 64.1 \times 10^{-3}$.kJ It is clear that $P_i \times V_i > P_f \times V_f$ and the system is therefore non ideal. This may be due to two factors:

Firstly at very low density, all gases approach ideal-gas behaviour, with the P-v-T relationship being given by the ideal-gas equation of state, however it must be noted that this law is only approximately true. To overcome this, the concept of the compressibility factor, Z is utilized. The compressibility factor was discussed in chapter 4 and is repeated here:

$$PV = ZnRT \qquad \text{Equation 6.8}$$

where

Z = compressibility factor

n = number of moles

R = gas constant (8.314 J/ mol K)

For an ideal gas, Z=1, and the deviation of Z from unity is a measure of the deviation of the actual relation from the ideal-gas equation of state. The precise nature of the behaviour of the intermolecular forces is complex. The qualitative nature of the compressibility factor diagrams of Oxygen, Nitrogen and Carbon dioxide are all different. It would therefore by highly complex to determine the compressibility factor of air accurately. This can be solved by introducing the concept of Reduced pressure and Reduced temperature. Whereby one reduces the properties with respect to the values at the critical point. The critical point is the pressure and temperature where this substance is a gas, liquid and a solid at the same time.

The second possible contributing factor is the presence of frictional forces in the blasthole.

The pressure versus volume graph can be drawn using the values above.
With:

$V_i = V_A = 404.0 \times 10^{-6} m^3$ (figure 6.11)

$V_f = V_C = 634.5 \times 10^{-6} m^3$ (figure 6.13)

And $V_B = \frac{V_A + V_C}{2} = 519.25 \times 10^{-6} m^3$

The pressure-volume relationship can now be graphically represented. To be able to determine the relationship between pressure and volume, it is vital to establish if there was a change in volume and exactly when the change started and the exact time it ended. Hence, it is vital to know if the stemming product moved, when it started moving and at what time it left the hole (figure 6.6 and 6.8).

6.5.5 Discussion and analysis

The individual test runs can now be divided into three categories as discussed before.

Category 1: During a number of test runs (8 of the 22) the stemming product was not ejected. This indicates that there was no volume change or pressure change that occurred during the test run. It also indicates that the static frictional force was larger than the maximum force that was applied to the product, as a result of the air pressure in the blasthole. The pressure volume relationship of each category has been investigated later in this chapter. Mathematically the relationship between the frictional force and the force as a result of the pressure can be expressed as:

$F_{compressed-air} < F_{friction}$

With

$F_{compressed-air}$ = force applied to the capsule as a result of the air pressure

$F_{friction}$ = resistive force that the stemming capsule experiences just before movement, due to static friction

using Boyle's law, the pressure volume relationship is represented by:

$P_i V_i = P_f V_f$ but with $\Delta P = \Delta V = 0$

A statistical analysis was done in order to determine the distribution of the pressures. The tests produced a inconsistent results and it was therefore necessary to determine the 95% confidence interval of the arithmetic mean. The standard deviation as well as the confidence about the mean for each category was also determined. Figure 6.9 indicates the statistical parameters for category 1.

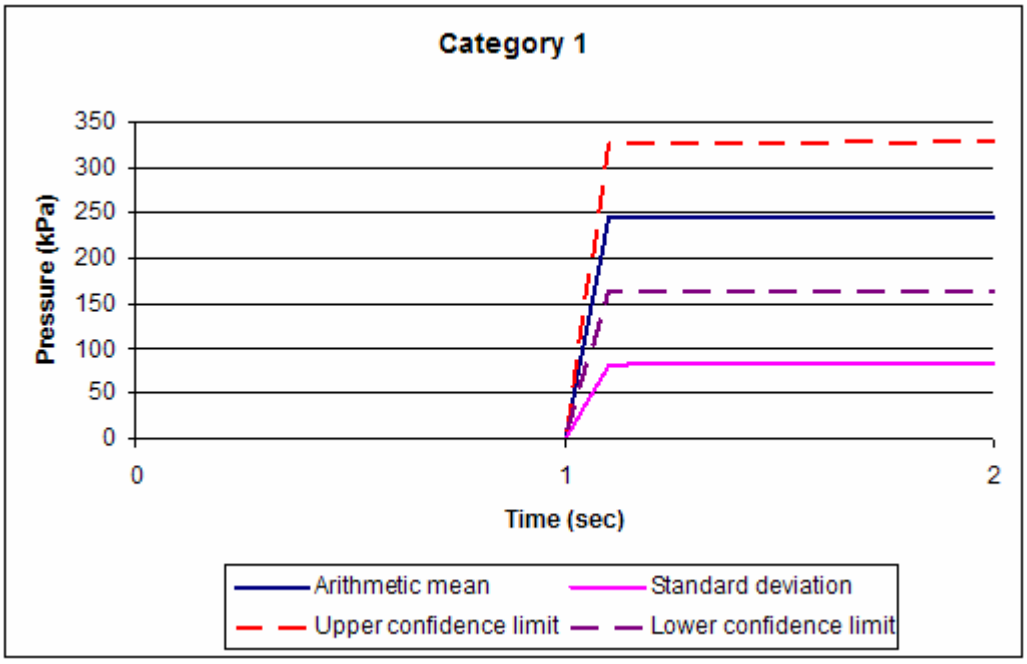

Figure 6.9: The statistical parameters of the first category of the tests with product A.

The statistical parameters in figure 6.9 give no indication of the performance of the stemming material. The data used to calculate these statistical parameters consisted of the data from the tests runs where the stemming withheld the pressure of the system (i.e. 8 of the 22 test runs). Hence, these statistical parameters merely describe the variance of the arithmetic mean of the system pressure.

Category 2: During fourteen test runs, the stemming capsule did not eject immediately. A pressure build-up of between 30 and 60 seconds occurred. During the pressure build up, the stemming capsule deformed. This observed deformation increased the static frictional coefficient and therefore the initial frictional force. As the pressure increased in the blasthole the force on the stemming capsule increased. Mathematically this can be expressed as:

$$F_{compressed-air} < F_{friction} \text{ with } \Delta F_{friction} \uparrow$$

Then a point is reached where the frictional force has reached its maximum:

$$F_{compressed-air} = F_{friction} \text{ with } \Delta F_{friction} = 0$$

This is followed by a phase where the frictional force was overcame by the force, due to the air pressure in the blasthole and then ejection of the stemming capsule occurred. This can be mathematically represented as follows:

$$F_{compressed-air} > F_{friction} \text{ with } \Delta F_{friction} \downarrow$$

The statistical parameters of the third category of the clay tamping in figure 6.10 describes the properties of the data accurately. The influence of the deviation of the system pressure has been eliminated as described in paragraph 6.2.3. The standard deviation in figure 6.10 approaches a classic bell shape distribution between seconds 1 and 3. There is a clear difference between the positions of the maximum deviation in figure 6.10 when compared to figure 6.9. This could indicate that deformation plays a big role in the friction against the sidewalls of the hole. In the test runs analysed in figure 6.9 the stemming capsule ejected from the blasthole without deformation. However, the test runs analysed in figure 6.10 experienced substantial deformation. The inconsistency in the measured pressures between consecutive runs where the stemming capsule has been deformed, could be as a result of the inconsistency in the factors that influenced the deformation. There are a variety of factors that influences the deformation process in the blasthole. This explains the large difference between the upper and lower confidence limits in the figure. These factors are discussed later in this chapter. A maximum deviation of 135.6 kPa was recorded at 1.9 seconds from t=0.

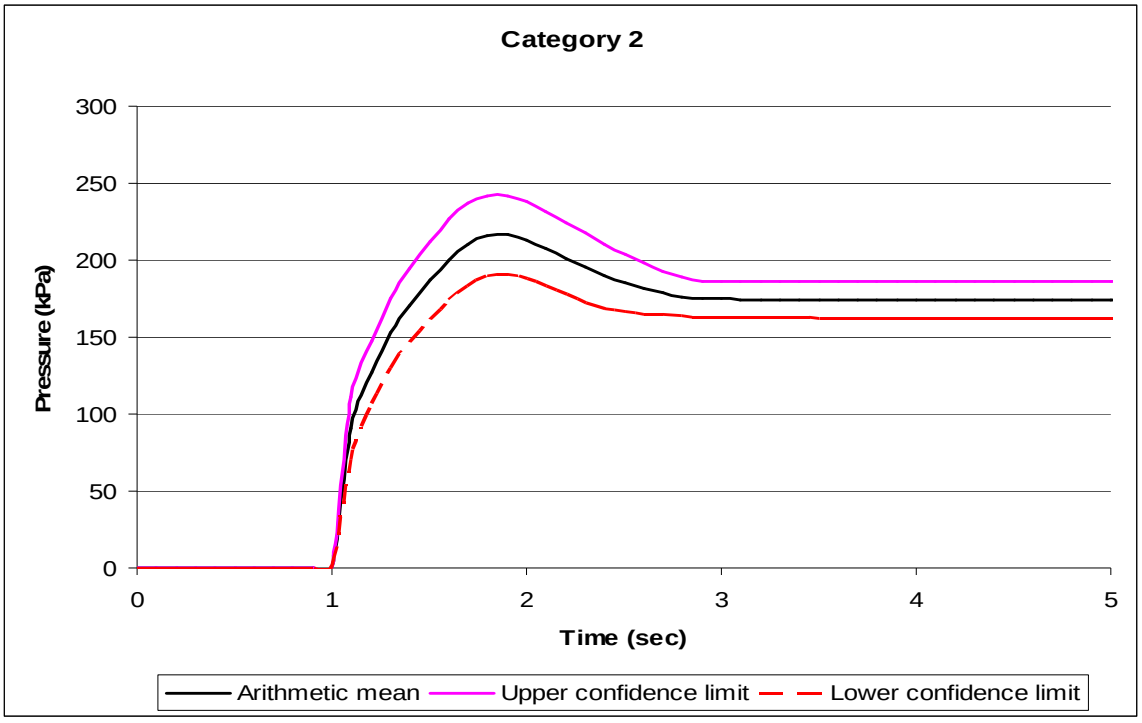

Figure 6.10: The statistical parameters of the 3rd category of tests with Product A.

The pressure-volume relationship was investigated for the test runs for all three categories. A clear difference between the three categories was identified and is indicated in figure 6.11. Category one is represented by single points ( ) in figure 6.11. The pressure-volume relationship determined for category two is represented by red and green horizontal lines in figure 6.11. The lines indicate a constant pressure during the time that the volume is changing. The behaviour of the relationship between the pressure and the volume for sub-category three approaches that of an ideal gas.

The pressure volume relationship in figure 6.11 indicates a clear distinction between the different test runs. These differences can be due to one or a combination of the following factors:

- inhomogeneous moisture content
- human error during the insertion procedure
- in homogeneity of the contents (clay) of the product

The third possible factor is a factor that can not be accounted for in the design of the product as this is part of the prescribed procedure for the use of this product. However, the first two factors can be altered and its contribution to its deviation reduced.

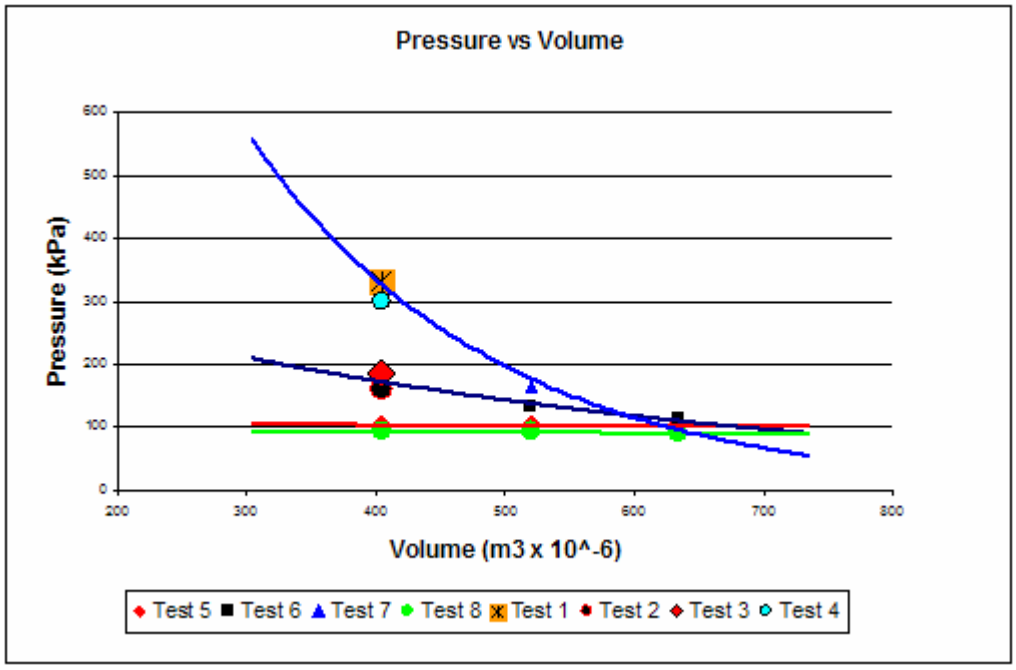

Figure 6.11: Pressure versus Volume for all the test runs.

6.5.6 Performance evaluation

It is difficult to determine a consistent trend on the performance of this product. The possible reasons for this observed inconsistent performance have been discussed. The design of the clay stemming capsule basically uses the same scientific laws as the coarse gravel stemming. One mayor difference can be observed between the two stemming materials: the gravel stemming capsule is inserted while still inside the plastic pouch while the clay stemming capsule is removed from its pouch and then inserted into the hole.

The pouch restricts the deformation of the gravel stemming but increases the coefficient of friction between the capsule and the insides of the hole. The opposite is true for the clay stemming capsule.

The maximum pressure that the stemming capsule can take is determined by the value of the force applied to the stemming at the point just before movement. The maximum force was achieved in the 1st test run and was 332MN. The lowest was achieved in the 8th test run and is 104MN. The interval of the mean at 95% confidence, at the time of maximum pressure, was $u = 294MN$ and $l = 106MN$.

6.6 Product B

6.6.1 Product description

This particular product is made up of coarse (0.5mm –1mm) soil grains with different shapes. These soil grains are held together in a cylindrical plastic pouch. The product is manufactured by Bintex, South Africa.

6.6.2 Prescribed use

The stemming capsule is to be soaked in clean water for about 10minutes before insertion. The stemming capsule is then inserted into the hole by hand. After each stemming capsule pouch is inserted by hand, a loading or charging stick is used to secure the plug as tight as possible. This procedure is then repeated until the remainder of the blasthole is filled with stemming capsule. The charge stick causes deterioration of the pouch and better contact between the hole and the stemming.

Figure 6.12: Course gravel stemming capsule.

6.6.3 Pressure test results

The pressure tests were performed on this specific product, using the experimental setup discussed in chapter 5.2. The data represented graphically in Figure 6.13 below has been adjusted in an effort to eliminate starting time differences.

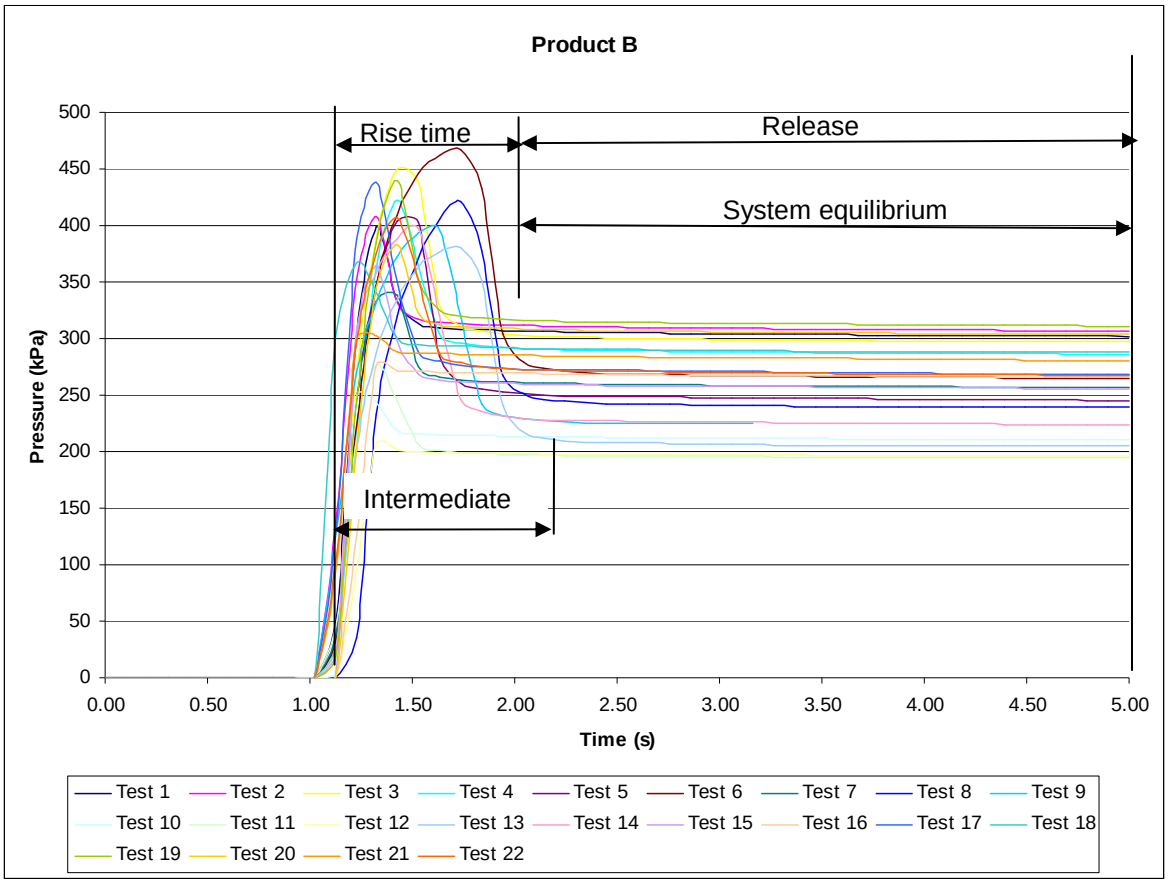

Figure 6.13: The pressure change over time for all the tests

To allow for changes in system pressure the pressure readings were adapted with a constant value equal to the difference between the mean and that particular test run as for product A. The mean value that was used is the pressure of the system after equilibrium was calculated. This system equilibrium is indicated in figure 6.13

6.6.4 Method of analysis

Boyle's gas law was also used to investigate the rate of stemming ejection of the test runs from product B. The data collected during test one of the test runs form product B have been used to investigate the behaviour of the air in the blast chamber.

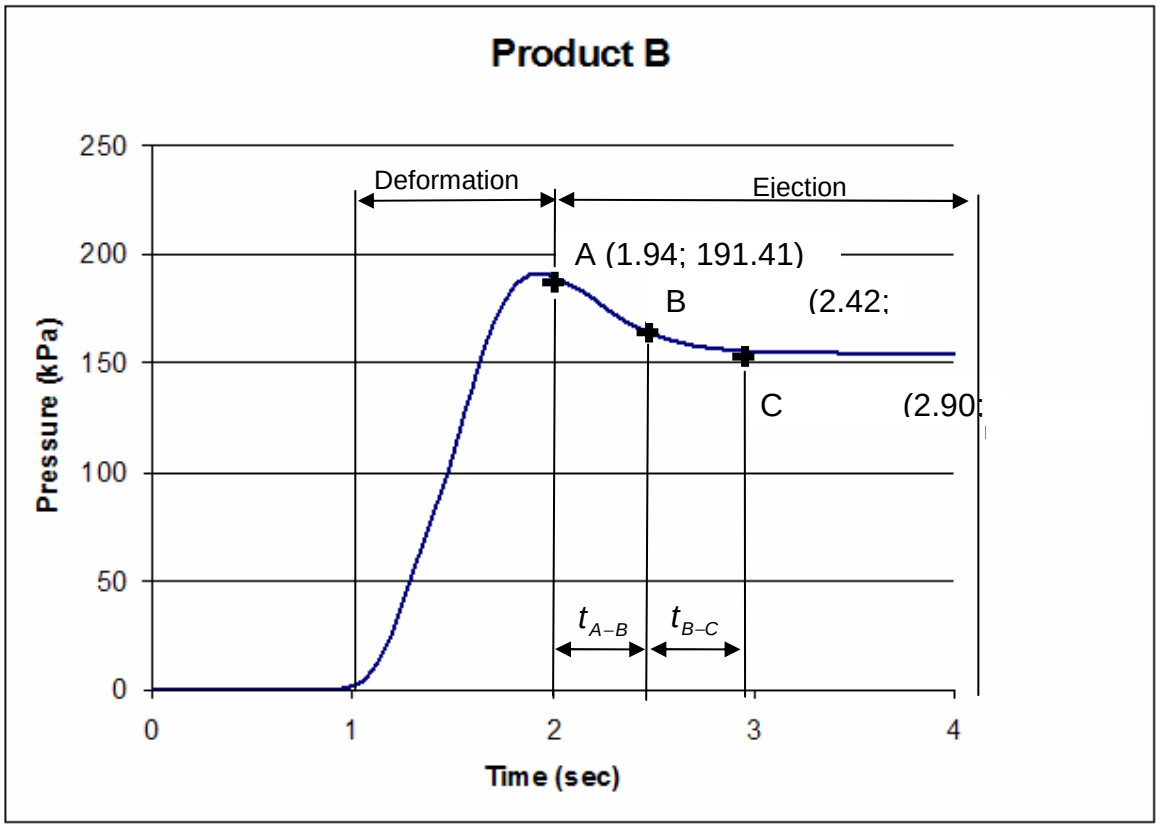

Figure 6.14: Test run 10 of Product B

The same logic used for product A was used for product B. In figure 6.14 above $t_{A-B} = t_{B-C}$. If it as assumed that the volume of compressed air in the blasthole only starts to change as soon as the projectile (i.e. the stemming capsule) starts to eject then point A in figure 6.14 indicates the start of the change in volume.

Similarly to the assumptions made for product A, it was assumed that any significant changes in the volume of the gas (air) in the blasthole occurs when the projectile (stemming product) starts moving out the hole. It needs to be determined whether the conditions in the blasthole follow Boyle's gas law. Boyle's law is expressed by the following mathematical equation:

The initial and final volume would be the same as for product A with:

$$V_i = 404.0 \times 10^{-6} m^3$$

and:

$$V_f = 634.5 \times 10^{-6} m^3$$

The validity of the equation can now be tested. The value of the initial pressure and the final pressure can be read off the graph in figure 6.14.

With $P_i = 191.41 kPa$ and $P_f = 166.66 kPa$, $P_i \times V_i = 191.41 \times 404 \times 10^{-6} = 77.3 \times 10^{-3}$

Where $P_f \times V_f = 166.66 \times 634.5 \times 10^{-6} = 105.7 \times 10^{-3}$. It is clear that $P_i \times V_i < P_f \times V_f$ and the system is therefore, non ideal. The relationship observed here is reversed from that of product A. Boyle's law does therefore not apply to product B. The behaviour of the product during deformation is the one factor that could have the largest impact on the friction forces that the product experience during deformation.

6.6.5 Discussion and analysis

The pressure versus volume graph can be mapped using the values above.
With:

$V_i = V_A = 404.0 \times 10^{-6} m^3$ (figure 6.6)

$V_f = V_C = 634.5 \times 10^{-6} m^3$ (figure 6.7)

And $V_B = \frac{V_A + V_C}{2} = 519.25 \times 10^{-6} m^3$

The pressure-volume relationship can now be graphically represented. The pressure-volume relationship can only be determined if there was a change in volume or a change in pressure over time. Hence, it is important to know if the stemming product moved, when it started moving and at what time it left the hole (figure 6.6 and 6.8).

The test runs can now be separated into groups that produced similar results. In this case only one category were distinguished.
Category 1: In all of the test runs stemming ejection did not occur immediately. A pressure-build up of between 60 and 90 seconds occurred. During this pressure build up stemming deformation occurred. The static frictional coefficient increased during the deformation. This caused the frictional force exerted on the stemming capsule to increase proportionally. The increase in pressure caused the force due to pressure on the stemming capsule to increase. Mathematically this can be expressed as:

$F_{compressed-air} < F_{friction}$ with $\Delta F_{friction} \uparrow$ (Phase A –figure 6.5)

Then a point is reached where the frictional force has reached its maximum. This is where the system equilibrium is reached:

$F_{compressed-air} = F_{friction}$ with $\Delta F_{friction} = 0$ (The point between Phase A and B –figure 6.5)

Immediately after the above equilibrium was reached the frictional force was overcome by the force due to the air pressure in the blasthole and then ejection of the stemming capsule occurred. Mathematically it can be expressed as:

$$F_{compressed-air} > F_{friction} \text{ with } \Delta F_{friction} \downarrow \text{ (Phase B –figure 6.5)}$$

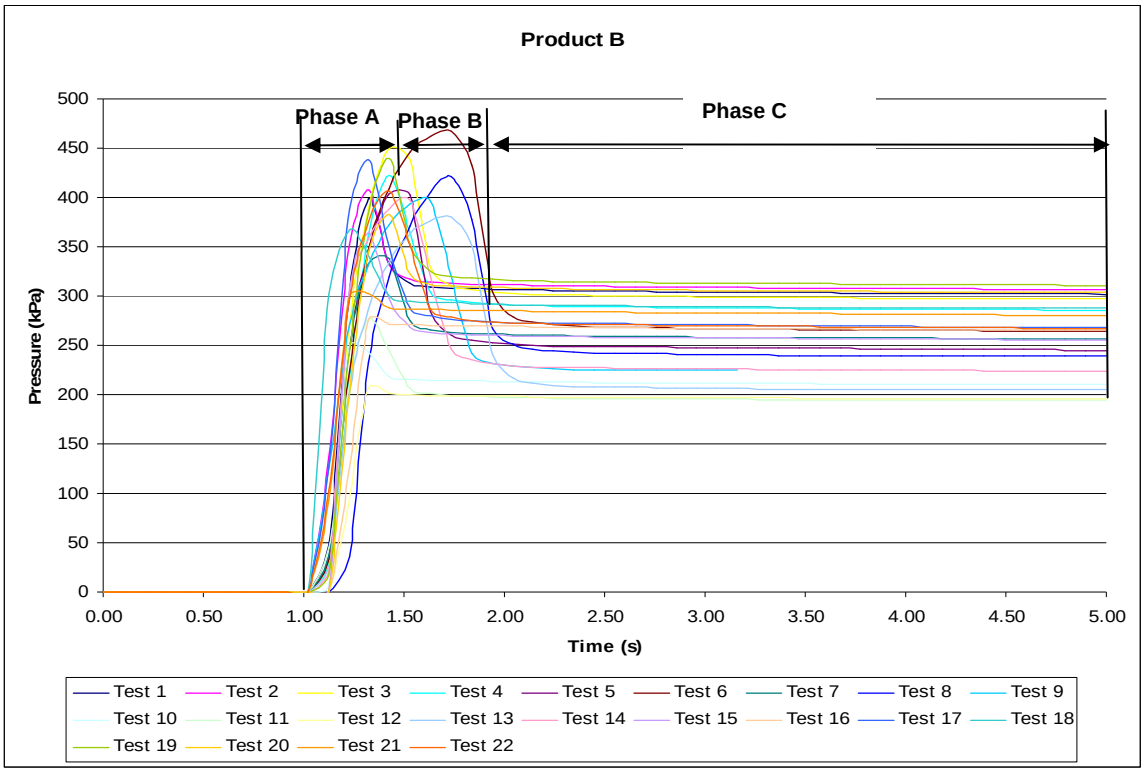

Figure 6.15: Test results from category 1 of product B.

The test runs behaved as described by the intermediate curve in figure 6.6. The last phase (phase C in figure 6.15) represents system equilibrium after ejection occurred. Here the moving air experiences friction against the sidewalls of the blasthole. The air friction provides a force in the opposite direction as the flow of the air. This causes a back pressure of approximately 154kPa and is equal to the pressure represented by phase C in figure 6.15.

A statistical analysis was conducted using on the data. Figure 6.16 indicates the Arithmetic mean, the Standard deviation and the upper and lower confidence limits at 95%. Refer to Appendix A1 for all the numerical values of the test results.

The upper and lower confidence limits have been indicated in figure 6.16 below. This indicates that the arithmetic mean is an accurate representation of the data from this category.

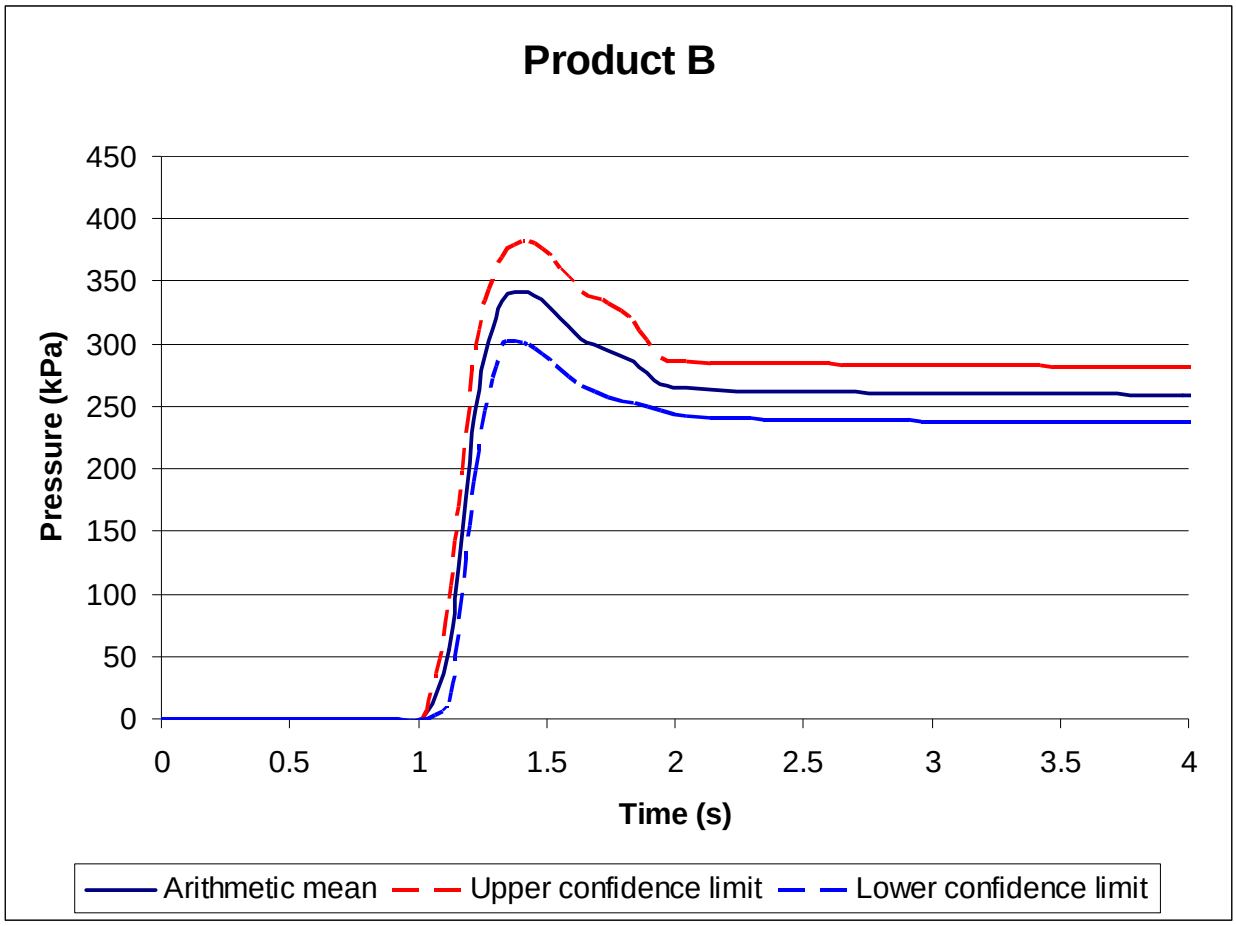

Figure 6.16: The arithmetic mean, upper and lower confidence limits as well as the standard deviation for the tests results for category 1 of product B.

6.6.6 Performance evaluation

A stemming product that experiences deformation to such a degree that the normal force of the stemming product on the sidewalls of the hole, would also experience an increase the frictional force experienced by the stemming product. (For a detailed discussion please refer to section 4.2.) Four of the 22 test runs have shown a poor pressure build up and ejection (figure 6.15), where there was no increase in the frictional force exerted on the sidewalls during the time that the pressure was applied.

Notably, in 18 of the 22 test runs there was pressure build-up during the run. In these runs the stemming capsule resisted the movement to a point where the force caused by the applied pressure overcame the resistance against the insides of the blast holes and was then ejected. The exact time of ejection of the stemming is shown by the sudden drop in the pressure graph shown in figure 6.16. The build up in pressure can be explained by a deformation and friction analyses.

As the pressure in the blasthole builds up the stemming capsule resists movement. This friction resistance is caused by the normal force that is exerted by the deformation of the stemming capsule during insertion. This normal force is applied perpendicular to the side walls of the blasthole. If the stemming capsule is merely pushed out the blasthole without further deformation then the pressure curves seen in the figures above will not have a peak follow by a sudden drop of pressure. However, if during the application of pressure, deformation takes place, then the normal force against the sidewalls of the blasthole will increase causing an increase in pressure. This increase in blasthole pressure will continue until the force parallel to the blasthole is larger than the resistive force in the opposite direction. At the point where these to forces are equal, movement occurs. The maximum pressure that the stemming capsule can take is determined by the value of the force applied to the stemming at the point just before movement. A maximum force of 283MN was observed in the 10^{th} test run, and the lowest of

152MN observed in the 5th test run. The interval of the mean is 187 ± 16 MN at 95% confidence interval.

6.7 Product C

6.7.1 Product description

This product is an aerosol foam stemming made up of Tris(chloroisopropyl)phosphate, less than 45% by weight and Diphenylmethane-4,4'-diisocyanate isomers and homologues, 30-45% by weight. Tris(chloroisopropyl)phosphate is a low viscous and low acidic flame retardant additive used in flexible and rigid polyurethane and Polyisocyanurate foam, unsaturated polyester resins, pvc, etc. Diphenylmethane-4,4-diisocyanate is a light yellow coloured solid. It is not soluble in water. It may be toxic by ingestion, inhalation, or skin absorption. If in a solution it may or may not burn, depending on the nature of the material and/or the solvent. The chemical products are pressurised inside an aerosol can with the use of an inert propellant. This froth hardens when in contact with air. The curing time depends on the conditions of the application.

6.7.2 Prescribed use

Remove white cap from aerosol can and attach injector tube to the top of the can. Insert injector tube into blasthole and suppress the black cap of the injector tube (see figure 6.17). The yellow foam will now be pushed into the hole under pressure. Release black cap of the injector tube after the blasthole is filled with foam.

The foam used during these tests was allowed to cure for 1½ hours before the pressure was applied. It was observed that the foam was only about 5% cured at this point. The 1½ hour waiting period was taken as the average time between charging up and blasting time. It was noted during the tests that the curing time for

the foam did not prove to be sufficient. This caused the foam to fail by sliding rather than friction on the sidewalls.

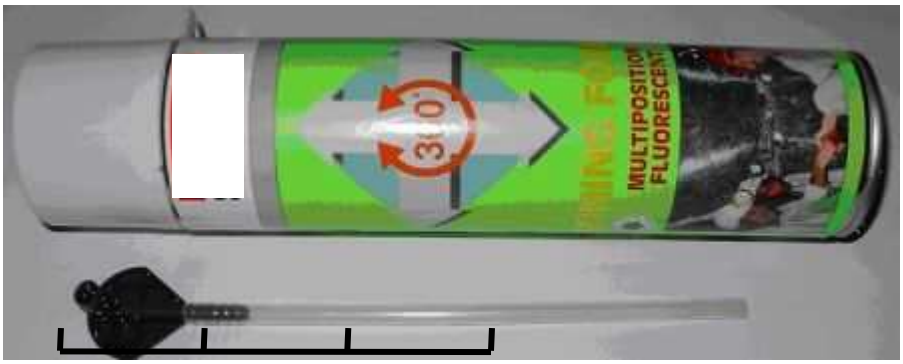

Figure 6.17: Photo of the aerosol foam stemming.

6.7.3 Pressure test results

Procedures were followed and corrections applied as per section 6.5.3. Figure 6.18 indicate the results graphically.

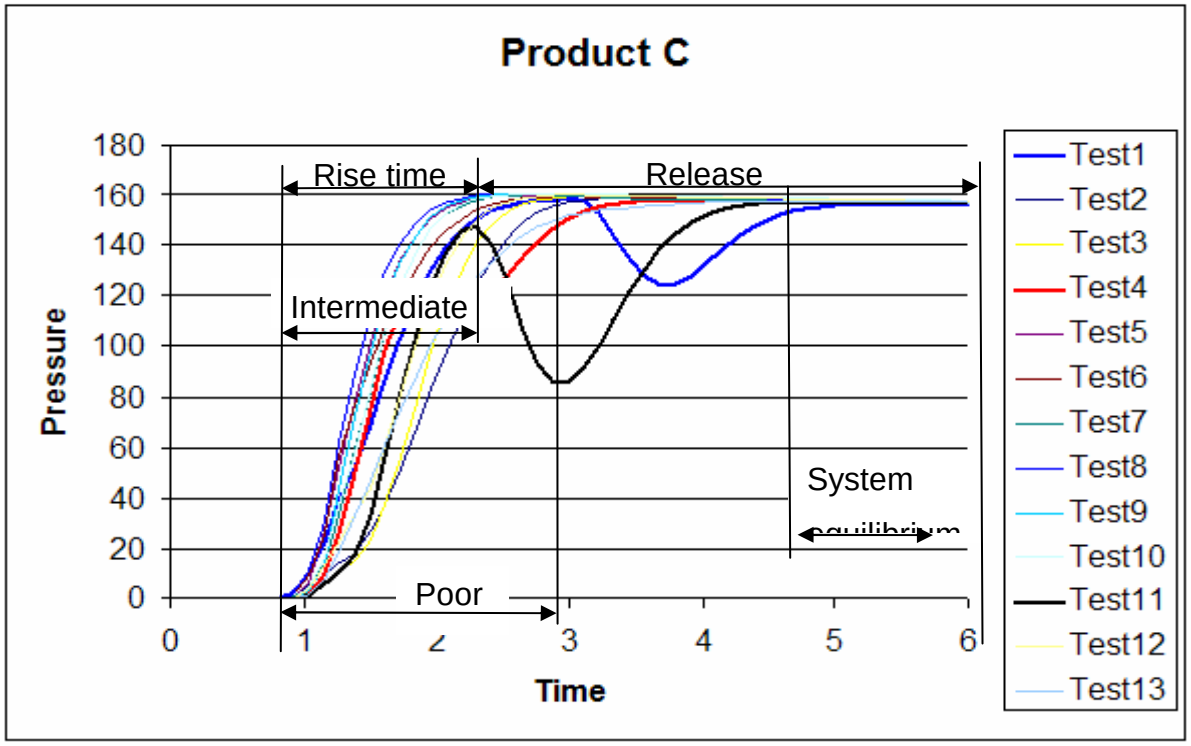

Figure 6.18: Pressure test results from the product C.

6.7.4 Method of analysis

Boyle's gas law was also used to investigate the rate of stemming ejection of the test runs from product B. The data collected during one of the test runs form product C will be used to investigate the behaviour of the air in the blast chamber.

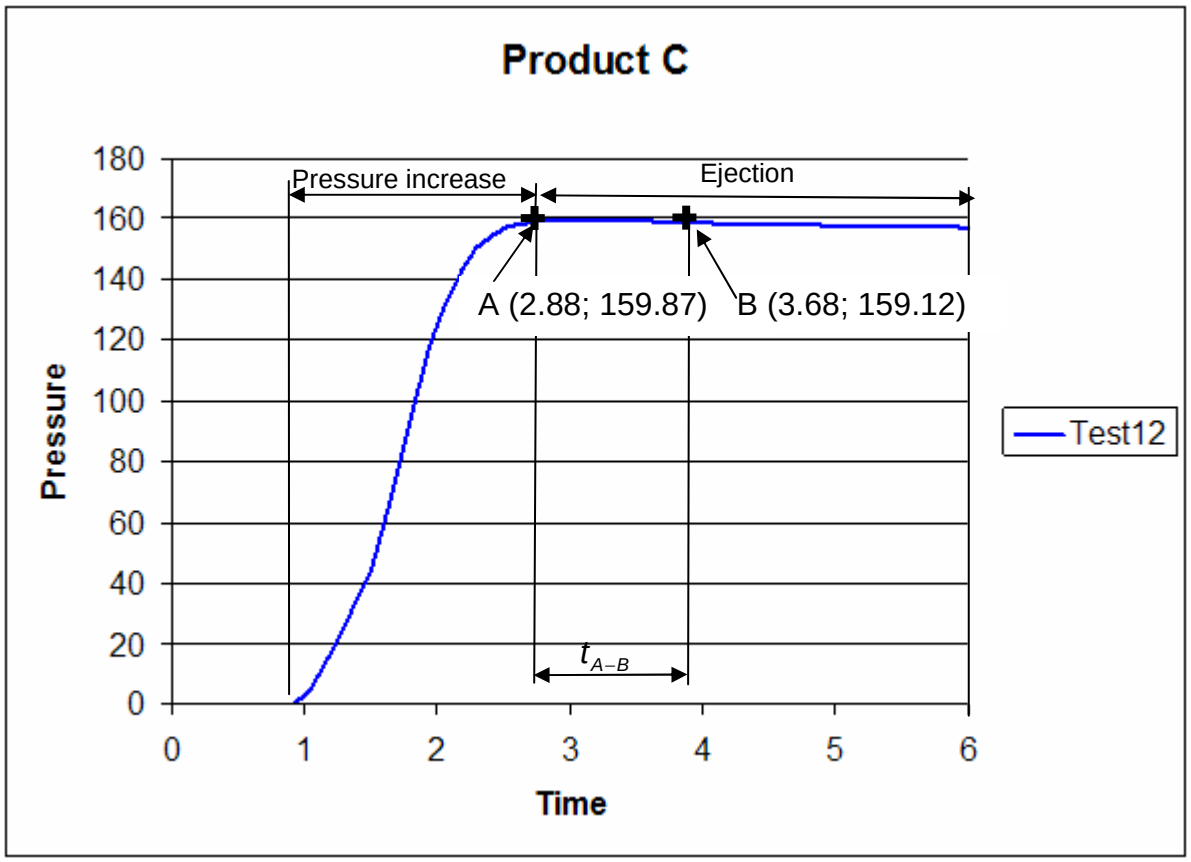

Figure 6.19: Test run 10 of Product B

The same logic used for the previous two products was applied to product C. The difference in pressure at point A and point B (figure 6.19) is negligible for all practical purposes. If it as assumed that the volume of compressed air in the blasthole only starts to change as soon as the projectile (i.e. the stemming capsule) starts to eject, then point A in figure 6.19 indicates the start of the change in volume.

It was again assumed that any significant changes in the volume of the gas (air) in the blasthole occurs when the projectile (stemming product) started moving out the hole. The applicability of Boyle's gas law was tested.

As for product A, the initial and final volume would be the same with:

$$V_i = 404.0 \times 10^{-6} m^3$$

and:

$$V_f = 634.5 \times 10^{-6} m^3$$

The validity of the equation can now be tested. The value of the initial pressure and the final pressure can be read off the graph in figure 6.19:

With $P_i = 159.87 kPa$ and $P_f = 159.12 kPa$,

$P_i \times V_i = 159.87 \times 404 \times 10^{-6} = 64.6 \times 10^{-3}$

Where $P_f \times V_f = 159.12 \times 634.5 \times 10^{-6} = 101 \times 10^{-3}$.

Hence, $P_i \times V_i < P_f \times V_f$ and the system is therefore, non ideal. Furthermore, it can be concluded that Boyle's does not apply to product C.

6.7.5 Discussion an analysis

The pressure-volume relationship was graphed using the values above.
With:

$V_i = V_A = 404.0 \times 10^{-6} m^3$ (figure 6.6)

$V_f = V_B = 634.5 \times 10^{-6} m^3$ (figure 6.7)

The pressure-volume relationship can only be determined if there was a change in volume measured over a change in time. Therefore, it is important to know if the stemming product moved, when it started moving and at what time it left the hole (figure 6.6 and 6.8).

The test runs can now be separated into groups that appeared to produce similar results. Two distinct categories can be distinguished: This product indicated only one group of results. In all the tests runs, stemming ejection occurred immediately. No pressure build-up or deformation of the stemming product was observed. The static frictional coefficient did not increase during the deformation.

Mathematically this can be expressed as:

$$F_{compressed-air} > F_{friction} \text{ with } \Delta F_{friction} \downarrow$$

During the whole testing phase the force exerted on the stemming product due to the compressed air was in excess of the frictional force experienced in the opposite direction. Mathematically this can be expressed as:

$$F_{compressed-air} > F_{friction} \text{ with } \Delta F_{friction} \downarrow$$

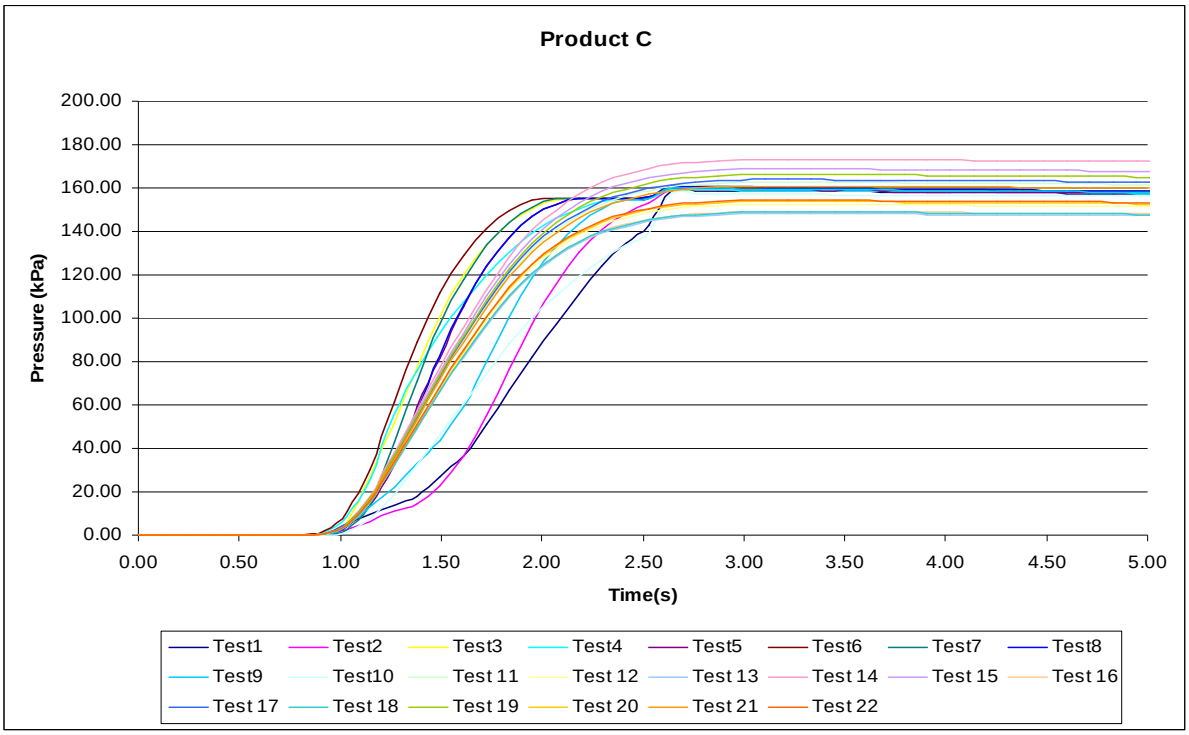

Figure 6.20: Test results from category 1 of product C.

These test runs are described by the poor curve in figure 6.2. A statistical analysis was conducted on these data. Figure 6.20 indicates the Arithmetic mean, the Standard deviation as well as the upper and lower confidence limits at 95%. All the numerical values of the test results are provided in Appendix A1.

Figure 6.20 shows that the upper and lower confidence limits follow the mean closely. This signifies that the arithmetic mean is an accurate representation of the data from this category. It also signifies that the variance about the mean is low

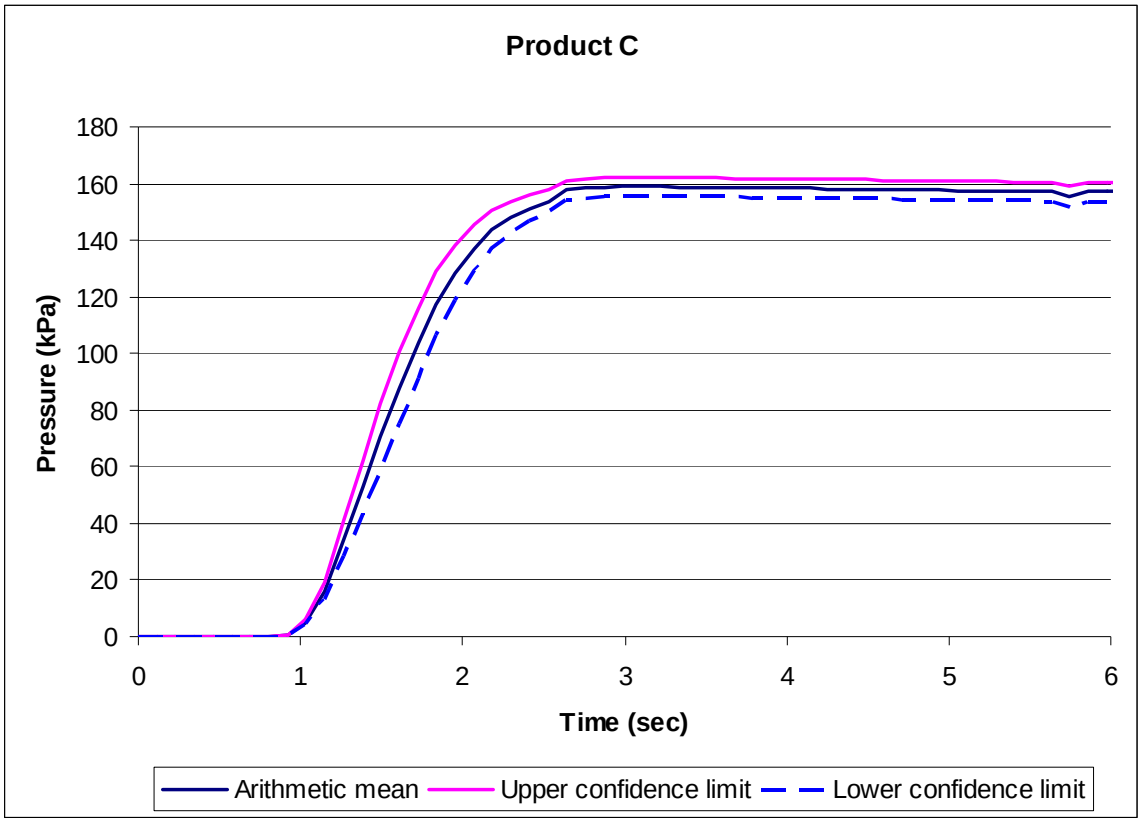

Figure 6.21: The arithmetic mean, upper and lower confidence limits as well as the standard deviation for the tests results for category 1 of product C.

6.7.6 Performance evaluation

If a stemming product experiences deformation to such a degree that the normal force that the stemming product exerts on the sidewalls of the hole increases, this would also increase the frictional force experienced by the stemming product

(detailed discussion is provided in section 4.2). All the test runs for Product C indicated a poor pressure build up and ejection (figure 6.2). In all cases there was no increase in the frictional force exerted on the sidewalls during the time that the pressure was applied.

All of the test runs indicated an even pressure increase. After the maximum pressure was reached, the pressure reached system equilibrium and stayed constant until the end of the test run. The maximum pressure recorded was merely the system back pressure. Hence, the foam was not able to withstand any pressure that was placed on it.

It is clear that the tests produced only one distinct category of results. The distribution of the 95% confidence interval of the arithmetic mean has indicated a standard deviation of less than 24kPa.

The data obtained paints a clear picture as to the performance of the foam stemming during the pressure tests. The pressure tests on the cured foam tests indicated different performance patterns. All of the tests indicated a poor, if any, resistance against air pressure.

The maximum pressure that the aerosol foam can withstand was determined by the value of the force applied to the stemming at the point just before movement. Test run 14 achieved the maximum pressure. The maximum force required to remove the stemming from the hole was 156MN. The minimum force required was measured in the 11^{th} test run and was 106MN. The upper and lower confidence limits of the mean at 95% confidence, at the time of maximum pressure was $u = 159MN$ and $l = 156MN$.

6.8 Product D

6.8.1 Product description

This product is made up of six components comprising several polymer components as well as one aluminium component. All six components are manufactured separately and joined (with friction) together to form a single unit. Figure 6.22 indicates the product in its separate components and Figure 6.23 indicates the product in assembled format. The product is manufactured by Denwa Engineering, situated in Johannesburg, South Africa.

6.8.2 Prescribed use

The stemming capsule is to be soaked in clean water for approximately 10min before insertion. The stemming capsule is then inserted into the blasting hole by hand. After each stemming capsule pouch is inserted, a loading or charging stick is used to secure the plug as tightly as possible. This procedure is then repeated until the remainder of the blasthole is filled with stemming capsule.

Figure 6.22: The mechanical plug disassembled.

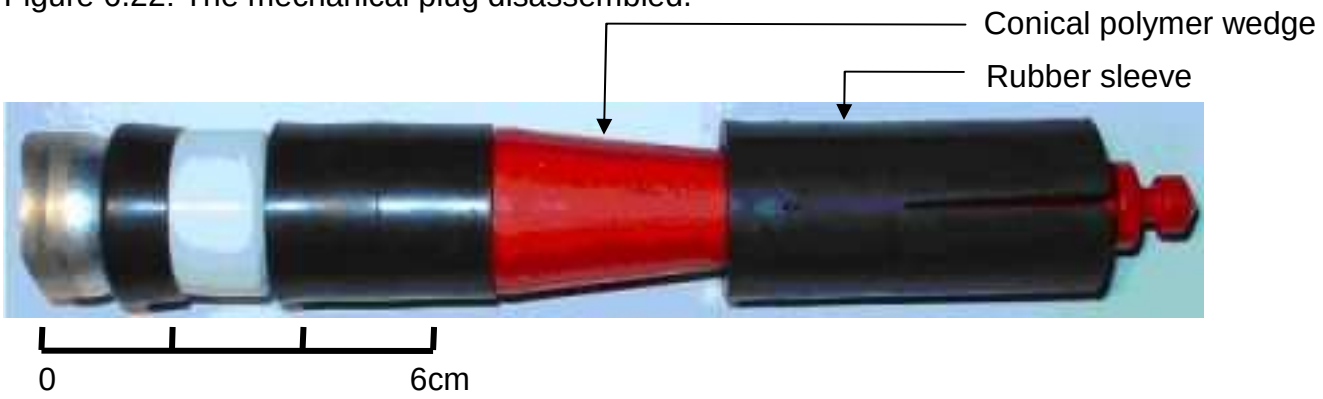

Figure 6.23: The mechanical plug assembled.

6.8.3 Pressure test results

The pressure test results are indicated in figure 6.24. These test runs indicated a variety of different pressure performance patterns. During some of the test runs the stemming products stayed in the hole, while during other test runs the compressed air leaked passed the stemming plug.

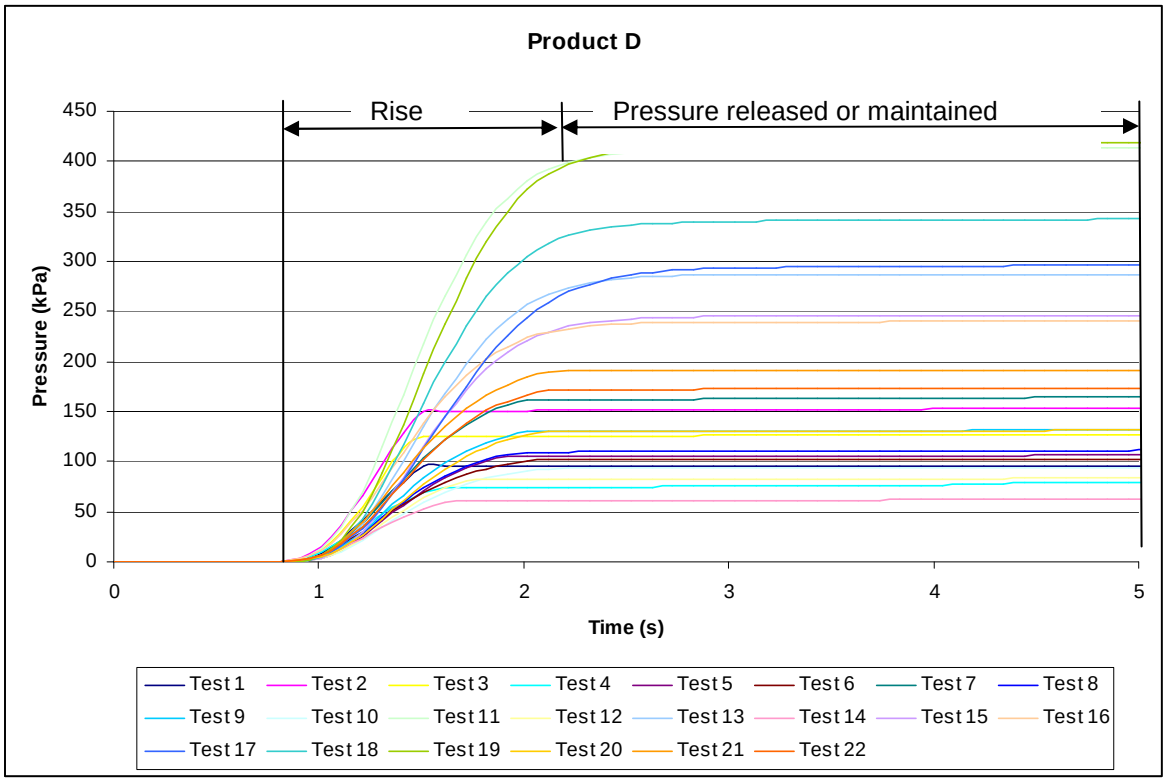

Figure 6.24: Results from pressure tests from product D.

The tests results were divided into three categories. The first category included the test runs where the stemming plug did not eject and no air leaked passed the plug. The second category comprised the test runs where the stemming plug stayed in the hole but compressed air leaked pass the sides of the plug. The last category included the test runs where the stemming plugs were blown out the hole. These three categories are discussed in detail in paragraph 6.8.4

6.8.4 Method of analysis

Category 1: The first category (test runs 11, 13, 15-22) produced a sudden rise to the maximum pressure and then held the pressure until the ten seconds testing epoch was over. During these tests, the stemming capsule was not blown out the hole, but managed to maintain the pressure throughout the test run. The maximum pressure that the product withstood was 332 kPa. Figure 6.36 indicates a slight increase in pressure between 3 and 6 seconds. This indicates that there was no loss in pressure in the system and the compressor had time to build up pressure. Hence, there was an increase in system pressure in this time period.

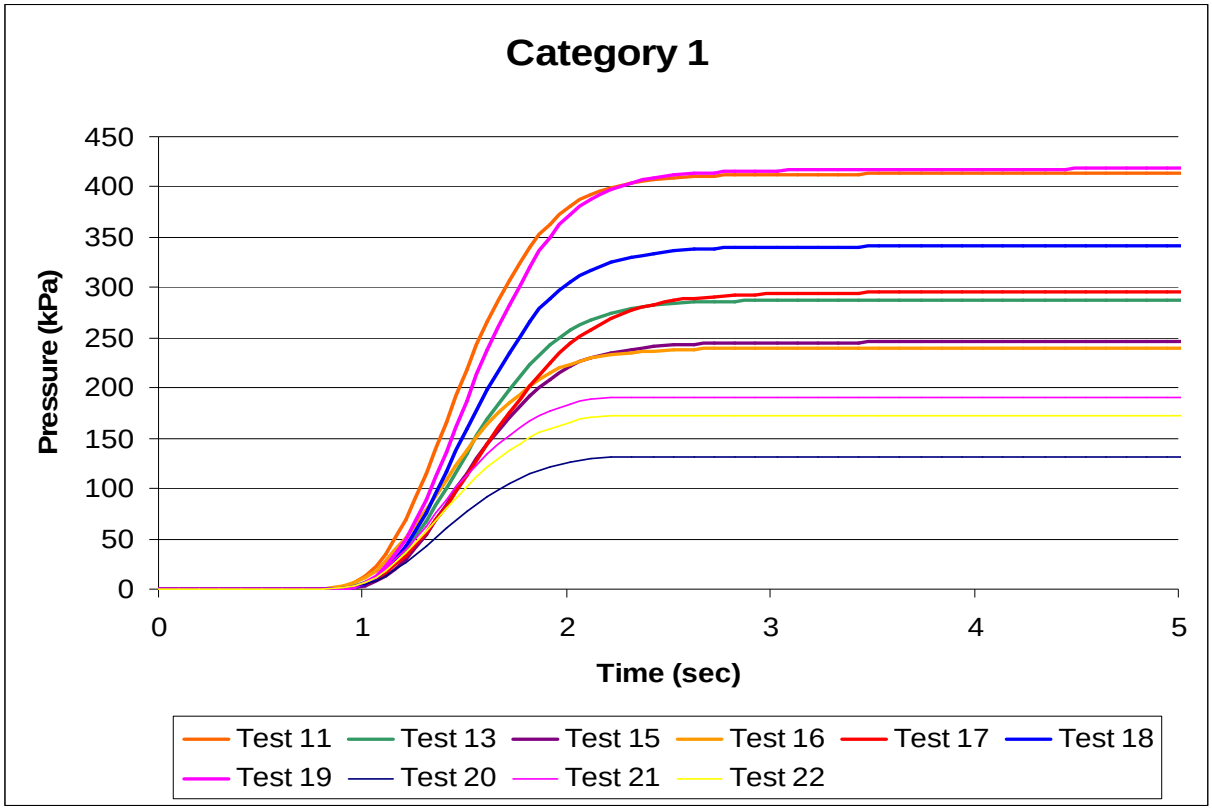

Figure 6.25: The pressure test results from product C category 1.

Category 2: The second category includes the test runs where the stemming plug stayed in the hole but the air leaked past the plug on the sides (test runs 5-9, 12 and 14). Figure 6.25 indicates that there was a slower build up in pressure which reached a maximum and then a slowly lost pressure towards the end of the test

run. The maximum pressures reached during these tests runs are considerably lower (between 60 and 170 kPa) compared to those reached during the test runs in category 1 (between 240-420 kPa).

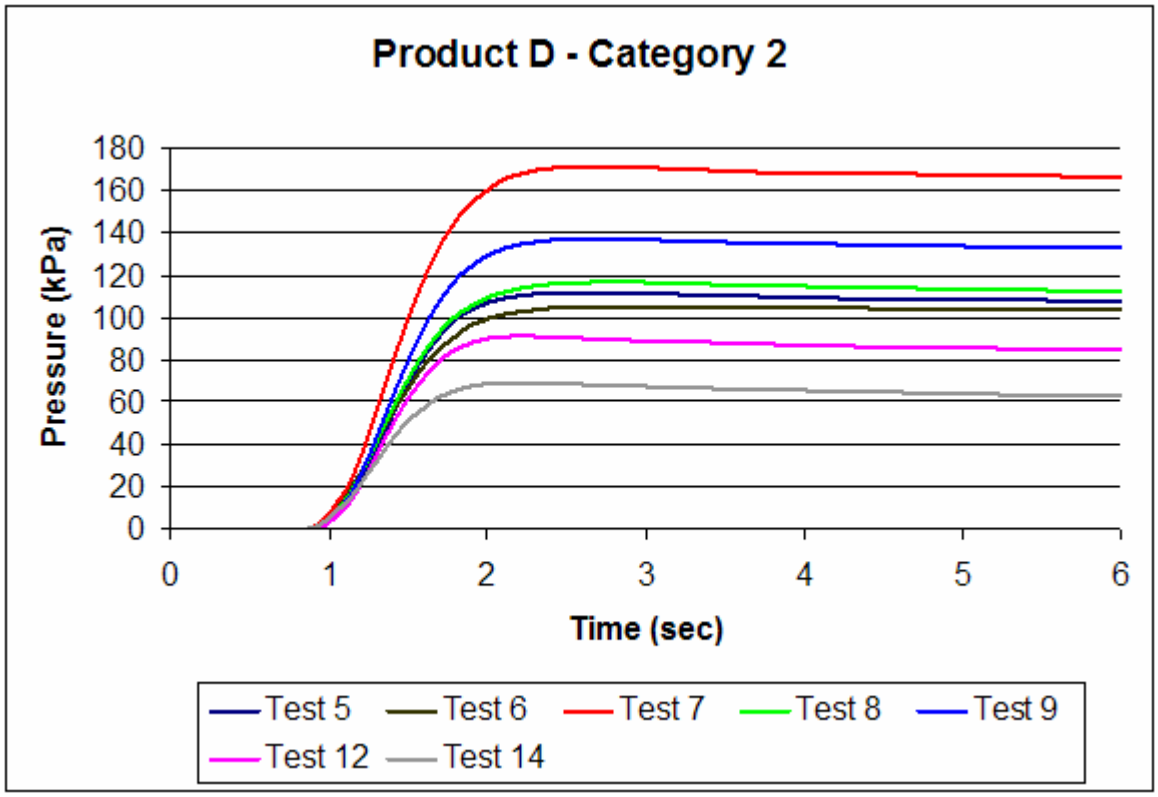

Figure 6.26: Pressure test results from product D category 2.

Category 3: This category includes those test runs where the stemming plug was blown out the hole (tests 1-4). The pressure in the hole during these test runs increased and decreased sporadically (figure 6.27).

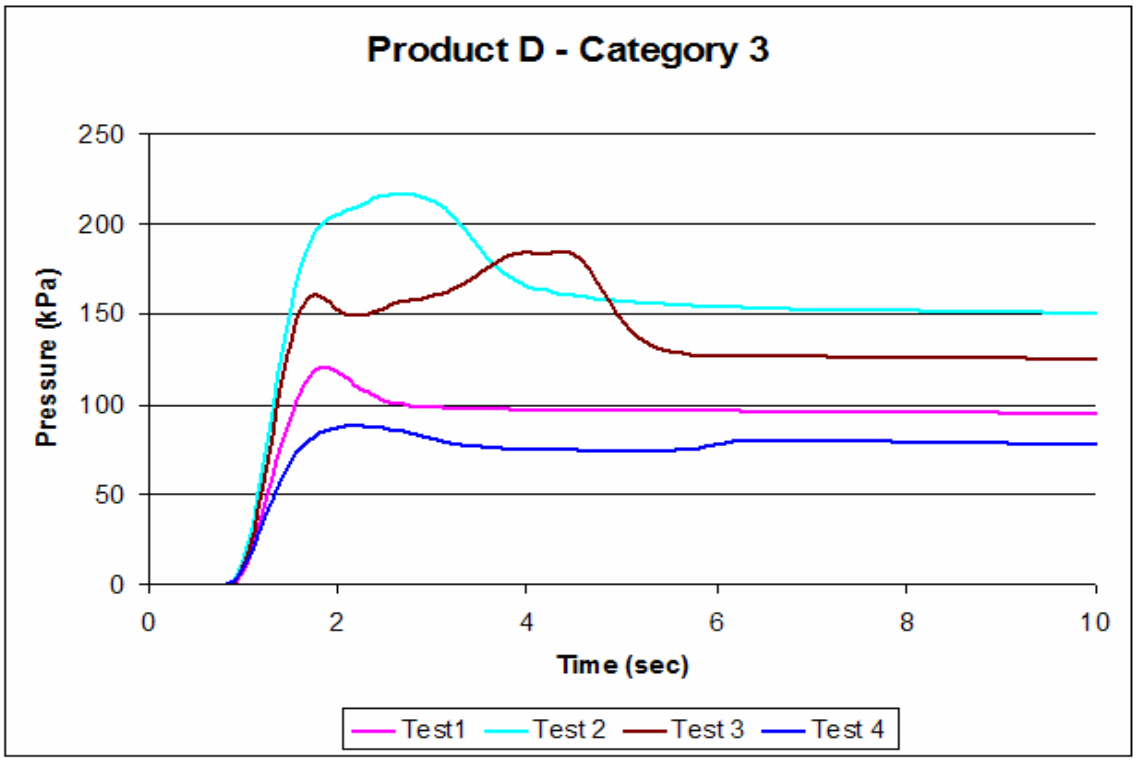

Figure 6.27: Pressure test results from product D category 3

6.8.5 Discussion and analysis

Category 1: The first category (test runs 11, 13, 15-22) comprised the group of test runs that produced a sudden rise to the maximum pressure and then held the pressure until the ten seconds testing epoch was over. During these tests the stemming capsule was not blown out the hole. Hence, there was no change in the volume during the test runs. This further indicates that the static frictional force was larger than the maximum force applied to the product, as a result of the air pressure in the blasthole. Using Boyle's law, the pressure-volume relationship is graphically represented in figure 6.28. Mathematically the relationship between the frictional force and the force as a result of the pressure, can be expressed as:

$$F_{compressed-air} < F_{friction}$$

With

$F_{compressed-air}$ = force applied to the capsule as a result of the air pressure

$F_{friction}$ = resistive force that the stemming capsule experienced just before movement, due to static friction.

Using Boyle's law, the pressure volume relationship is represented by:

$P_i V_i = P_f V_f$ but with $\Delta P = \Delta V = 0$

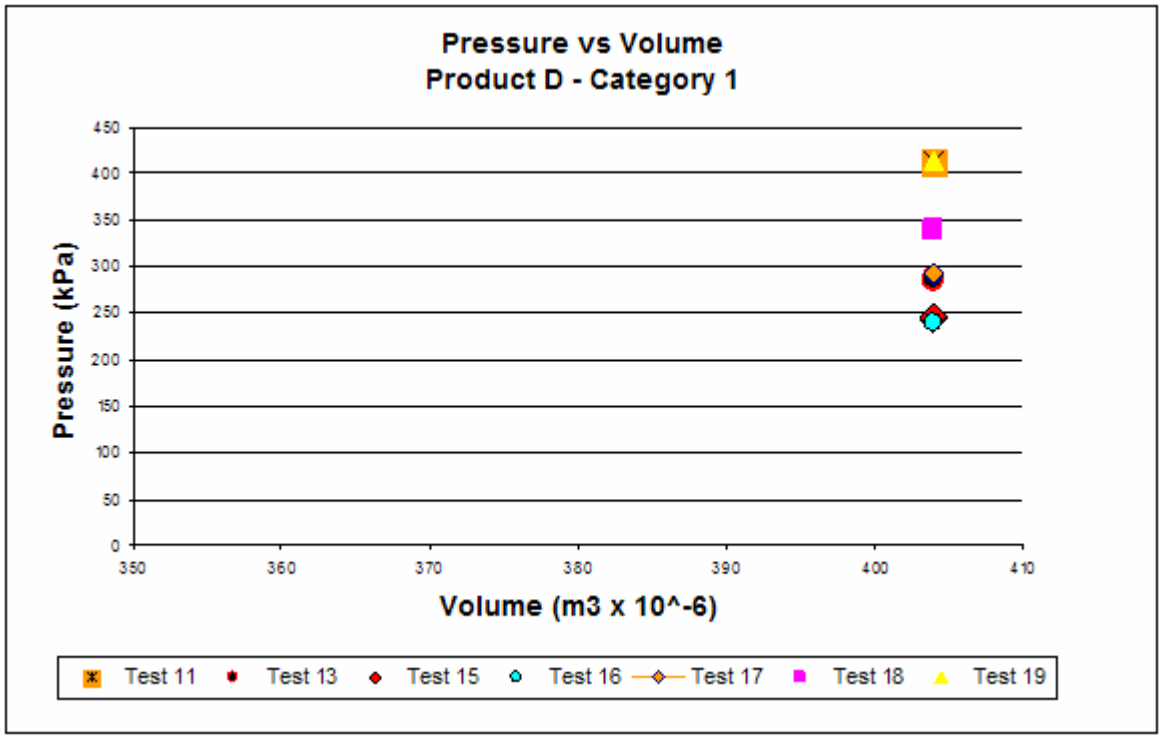

Figure 6.28: The statistical parameters of product D category 1.

The pressure volume relationship has been indicated by a single point in figure 6.22 because $\Delta P = \Delta V = 0$. This equation is only valid for the time after maximum pressure was reached. As explained above, there was no volume change during these test runs. The pressures indicated in figure 6.28 were measured at two different points in time after maximum pressure was reached (t=x and t=y), as this would have been the period during which a change in volume would have occurred.

Statistical analyses were done in order to determine the distribution of the data. The test runs revealed a high variability in measured pressure and the 95% confidence interval of the arithmetic mean was therefore calculated. The standard

deviation as well as the confidence about the mean for each category was also determined. Figure 6. 29 indicates the statistical values of the first sub-category.

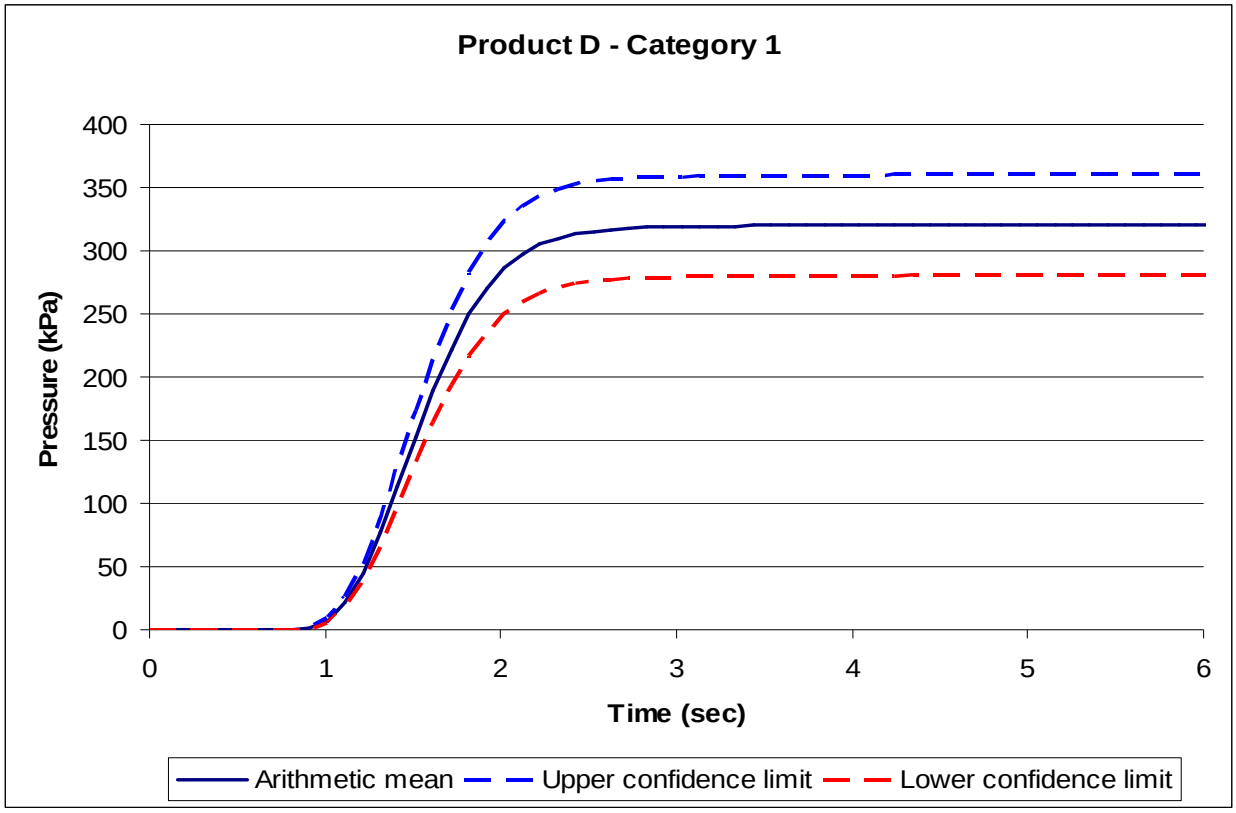

Figure 6.29: The arithmetic mean, upper and lower confidence limits as well as the standard deviation for the tests results for category 1 of product D.

The data from which these statistical parameters were calculated are comprised of those tests runs where the stemming plug withheld the pressure of the system and notably sealed the hole well enough to ensure no leakage of compressed air takes place. Hence, the statistical parameters in figure 6.29 merely describe the variance of the arithmetic mean of the system pressure, and give no indication of the performance of the stemming material.

Category 2: The second category includes test runs 5-9, 12 and 14 where the stemming plug remained in the hole but the compressed air bypassed the plug. As

in category 1 of product D, no change in the volume occurred during the test runs. Hence, the static frictional force was also larger than the maximum force that was applied to the product as a result of the air pressure in the blasthole. Due to some of the air bypassing the plug, the force induced on the plug by the compressed air in category 2 is less than that of category 1. The pressure volume relationship has been indicated in figure 6.30. Mathematically the relationship between the frictional force and the force as a result of the pressure can be expressed as:

$$F_{compressed-air} < F_{friction}$$

With

$F_{compressed-air}$ = force applied to the capsule as a result of the air pressure

$F_{friction}$ = resistive force that the stemming capsule experience just before movement, due to static friction.

Using Boyle's law, the pressure volume relationship is represented by:

$P_i V_i = P_f V_f$ but with $\Delta P = \Delta V = 0$

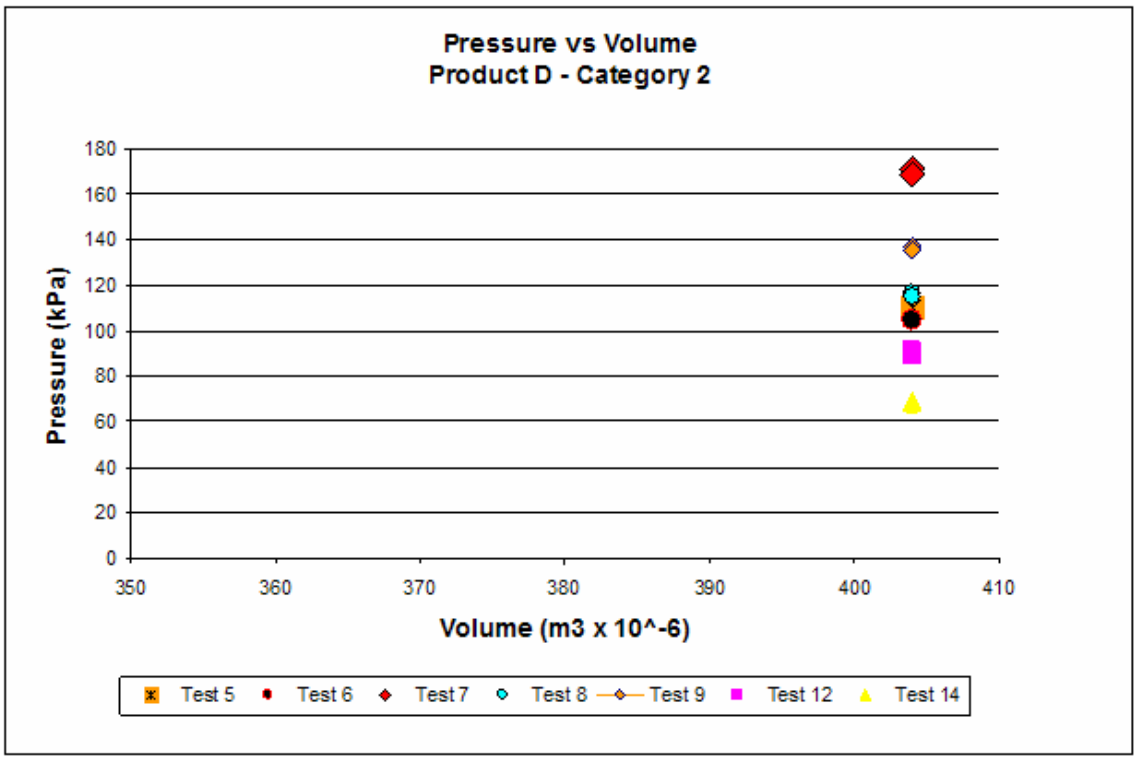

Figure 6.30: Pressure volume results from product D category 2.

The data included in category 2 were statistical analysed. Figure 6.31 indicates the arithmetic mean, standard deviation and 95% upper and lower confidence limits. Numerical values for all the test results are provided in appendix A1.

The upper and lower confidence limits follow the mean closely. This signifies that the arithmetic mean is an accurate representation of the data for this category.

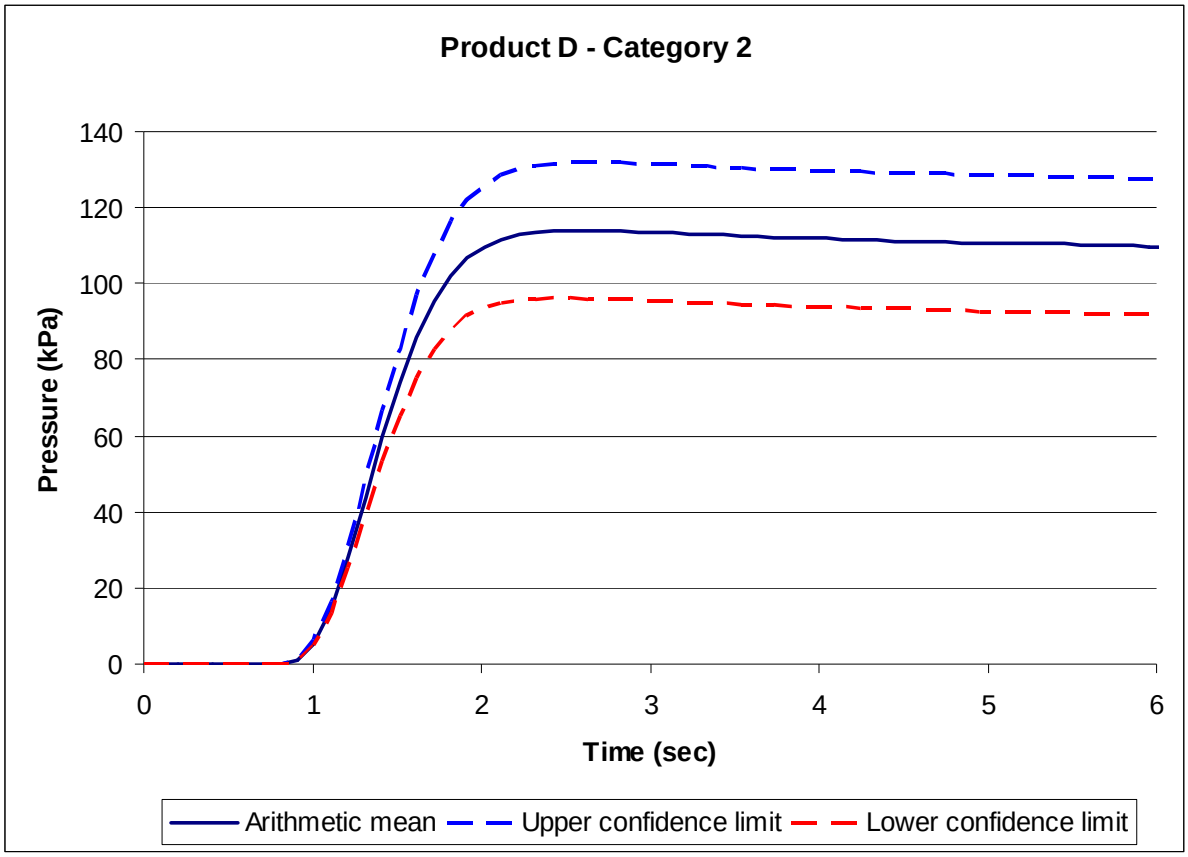

Figure 6.31: The statistical parameters of the product B category 2.

Category 3: This category includes the first four runs. During these test runs the stemming capsule did not eject immediately. The pressure curve of test run 1 followed a similar pattern to that of the other products. During the time that the pressure was applied the stemming product deformed. This deformation was not due to a lack in integrity of the plug, but rather was a result of the interaction of the separate parts. The black rubber sleeve (figure 6.26) moved up the red conical

polymer wedge during the deformation stage. This increased the normal force on the insides of the blasthole and therefore increased the friction that the plug experienced against the sidewalls of the hole. Mathematically it can be expressed as follows:

$$F_{friction} = \mu_s N$$

Where:

$F_{friction}$ = friction force exerted on stemming (N)

μ_s = coefficient of static friction

N = normal force (N)

In the above equation, if the normal force increases and the coefficient of static friction stay constant, the frictional force exerted on the stemming will increase.

The pressure build-up was erratic and no consistent deformation behaviour was observed. This inconsistent behaviour could be ascribed to the small differences in the applied pull force that was used to secure the plug in position. These inconsistencies introduced from human handling should be considered when a plug is designed. In general the static and dynamic coefficient of friction of the contact between the rubber sleeve of the plug and the sides of the hole increased and decreased irregularly. This influenced the frictional force and therefore, influenced the force that the compressed air applied to the plug.

Initially the applied force on the plug was smaller than the maximum static frictional force. Mathematically it can be expressed as:

$$F_{compressed-air} < F_{friction} \text{ with } \Delta F_{friction} \uparrow$$

Then a point is reached where the frictional force has reached its maximum:

$$F_{compressed-air} = F_{friction} \text{ with } \Delta F_{friction} = 0$$

This is followed by a phase where the frictional force was overcome by the force due to the air pressure in the blasthole and then ejection of the stemming capsule occurred. Mathematically it can be expressed as:

$$F_{compressed-air} > F_{friction} \text{ with } \Delta F_{friction} \downarrow$$

The above cycle was repeated and there was therefore an increase in the pressure in the hole after the initial peak was observed.

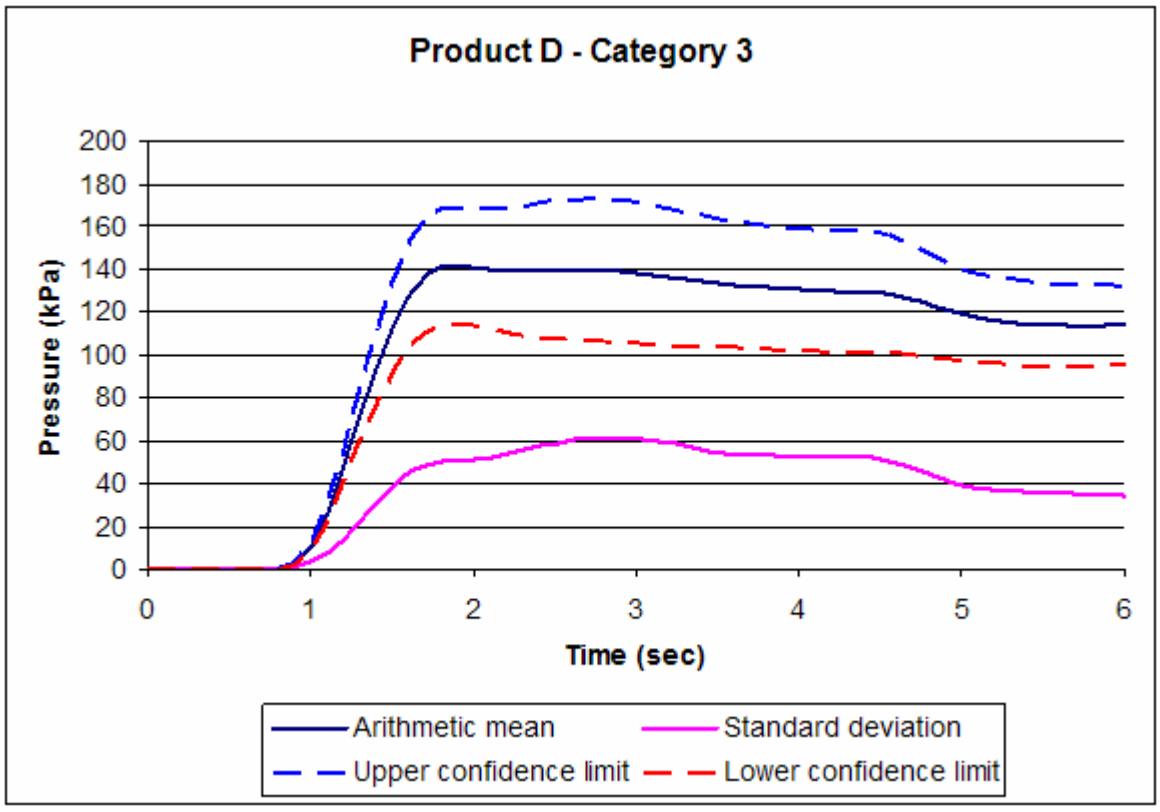

Figure 6.32: The statistical parameters from the pressure test results form product D category 3.

The statistical parameters of the third category of the product D in figure 6.32 do not describe the properties of the data accurately. The influence of the deviation of the system pressure has not been eliminated because that would have influenced

the observed pressure to such a degree that the statistical analysis would have been inaccurate. The standard deviation in figure 6.32 indicates a decline in the pressure as the time approached the end of the test time window. This is a clear indication that the stemming plug did not obstruct the compressed air to a large degree. The upper confidence limit of the data observed at any given time in figure 6.43 is lower than that observed for the same time of category 1 product D. the confidence limits in figure 6.32 were calculated at a 95% confidence.

The pressure volume relationships for each of the four test runs are graphed in figure 6.33.

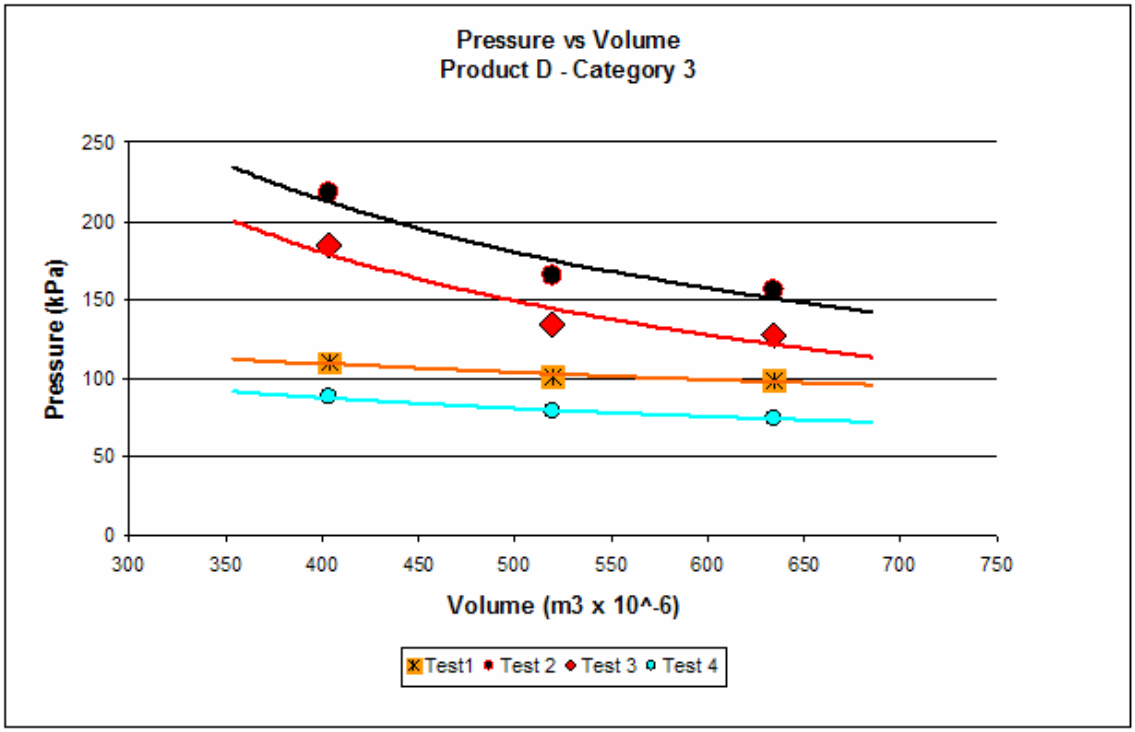

Figure 6.33: Pressure versus Volume for all the test runs.

6.8.6 Performance evaluation

This product produced pressure performance results that could be divided into three distinct categories. Two of these categories had a small standard deviation from the mean. In forty percent of the test runs, the plug stayed in the hole and

was able to maintain the pressure in the hole. In another forty percent of the test runs the plug also stayed in the hole but the compressed air bypassed the plug (i.e. air leak). In the last twenty percent of the test runs the plugs was blown out of the hole.

The maximum pressure that the stemming capsule can take is determined by the value of the force applied to the stemming at the point just before there was a sharp decrease in the pressure. The maximum force was achieved in the 19th test run and was 334N, the lowest was achieved in the 14th test run and was 56N. The interval of the mean at 95% confidence, at the time of maximum pressure was $u = 288N$ and $l = 77N$.

6.9 Product E

6.9.1 Product description

This product consists of a combination of three different materials combined in a plastic pouch. The largest part of the ingredients in the plastic pouch consists of coarse granules. The other two ingredients are a mixture of ghries and clay. The one end of the plastic pouch has been cut of at an angle to form a sharp point. The sharp point of the plastic pouch is filled with the ghries-clay mixture (figure 6.34).

6.9.2 Prescribed use

The stemming capsule is inserted into the hole by hand. The stemming capsule must be inserted into the hole with the sharp end first. A loading or charging stick was used to secure the plug as tight as possible. One stemming capsule is used per hole.

Figure 6.34: Product E.

6.9.3 Pressure test results

The pressure tests were performed on this specific product, using the experimental setup discussed in chapter 5.2. The data represented graphically in figure 6.46 below has been manipulated in an effort to eliminate starting time differences.

The second correction that was applied to the data was necessary to account for the differences in system pressure. The compressed air system used in this experiment used a pressure vessel that is pumped to a high pressure with a piston air pump. When air is drawn for the first run the pressure is high (up to 600kPa), for each consecutive test run thereafter the system pressure will be lower until the pressure drops too low (below 300 kPa). At this point the pump automatically starts again and pumps the vessel to a high pressure.

To allow for these changes in system pressure, the variance of the system pressure was determined and the pressure readings for each of the tests runs were adapted to accommodate for the limitations of the system.

The product performed with reasonable consistency. All of the test runs reached local maximum pressures between 200kPa and 300kPa. During all of the test runs the stemming capsule was ejected.

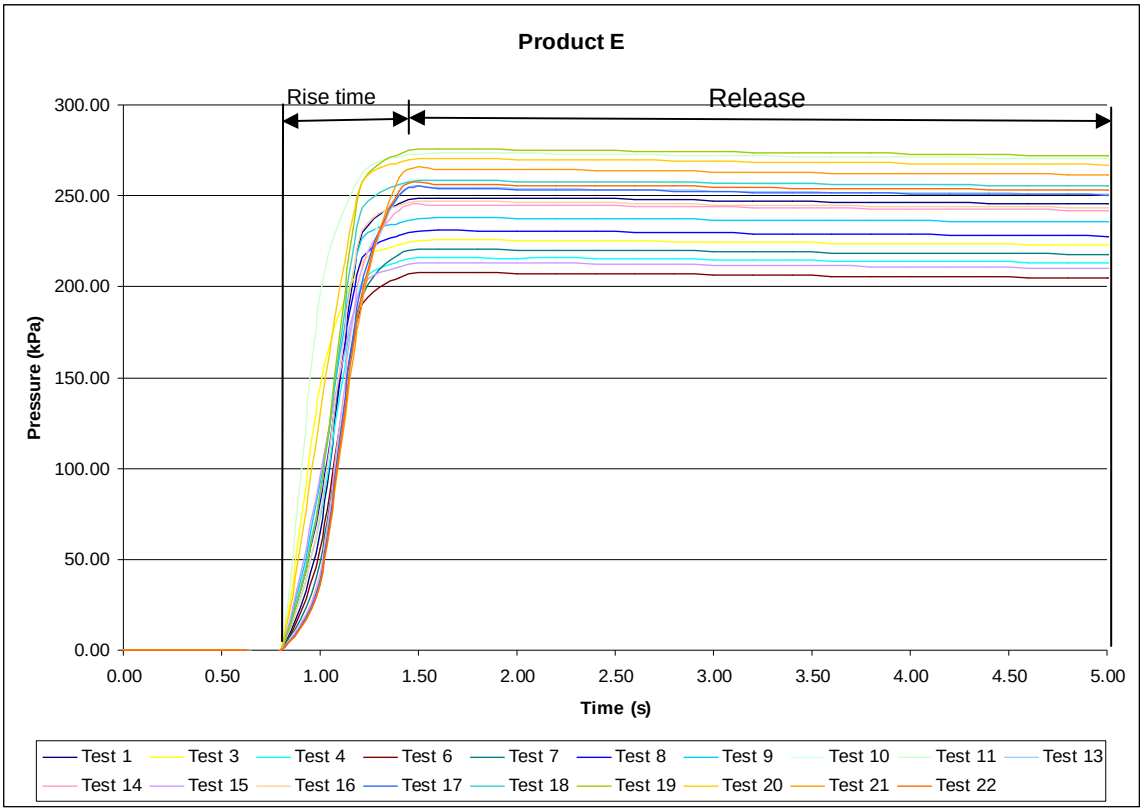

Figure 6.35:The pressure change over time for all the tests.

6.9.4 Method of analysis

Boyle's gas law was also used to investigate the rate of stemming ejection of the test runs for product E. The same logic used for all the other products was used for product E. It is assumed that the volume of compressed air in the blasthole only starts to change as soon as the projectile (i.e. the stemming capsule) starts to eject then point A in figure 6.15 indicates the start of the change in volume.

Similarly to the assumptions made for all the other products, it was assumed that any significant changes in the volume of the gas (air) in the blasthole occurs when the projectile (stemming product) starts moving out the hole. The question that arises is whether the conditions in the blasthole follow Boyle's gas law or not. The

pressure volume relationship was investigated by plotting this relationship on a graph.

The initial and final volume would be the same as for the other products with:

$$V_i = 404.0 \times 10^{-6} m^3$$

and:

$$V_f = 634.5 \times 10^{-6} m^3$$

6.9.5 Discussion an analysis

The pressure-volume relationship can now be graphed using the value above. The pressure-volume relationship can only be determined if there was a change in volume measured over a change in time. In other words, it is important to know if the stemming product moved, when it started moving and at what time it left the hole (figure 6.6 and 6.8).

As in the analysis of the other products, the test results can now be separated into groups that appeared to produce similar results. The data produced all similar results and no separate categories could be recognised.

Stemming product retention did not occur during any test run. Hence, ejection occurred before maximum air pressure was applied. This indicates that the initial static friction between the sidewalls of the blasthole and the stemming product was inadequate to cause retention of the capsule. Without adequate retention, little to no deformation is possible. With inadequate deformation the normal force against the sidewalls does not increase as increased pressure is applied. The result is premature ejection of the stemming capsule.
Mathematically the process can be expressed as:

$$F_{compressed-air} \uparrow > F_{friction} \rightarrow$$

where:

$F_{compressed-air} \uparrow$ indicates that the force due to the compressed air increases over time (phase A figure 6.18)

$F_{friction} \rightarrow$ indicates that friction in the blasthole stays constant

The above mathematical equation relates to Boyle's law and the pressure volume relationship is represented by:

$$P_i V_i \neq P_f V_f \text{ however with } \Delta P \approx 0 \text{ and } \Delta V \neq 0$$

The initial pressure depicted in the above equation must, according to Boyle's law, coincide with the initial volume. The initial volume was taken to be the volume of air in the blasthole just when movement of the stemming capsule started. The initial pressure would then be the pressure in the blasthole at the point of equilibrium between the frictional force and the force exerted of the stemming capsule due to the air pressure.

The statistical parameters of the product E in figure 6.36 describe the properties of the data rather accurately. The influence of the deviation of the system pressure has been eliminated as described above. The standard deviation in figure 6.36 indicates a wider distribution just after the first second. The distribution narrows down closer towards the 2nd second. A maximum deviation of 36.39 kPa was recorded after 1 second. This explains the small difference between the upper and lower confidence limits.

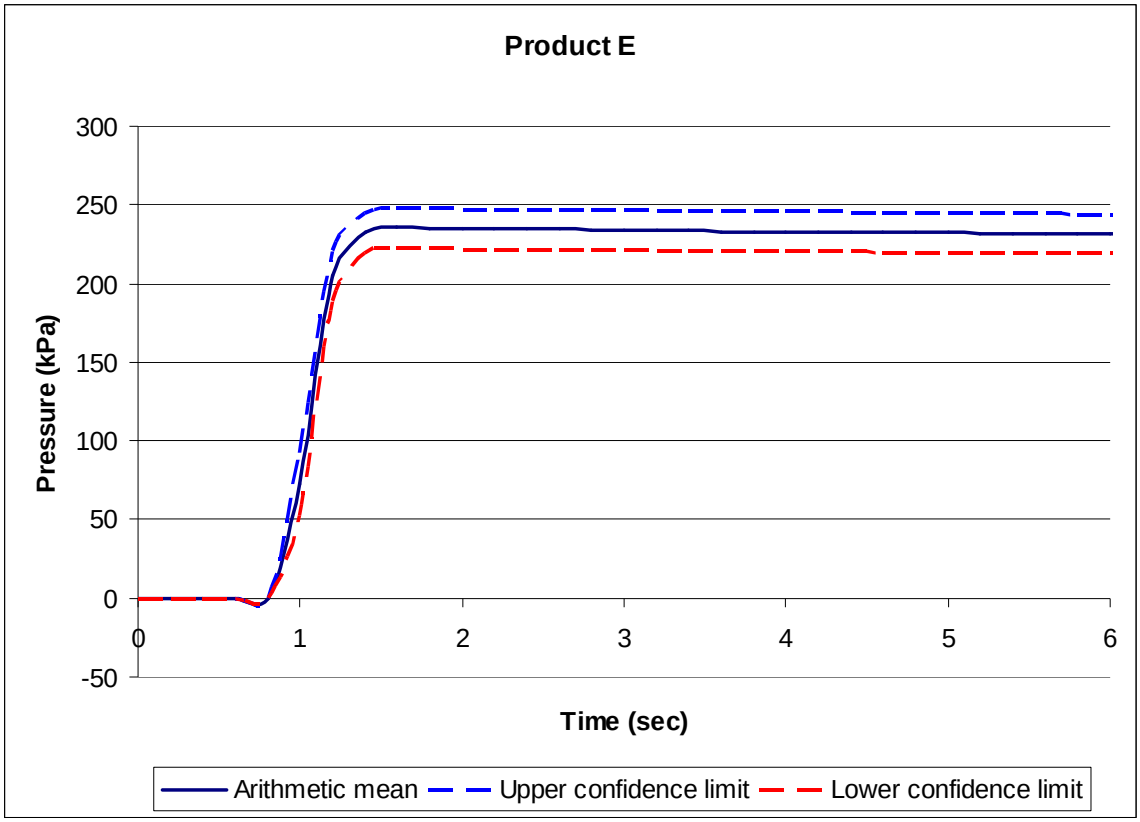

Figure 6.36: The statistical parameters from Product B.

6.9.6 Performance evaluation

The stemming capsule was not retained in any of the test runs. All of the test runs indicated poor resistance to the air pressure. In all the test runs there was no increase in the frictional force exerted on the sidewalls during the time that the pressure was applied. No deformation after pressure application was observed.

It can be observed from figure 6.36 that there was a slight decrease in pressure after the maximum pressure was reached. This indicates that the stemming capsule was out the hole and that there was no retention of the air pressure in the hole. If the stemming capsule is merely pushed out the blasthole without further deformation then the pressure curves seen in the figures above will not have a

peak follow by a sudden drop of pressure. The interval of the mean was 236 ± 23 kPa which equates to 189 ± 19 N at 95% confidence interval.

7 DATA ANALYSIS – HIGH PRESSURE TESTS

7.1 Introduction

The experimental testing for the second phase used exactly the same products that were used for the first phase. A brief summary of the various products has been included in table 7.1 below in no particular order.

Table 7.1: Summary of the products tested

Product description	Code name
Homogeneous clay ampoule	Product A
Homogeneous gravel ampoule	Product B
Polyutherane foam	Product C
Mechanical plug	Product D
Heterogeneous gravel ampoule	Product E
Control test runs	No stemming

The experimental setup that was used for these tests was fundamentally different to those of the first phase. A complete description of the experimental setup is provided in chapter 5. Various stemming materials were analysed for their ability to resist gas pressure during the detonation of ballistite. The test results of the different stemming material's performance were analysed individually and sorted into categories of similar performance based on the characteristics of a "good" stemming as described in chapter 6. The pressure test results for each of the

products were also statistically analysed and the end of each section, similarly to chapter 6.

7.2 Product description and use

The product description and use of each of the products have been described in chapter 6.

7.3 Sampling rate and data correction

The sampling rate was first set to 100 Hz, but it was observed that this sampling rate was too low and only a single pressure value was obtained. The sampling rate was then increased to 200 kHz. This sampling rate was found to be sufficient. Only one correction was applied to the data: The starting times of all the test runs were not identical hence, the starting times were normalised to coincide with one another. The pressure system was calibrated with atmospheric pressure taken to be zero.

7.4 Method of analysis

The performance analysis of the stemming products was based on two separate factors. The maximum pressure was analysed followed by an analyses of the pressure versus volume behaviour. The pressure distribution was statistically analysed. The pressure-volume analyses were based on the same basic principles that were used during the low pressure tests.

The results from test run 7 are provided here to provide an explanation of the method of analysis. According to the results obtained from the switch at the end of the steel pipe, ejection only starts immediately after maximum pressure was reached (Point A, figure 7.1). The stemming plug will then be fully ejected as soon as the pressure in the system has returned to a value that is the same as the average value obtained from the control tests. (Point B, figure 7.1). With no stemming (i.e. control test) it is an open system with restricted vent. The pressure

time curve will then vary according to factors determined by the characteristics of the ballistite. The volume change that occurs during this period of time is exactly equal to that of the low pressure tests.

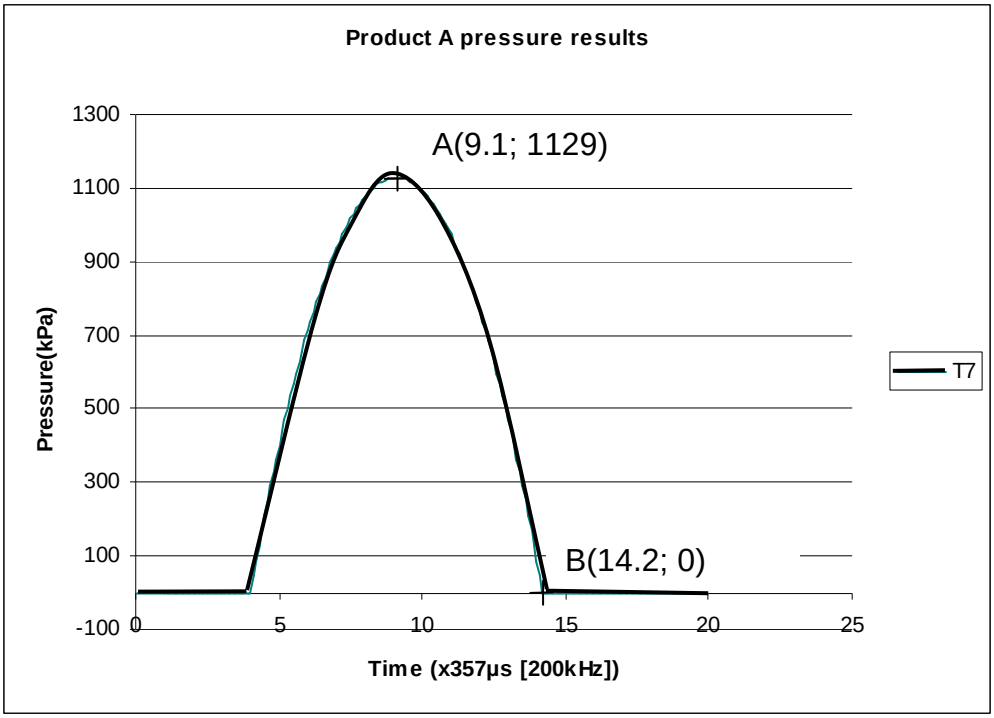

Figure 7.1: Results from pressure tests from product A

It was tested if Boyle's law holds true for this particular experimental setup. Boyle's law can be expressed by the following mathematical equation:

$$P_i V_i = P_f V_f \qquad \text{Equation 7.1}$$

where:

P_i = Initial Pressure (kPa)

V_i = Initial Volume(m^3)

P_f = Final Pressure (kPa)

V_f = Final Volume (m^3)

The initial and the final pressures can be read off the graph in figure 7.1 above. The initial and final volumes have to be calculated. The initial volume of air in the blasthole can be taken as:

$$V_i = \frac{\pi d^2}{4} \times (\lambda_{blasthole} - \lambda_{eject}) \qquad \text{Equation 7.2}$$

where:

ΔV = change in volume of the blast hole (m^3)

D = diameter of the blasthole (m)

$\lambda_{blasthole}$ = the length of the steel pipe protruding form the pressure vessel (m)

λ_{eject} = the length of stemming that has been ejected (m)

$$V_i = \frac{\pi 0.034^2}{4} \times (0.5 - 0.3) = 181.6 \times 10^{-6} m^3$$

and:

$$V_f = \frac{\pi d^2}{4} \times (\lambda_{blasthole})$$

$$V_f = \frac{\pi 0.034^2}{4} \times (0.5) = 454.0 \times 10^{-6} m^3 \qquad \text{Equation 7.3}$$

The validity of the equation can now be tested. The value of the initial pressure and the final pressure can be read off the graph in figure 7.1.

With $P_i = 1129kPa$ and $P_f = 0kPa$ (Pressure reading equipment has been calibrated so that atmospheric pressure is zero). Therefore:

$P_i \times V_i = \left(1129 \times 10^3\right) \times \left(182 \times 10^{-6}\right) = 205$ with, $P_f \times V_f = 0 \times 454 \times 10^{-6} = 0$. It is clear that $P_i \times V_i > P_f \times V_f$ and the system is therefore non ideal. At very low density, all gases approach ideal-gas behaviour, with the P-v-T relationship being given by the ideal-gas equation of state. However, it must be noted that this law is only approximately true.

7.5 No stemming product

The test runs that were performed with no stemming were done to act as a control run. The results from these runs were used to act as a pressure bench mark against which the other products could be measured. It also served as a measure of the consistency of the pressure in the test chamber.

7.5.1 Pressure test results

The pressure test results are provided in figure 7.2. The pressure tests did not indicate a clear difference between pressures that could be separated into individual groups. The results indicated a random distribution.

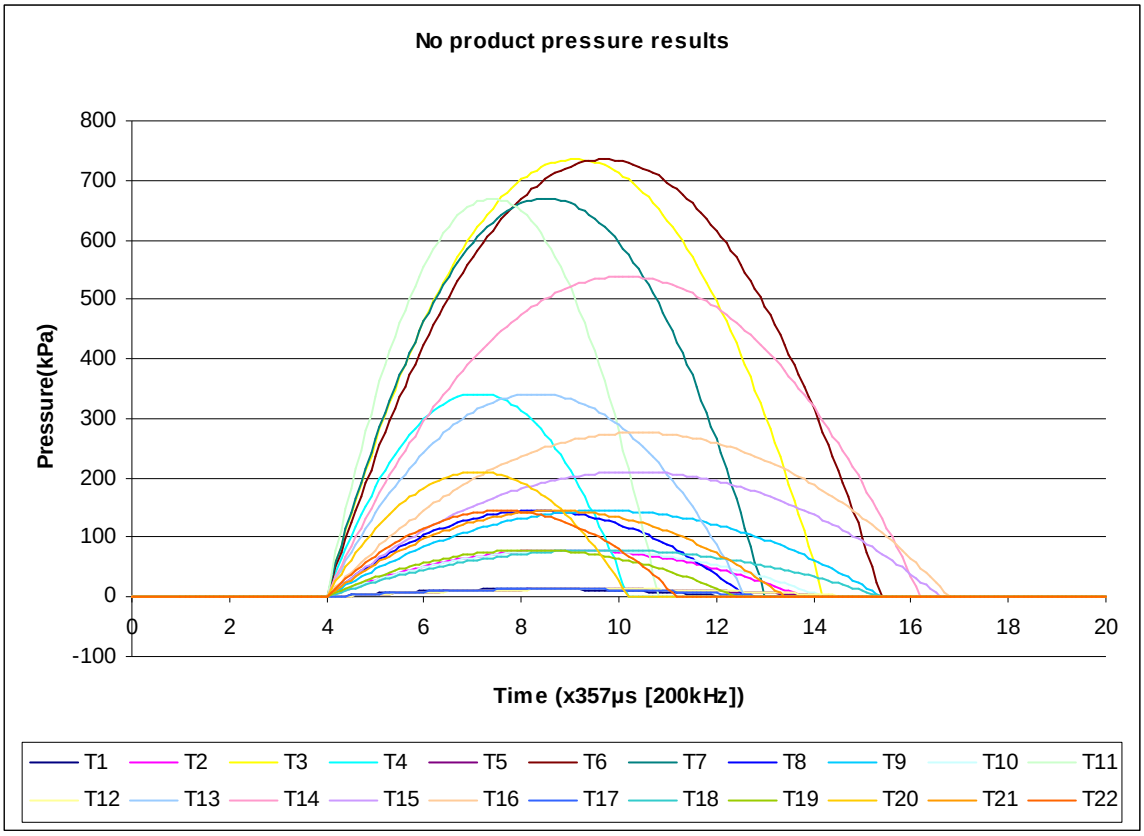

Figure 7.2: Results from pressure tests with no product

The pressure test results displayed an inverted parabolic shape when plotted versus time. All of the pressure test results indicated that the pressure returned to

zero after deflagration of the ballistite occurred. It is important to remember that the zero value for the pressure actually represents the ambient pressure with $P_i \times V_i = P_f \times V_f$. The variances in the pressures represented in figure 7.2 indicate the variance of the system. This was done in order to determine the variance that the system introduced into the pressure results of each individual product.

7.5.2 Discussion and analysis

The distribution of the pressure test results of the system without any stemming product was non uniform and no clear category separation was visible in these pressure test results (figure 7.2). The relationship between the volume and the pressure of the individual test runs was investigated and the results are provided in figure 7.3.

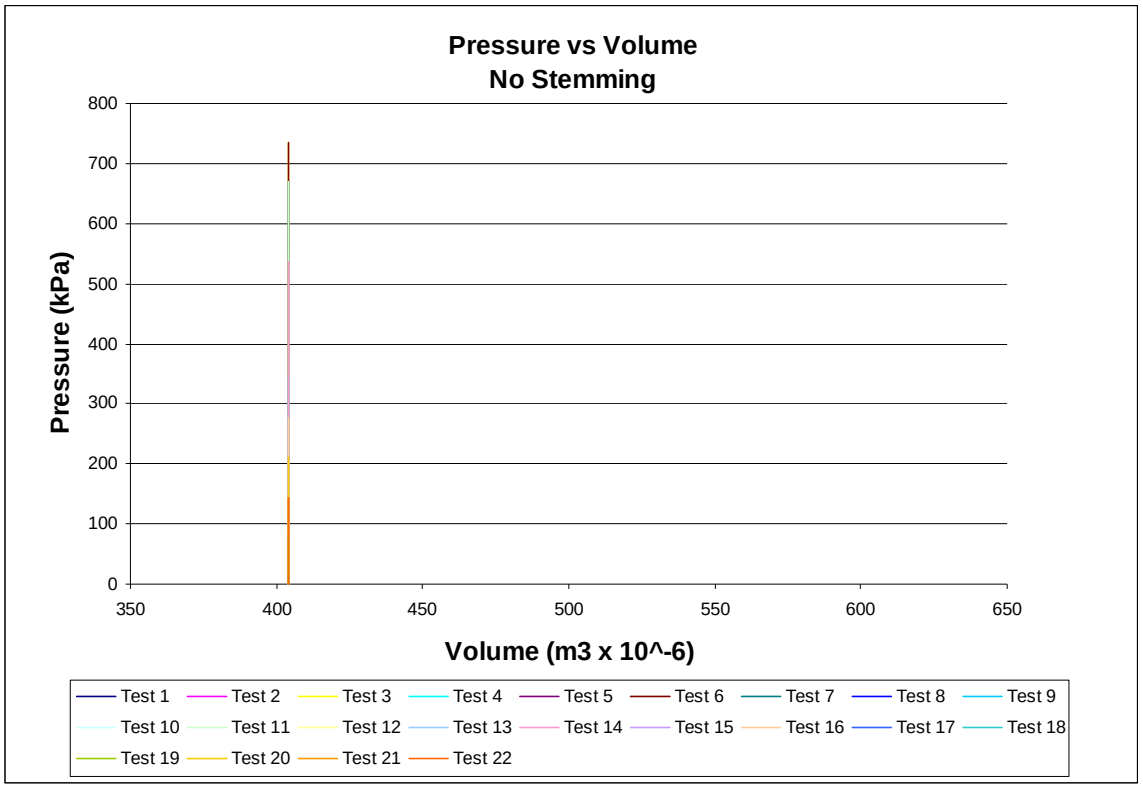

Figure 7.3: Pressure versus volume for the system without any stemming product.

Figure 7.3 clearly shows that as the volume in the pressure chamber increased, the pressure dropped. The resultant decrease in pressure did not show a hyperbolic shape but rather the inverse. The slope of the graph at V=401m^3 has $m \to 0$. As the volume increased with $V \to 635m^3$, the slope reduced with $m \to -1$. If pressure of the gas inside the chamber followed the laws of an ideal gas, the behaviour would have been inversely proportionate to that observed in figure 7.3. This phenomenon could probably be ascribed to the following: the fact that the pressure reduced to zero (atmospheric/ambient pressure) at the end of the test time.

7.5.3 Performance evaluation

Contrary to what was expected, the pressure tests results displayed a wide distribution. The variation in the pressure could only be ascribed to the inconsistent deflagration or detonation of the balistide. All the other factors were kept constant. These factors include:

1. Type of explosive
2. Mass of the ballistite
3. Position of explosives in blasting chamber
4. Position of detonator in explosives

The purpose of the tests without any stemming material was to determine the variance of the setup. The aim was to exclude the effect of the variance in the stemming material from the pressure calculations. A statistical analysis was conducted on the test results obtained from the pressure readings.

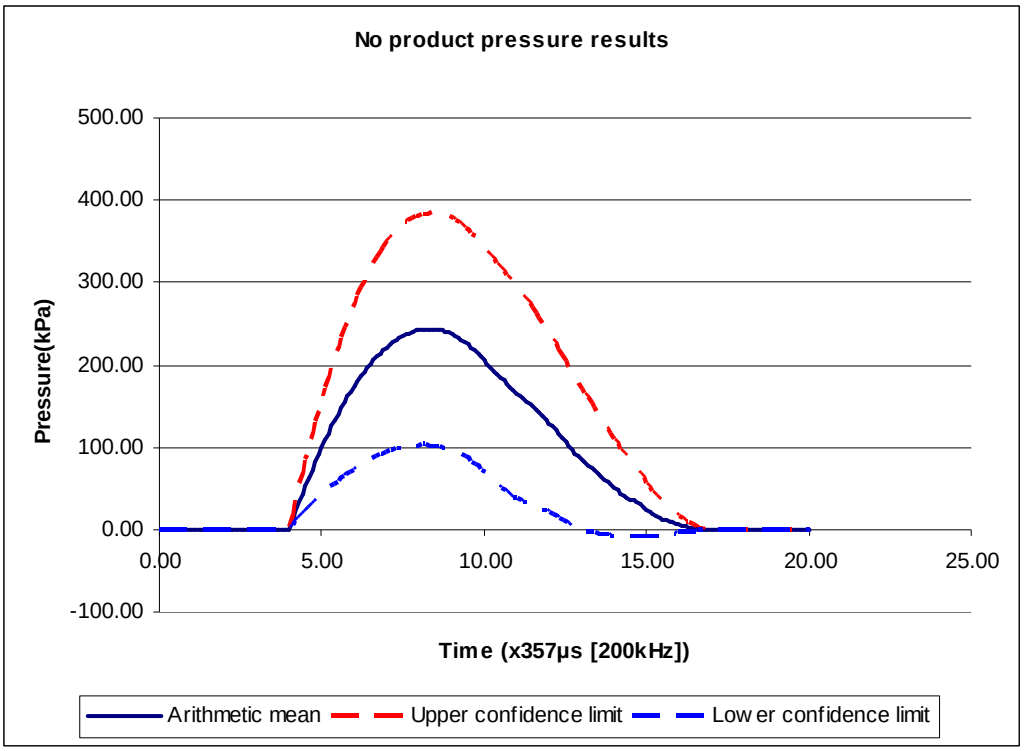

Figure 7.4: The arithmetic mean as well as the upper and lower confidence limit for no product pressure results.

The maximum force that would have been applied to a stemming capsule if one was inserted into the steel pipe was calculated using the maximum pressure in the vessel. The smallest force was calculated using the lowest local maximum pressure. The maximum force was achieved in the 3rd and 6th test run and was 668N, the lowest was achieved in the 17th test run, i.e. 12N. The interval of the mean at 95% confidence, at the time of maximum pressure, was $u = 350N$ and $l = 93N$.

7.6 Product A

7.6.1 Pressure test results

The pressure test results are indicated in figure 7.4. The stemming product did not remain in the pipe after detonation for any of the test runs. The pressure tests did not indicate a clear difference between individual groups. The results indicated a

more random distribution. The maximum pressure that product A was able to withstand was 1129kPa. The minimum pressure was 210kPa.

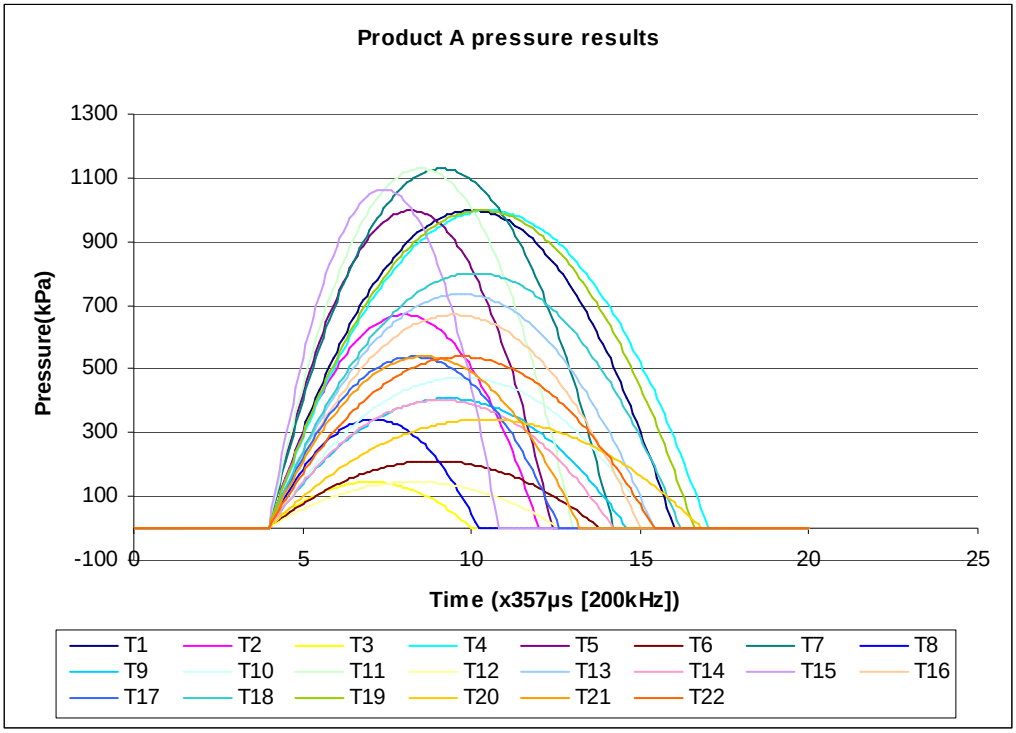

Figure 7.5: Results from pressure tests for product A

The test results displayed a parabolic shape when pressure was plotted versus time. All of the pressure test results indicated that the pressure returned to zero after ejection occurred. This indicates that the stemming plug was not retained in the hole but instead ejected. The time of ejection coincided with the maximum pressure value for all of the test runs.

7.6.2 Discussion and analysis

The distribution of the pressure test results of product A is non uniform and no clear category separation was visible in these pressure test results (figure 7.5). The high variance evident from the figure is suggesting that the product used in the test varies in its ability to withstand borehole pressure, from one capsule to another. If the pressure variance of the test runs where no stemming was used are considered, it is evident that the variance of the pressures generated by the

ballistite also plays a role in the consistency of the pressure results. Another factor that must also be considered is the human factor. Each stemming capsule has been manually loaded, and even though care was taken to stem the hole as consistently as possible, the human factor could well have had an influence. For example, a variance in pressure applied when stemming material was manually inserted, variance in moisture content and alignment in the blasthole. The relationship between the volume and the pressure of the individual test runs was investigated and is provided in figure 7.6.

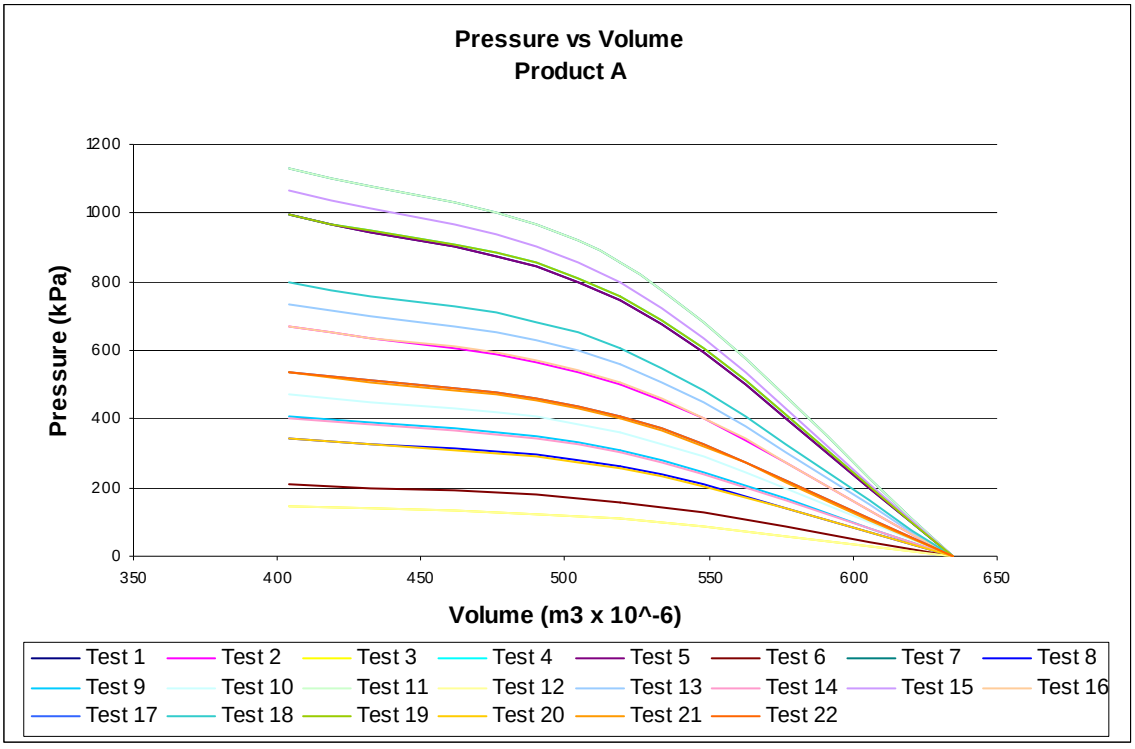

Figure 7.6: Pressure versus volume for product A

The pressure versus volume graph (figure 7.6) indicates the reverse of the relationship expected between pressure and volume for an ideal gas. This phenomenon could probably be ascribed to the following: the fact that the pressure reduced to zero (atmospheric/ambient pressure) at the end of the test time. The non-linearity of the pressure volume relationship indicates that it is a non-ideal system. An ideal system would have yielded a linear relationship.

7.6.3 Performance evaluation

It is difficult to determine a consistent trend on the performance of this product. The possible reasons for this observed inconsistent performance were discussed in section 7.6.2 above. The inconsistencies in the performance of the balistide could have contributed to the inconsistent performance of the stemming product tested. It was noted during the test runs that the stemming product was shot out the hole at high velocity. The product was completely disintegrated. This was evident from the size of the debris that was picked up in the vicinity of the test site. The product was not able to withstand the substantial pressure that was exerted on the product from the pressure in the blast chamber.

There were some difficulties experienced during manual loading of product A into the blasthole. The tolerance of the diameter of this product was ±2mm. Some samples of product A were oversized and hence, had to be reduced in diameter to ensure a snug fit in the hole.

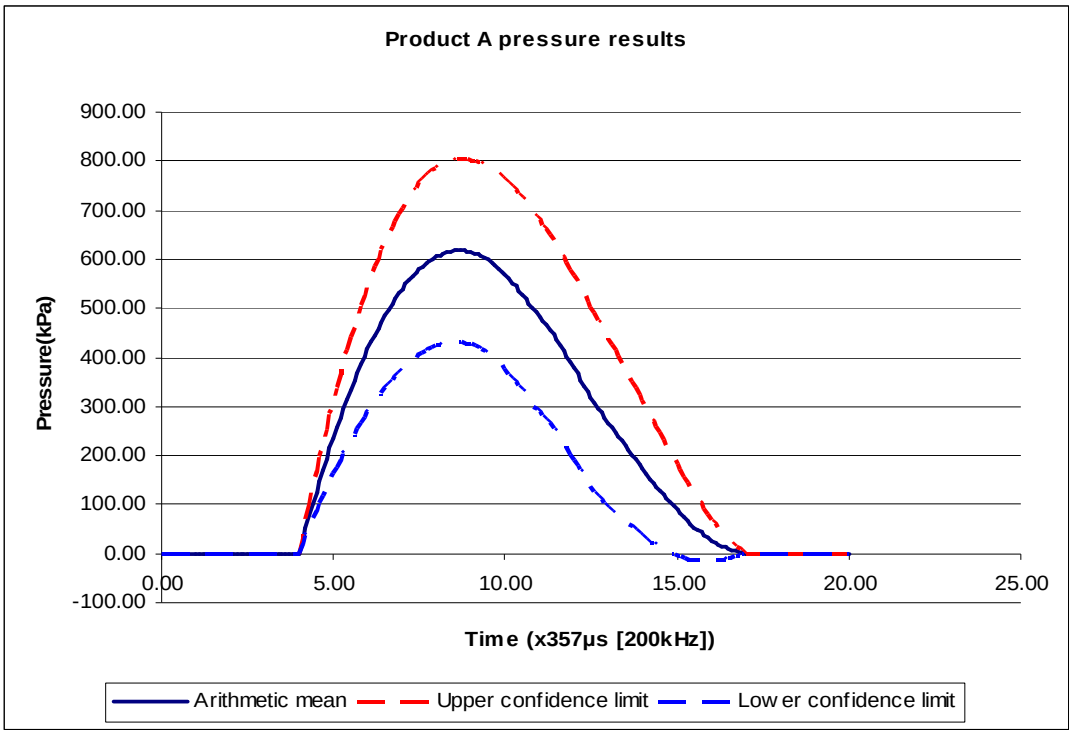

Figure 7.7: The arithmetic mean and the upper and lower confidence limit derived from the pressure test results of product A.

The maximum pressure that product A was able to withstand was determined by the value of the force applied to the stemming at the point just before movement of the stemming material. The maximum force was achieved in the 7th and the 11th test run and was 1017N, the lowest was reached in the 3rd and the 12th test run and was 131N. The interval of the mean at 95% confidence, at the time of maximum pressure was $u = 731N$ and $l = 392N$.

7.7 Product B

7.7.1 Pressure test results

The discussion on the pressure tests that was used to determine the performance of these products is provided in chapter 5. The data represented graphically in figure 7.8 below have been altered in an effort to eliminate starting time differences.

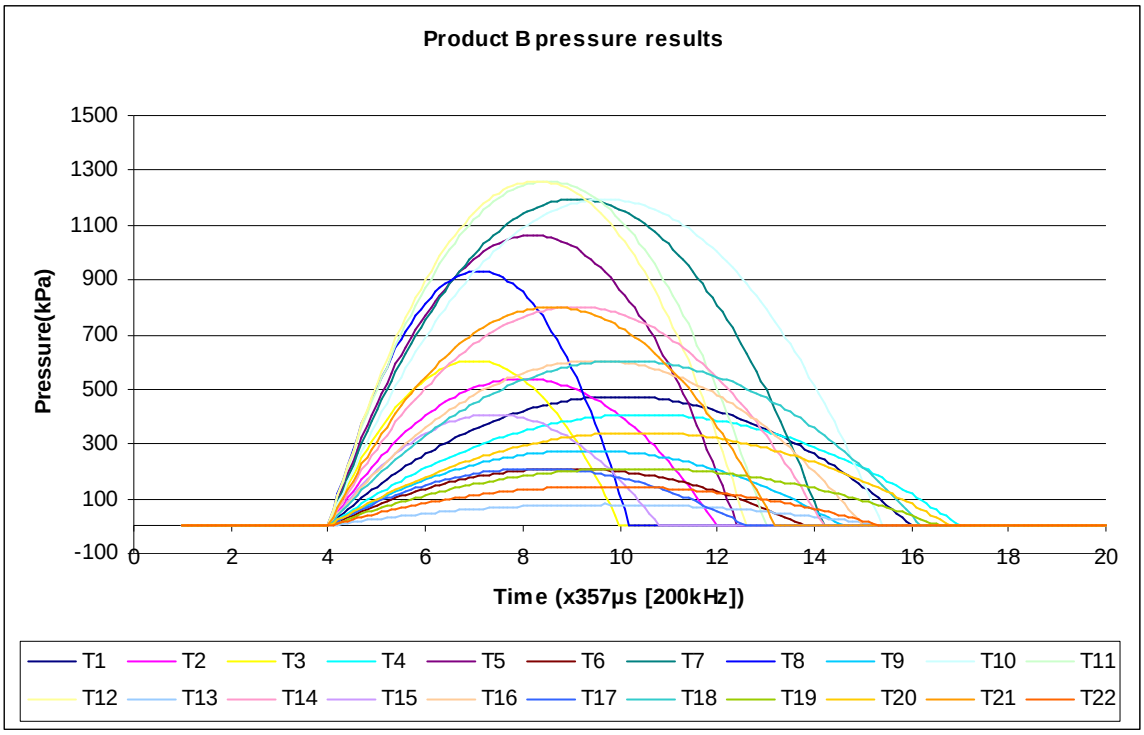

Figure 7.8: The pressure change over time for all the tests for product B.

The rate at which the pressure is increasing is variable. This is due to the variability both, in the pressure generated by the ballistite, and the diameters of the stemming products.

7.7.2 Discussion and analysis

The pressure versus volume graph can be mapped using the values above, with:

$V_i = V_A = 404.0 \times 10^{-6} m^3$ (figure 6.6)

$V_f = V_C = 634.5 \times 10^{-6} m^3$ (figure 6.7)

And $V_B = \frac{V_A + V_C}{2} = 519.25 \times 10^{-6} m^3$

The pressure-volume relationship that the stemming product experienced over time can now be graphed. It would only be of value to graph the pressure-volume relationship if there had been a change in volume. Therefore, it is important to determine if the stemming product moved, when it started moving and at what time it left the hole (figures 6.6 and 6.8).

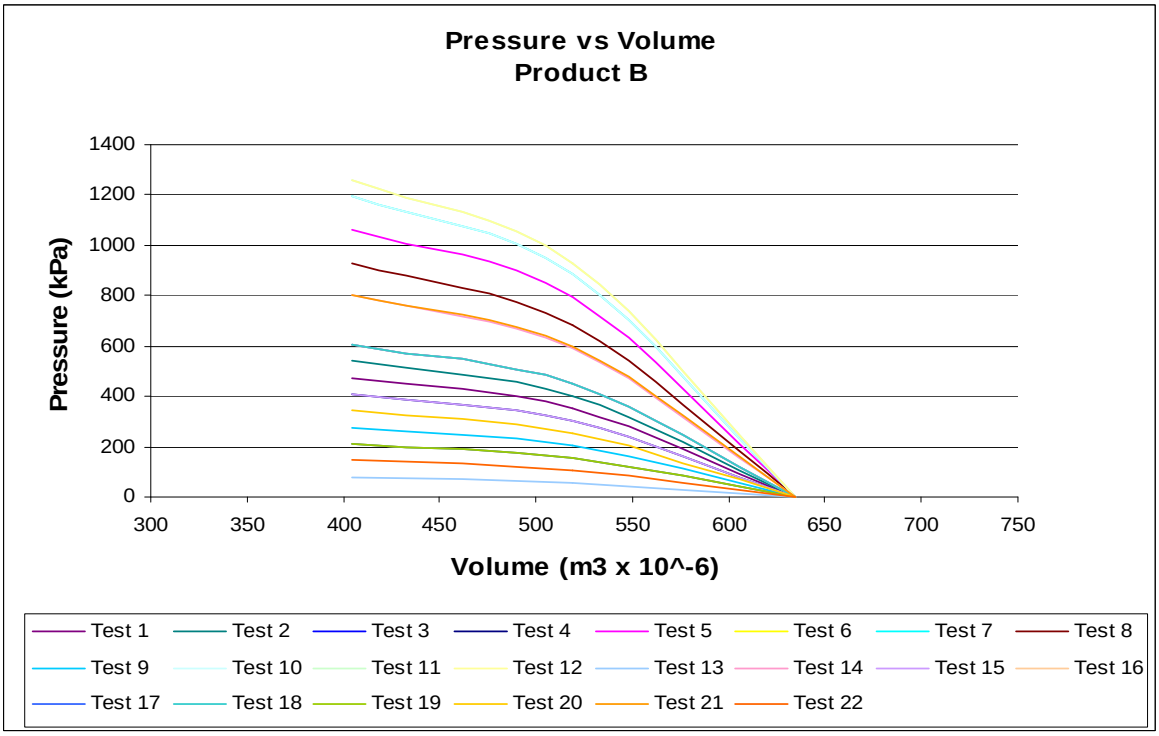

Figure 7.9: The pressure volume relationship for product B.

The statistical parameters that have been determined from the pressure test results from product B are indicated in figure 7.10 below. The interval about the mean at a 95% confidence limit widens from the fourth time unit to reach the widest distribution at peak pressure. The interval about the mean narrows down again to a small interval about the mean at the 16th time unit (figure 7.10). At maximum pressure a mean of 589kPa was recorded. At this point the confidence about the mean of 227kPa was recorded resulting in an upper confidence limit of 816kPa and a lower confidence limit of 362kPa.

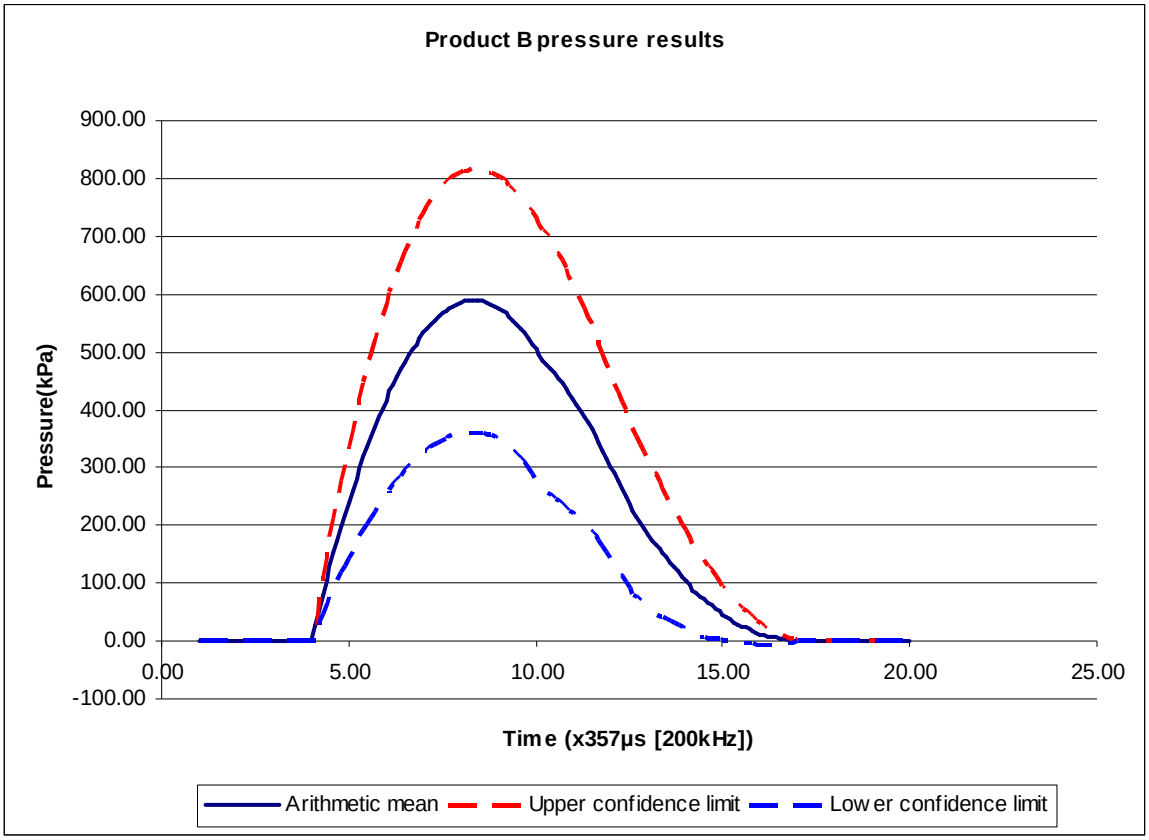

Figure 7.10: The arithmetic mean as well as the upper and lower confidence limit of product B.

7.7.3 Performance evaluation

Product B was designed to utilize the “interlocking effect” of irregular shaped particles. The concept is based on the theory that if a force is applied to the one

side of the stemming ampoule, the stemming ampoule would deform. This deformation would then cause the normal force working perpendicular to the sidewalls of the hole to increase. The interlocking effect would then cause individual particles to "interlock" with one another and therefore increase the normal force and hence, increase resistance to movement of the ampoule. None of the test runs produced any resistance to movement. All capsules were blasted directly out of the steel pipe. The maximum pressure was achieved in the 11th and 12th test run and was 1256kPa.

For all of the test runs, there was no increase in the frictional force exerted on the sidewalls during the time that the pressure was applied and each stemming capsule was pushed out the blasthole without further deformation. This is clearly visible in the pressure curves seen in the figures above.

The maximum pressure that the stemming capsule can take is determined by the value of the force applied to the stemming at the point just before movement. The product displayed a wide distribution of pressures but without outliers. The maximum resistive force was observed in the 11th and 12th test run and was 1144N, the lowest was observed in the 13th test run and was 72N. The upper and lower confidence limits were determined using a 95% confidence interval. The upper and lower confidence limits were 741N and 328N respectively.

7.8 Product C

7.8.1 Pressure test results

As described in chapter 6, product c was fundamentally different from all the other products in that it is aerosol foam contained in a canister and not a type of longitudinal ampoule or capsule manually positioned in a blasting hole. A detailed discussion is provided in section 6.7.1 and 6.7.2. Figure 7.11 graphically summarises the results of the high pressure tests for product c.

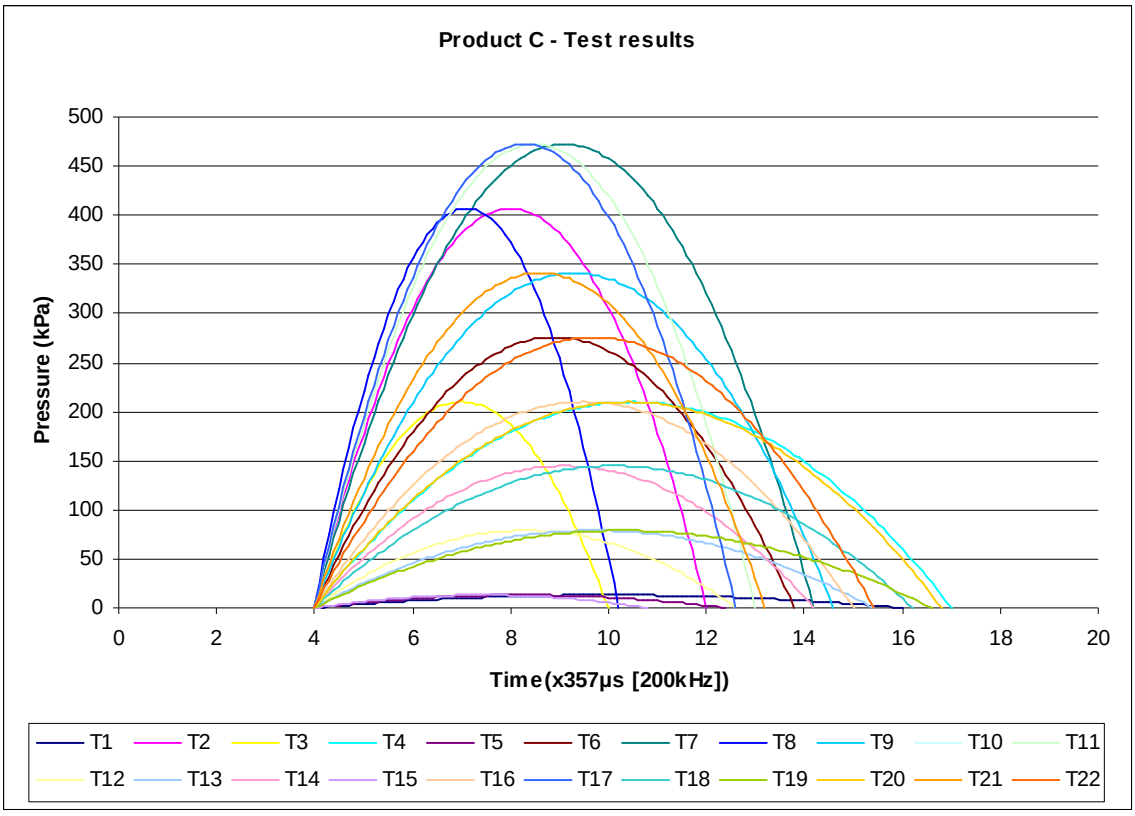

Figure 7.11: The pressure test results from product C.

The variance in the rate at which the pressure is increasing is indicative of the variance the pressure generated by the ballistite. The variability of the tolerances of the stemming product plays a lesser role as it is diminutive.

7.8.2 Discussion and analysis

Similarly, the pressure versus volume graph can be derived using the values above, with:

$V_i = V_A = 404.0 \times 10^{-6} m^3$ (Figure 6.6)

$V_B = 519.2 \times 10^{-6} m^3$ (Figure 6.7)

$V_f = V_C = 634.5 \times 10^{-6} m^3$ (Figure 6.8)

With reference to figure 7.1 the values of V_A and V_B were used together with V_C to determine the relationship between the pressure and the volume during detonation. The pressure-volume relationship can now be graphed. If $\Delta V = \Delta P = 0$, then plotting the relationship between the volume and the pressure would be of no value.

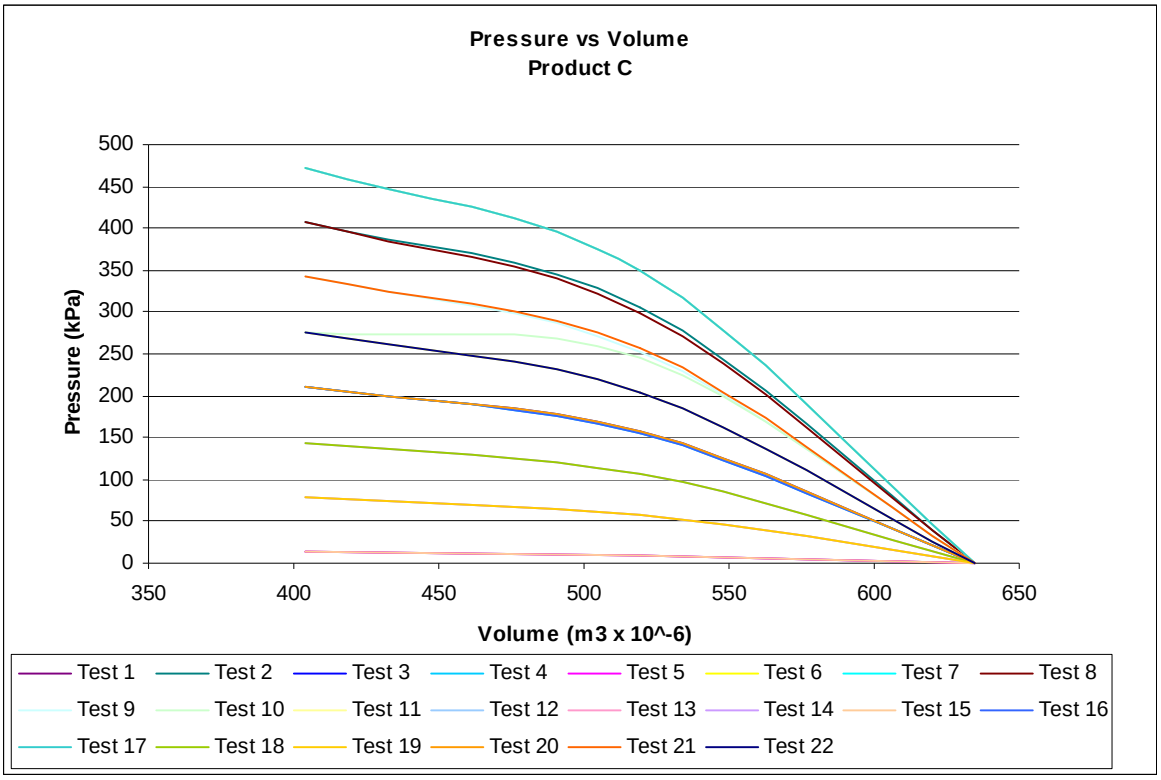

Figure 7.12: Pressure volume relationship for product C.

For all of the test runs for product C, all the capsules were ejected. Therefore, for all 22 test runs a change in volume occurred. From figure 7.12 the following mathematical assumptions can be made:

$$V_C - V_B = V_B - V_A \qquad \text{Equation 7.4}$$

However, for the pressure the same relationship does not apply. In this case is:

$$P_C - P_B > P_B - P_A \qquad \text{Equation 7.5}$$

This could indicate that the stemming product does not move out the hole at a constant speed but tends to increase speed during ejection.

7.8.3 Performance evaluation

The results from the test runs of product C were similar to the results obtained during the test runs with no product in the test vessel. The deformation that the stemming product experienced would be difficult to determine as the degree of deformation that the foam experienced depends on the degree of curing that occurred. Notably, the design concept of this product is uniquely different to those of the other products. The functioning of this product does not depend on the actions of the normal force acting on the sidewalls of the pipe, but rather the amount of friction that the product experiences due to the ability of the foam to stick to the inner walls of a blast hole.

For all the test runs for product c, there was no increase in the frictional force exerted on the sidewalls during the time that the pressure was applied. The statistical results indicated a wide distribution of the data around the arithmetic mean. Hence, the data are highly variable and the mean is unlikely to be a reliable representation of the data. The maximum pressure that the aerosol foam can take was determined by the value of the force applied to the stemming at the point just before movement. Test run 7, 11 and 17 achieved the same maximum pressure. The maximum force required to remove the stemming from the hole was 429N. The minimum occurred in the 1st and the 15th test run and was 12N. The upper and lower confidence limits of the mean (204N) at 95% confidence, at the time of maximum pressure was $u = 283N$ and $l = 121N$.

7.9 Product D

7.9.1 Pressure test results

The pressure test results are indicated in figure 7.13. These test runs indicated a variety of different pressure performance patterns. During all of the test runs the plugs were completely destroyed and shot out of the hole of the test chamber.

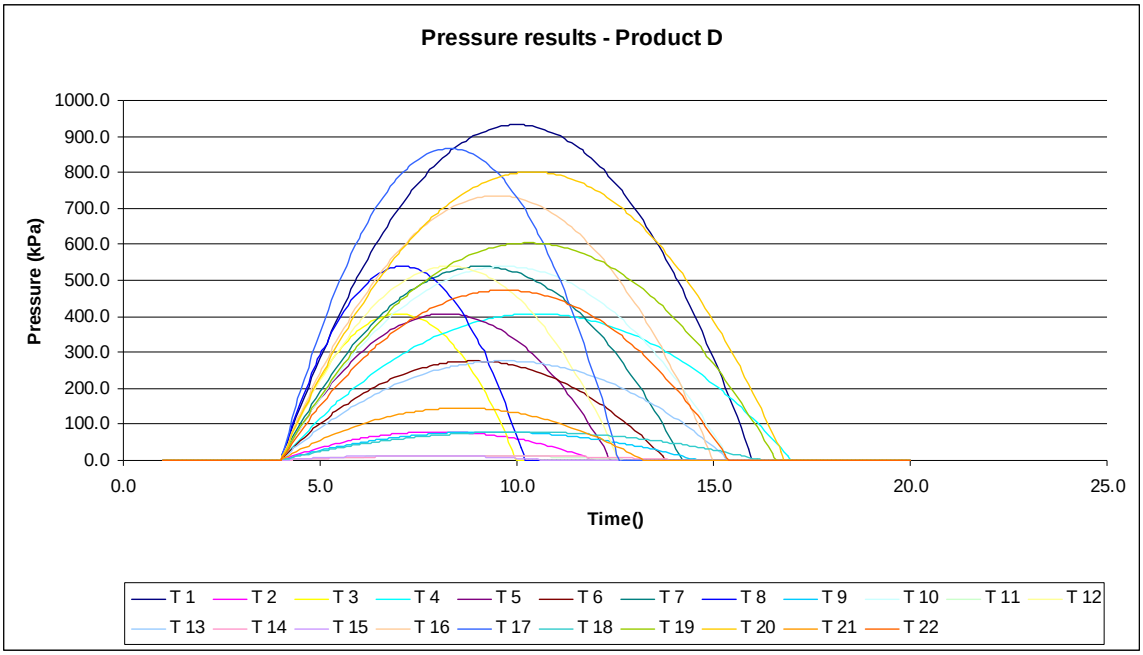

Figure 7.13: Results from pressure tests from product D.

There were no individual categories that could be identified. Figure 7.13 shows the range of pressures that was obtained during the test runs for product D.

7.9.2 Discussion and analysis

During all the test runs the stemming capsule was ejected immediately. The pressure curves follow a similar shape when compared to those of the other products. During the pressure application, the stemming product experienced deformation. This plug was designed to react with two movements and is explained with reference to figure 7.14:

During the first movement, the black rubber sleeve (part 6) moves up the red conical polymer wedge (part 5). This is the insertion stage. In the second movement of detonation, the aluminium shield (part 1) should flange open, and the rubber washer (part 2) should absorb some of the shock, giving the white polymer (part 3) time to move into the second black sleeve (part 4:).

Evidence of the last stage of deformation can be seen in figure 7.15.

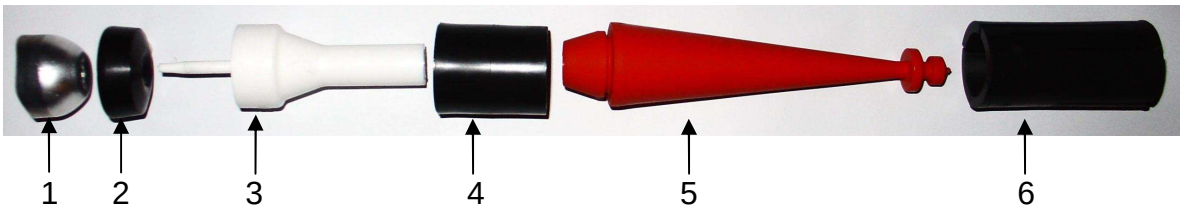

Figure 7.14: Product D separated into its individual parts

Figure 7.15: Deformation of part 3 and 4

The deformation displayed in figure 7.15 increased the normal force on the insides of the blasthole and therefore increased the friction that the plug experienced against the sidewalls of the hole. Mathematically it can be expressed as follows:

$$F_{friction} = \mu_s N \qquad \text{Equation 7.6}$$

Where:

$F_{friction}$ = friction force exerted on stemming (N)

μ_s = coefficient of static friction

N = normal force (N)

In the above equation, if the normal force increases and the coefficient of static friction stays constant, the frictional force exerted on the stemming will increase.

The pressure build-up was erratic and no consistent deformation behaviour was observed. This could be ascribed to the small differences in the applied pull force

that was used to secure the plug in position as well as the differences in pressure observed in the control run (section 7.5). Initially the force experienced by the plug was smaller than the maximum static frictional force. Mathematically it can be expressed as:

$$F_{ballistite} < F_{friction} \text{ with } \Delta F_{friction} \uparrow$$

This is followed by a moment where the frictional force has reached its maximum. In this scenario, the following mathematical rule applies:

$$F_{ballistite} = F_{friction} \text{ with } \Delta F_{friction} = 0$$

This is followed by a phase where the frictional force was overcome by the force due to the air pressure in the blasthole and then ejection of the stemming capsule occurred. Mathematically it can be explained as follows:

$$F_{ballistite} > F_{friction} \text{ with } \Delta F_{friction} \downarrow$$

The above cycle happened within 4 milliseconds (figure 7.13) and was observed for all test runs. Hence, there was an increase in pressure in the hole after the initial peak was observed.

Using the above mathematical relationship, the pressure volume relationship for each of the test runs can now be determined.

The pressure volume relationship of product D behaved inversely from the behaviour predicted for an ideal gas. This could be due to the influence that the explosion had on the gas pressures and the velocity that the projectile left the test equipment, causing a reduction in pressure immediately after ejection.

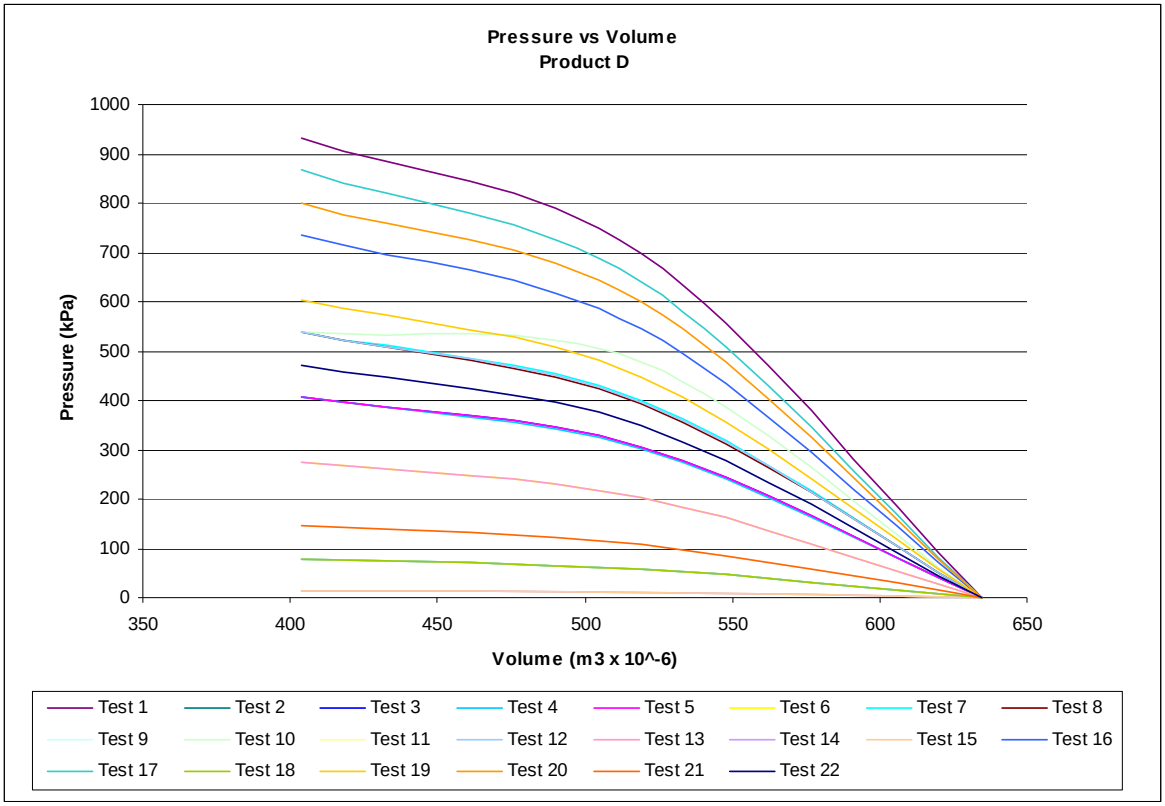

Figure 7.16: Pressure versus Volume for all the test runs of product D.

7.9.3 Performance evaluation

According to the theory on which the design of the product was based, the rubber sleeve must move over the white conical segment. This would then increase the normal force working perpendicular to the sidewalls of the hole. The stemming plugs were ejected before any significant pressure build up was displayed in the pressure curves.

The statistical parameters for product D indicate a maximum mean pressure of 374kPa after approximately 3 milliseconds (figure 7.17). The highest pressure was achieved in the 1st run and delivered a force of approximately 846N. The lowest pressure was achieved in the 14th test run and was 12N. The upper- and lower confidence limits indicate a wide distribution of values around the mean (340N). At

maximum pressure, the upper- and lower confidence limits of the product delivered a force of 484N and 190N. The confidence interval was determined at 95%.

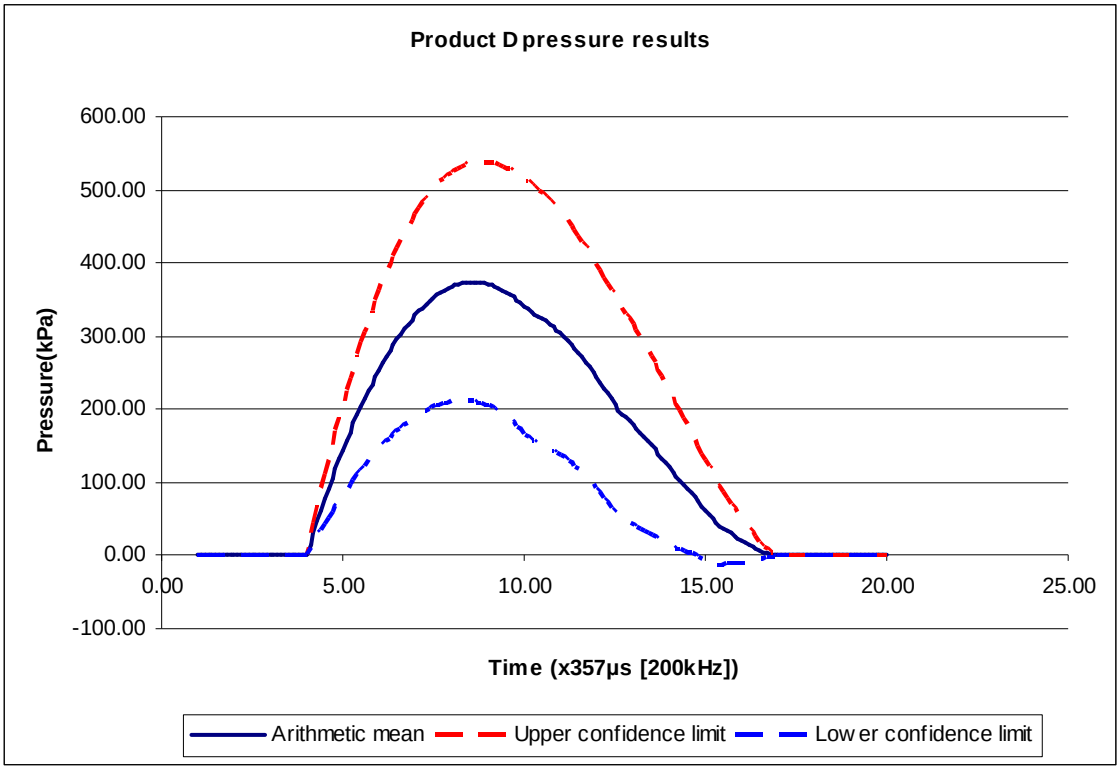

Figure 7.17: The statistical parameters from the pressure test results from product D.

7.10 Product E

7.10.1 Pressure test results

The pressure tests were performed on this product using the experimental setup discussed in section 5.2.

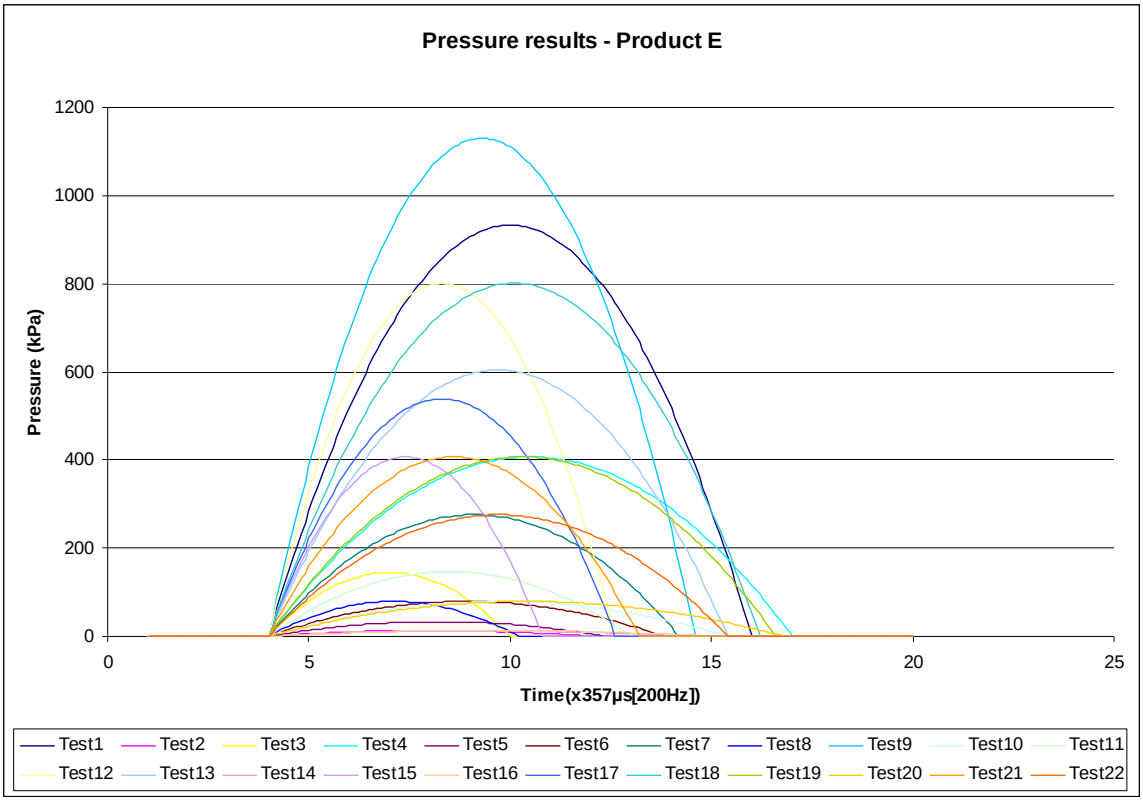

Figure 7.18: The pressure change over time for all the tests from product E.

The stemming capsule was ejected during all of the test runs. This product yielded inconsistent results (figure 7.18) which could most likely be ascribed to the non-homogeneity of the product's content. The maximum pressure was recorded in test run 9 and was in excess of 1000kPa.

7.10.2 Discussion an analysis

The design and method of application of product E was similar to that of product B however a couple of distinctions can be made. Product B consists as described earlier of bentonite that have hydrophilic characteristics. Product E however consists of two different types of gravel, with a finer gravel to the front and a coarser gravel to the back. In this case the stemming product also failed to be retained during all the test runs. This indicates that the initial static friction between the sidewalls of the blasthole and the stemming product was inadequate to cause

retention of the capsule. With adequate deformation of the stemming product by the applied pressure, the normal force against the sidewalls does not increase as increased pressure is applied. This would result in premature ejection of the stemming capsule.

Mathematically the above process can be expressed as:

$$F_{ballistide} \uparrow > F_{friction} \rightarrow$$

where:

$F_{ballistide} \uparrow$ indicates that the force due to the compressed air increases over time (phase A figure 6.18)

$F_{friction} \rightarrow$ indicates that friction in the blasthole stays constant

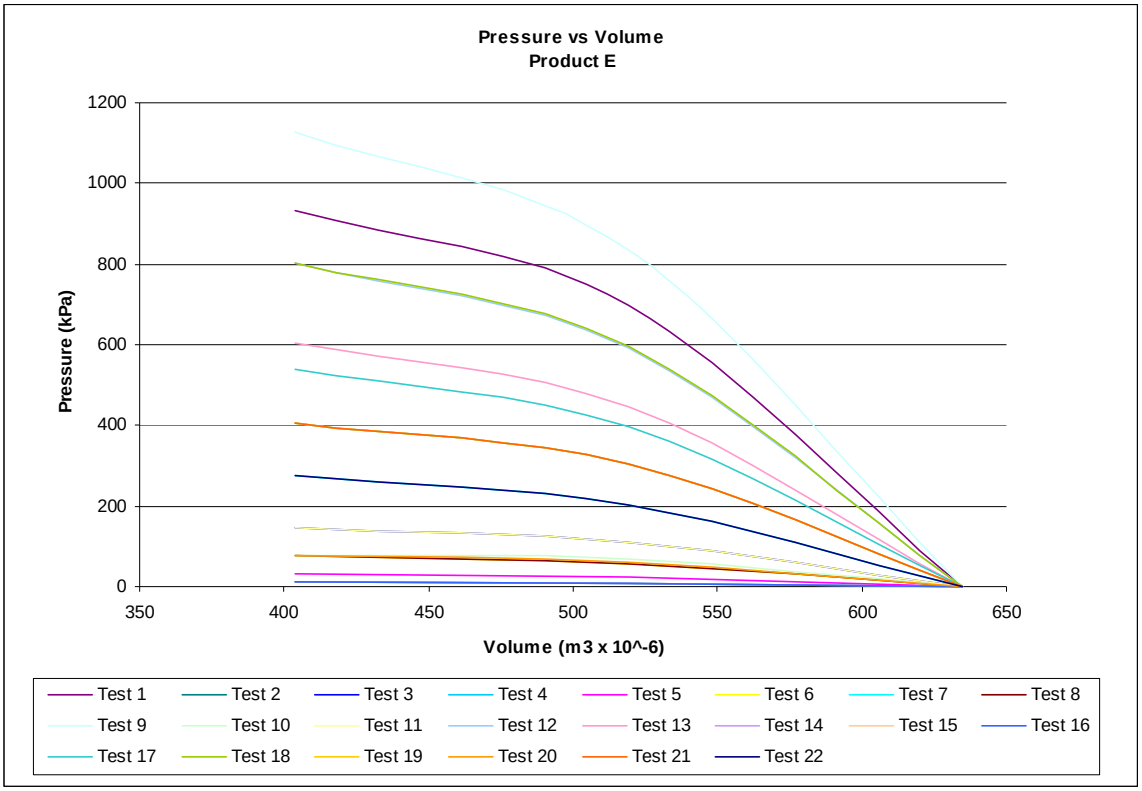

Figure 7.19: Pressure versus Volume for all the test runs of product E.

As described earlier, the pressure-volume relationship does not relate to Boyle's law. Hence, the pressure-volume relationship can be expressed as below:

$P_i V_i \neq P_f V_f$ however, with $\Delta P \neq 0$ and $\Delta V \neq 0$

The initial pressure was taken to be the maximum pressure. The initial volume is the volume in the pipe of the test rig just before movement of the stemming capsule occurred. The final pressure is the pressure just after complete ejection.

7.10.3 Performance evaluation

The test runs exhibited pressures between 200kPa and 500kPa. In all the test runs there was no increase in the frictional force exerted on the sidewalls during the time that the pressure was applied. No deformation was observed after pressure application.

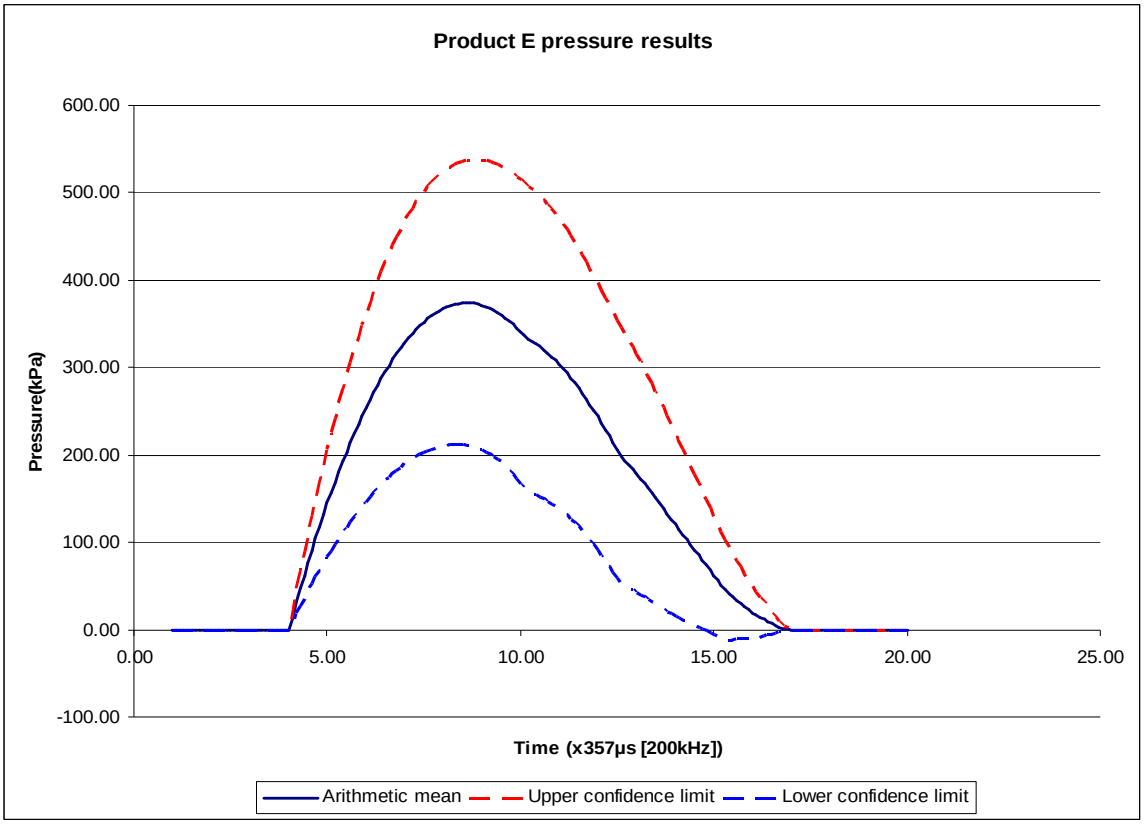

Figure 7.20: The statistical parameters for Product E.

The statistical parameters for product E are provided in figure 7.20. The widest distribution of the pressures around the mean was observed at maximum pressure. A maximum deviation of 330.27 kPa was recorded after 3.4 milliseconds. This explains the large difference between the upper and lower confidence limits in the figure.

A maximum force of 1025N was generated in test run 9. The smallest force that occurred during any test run for this product was observed in the second test run and reached a force of 11.7N. At maximum pressure, the upper- and lower confidence limits of the product delivered a force of 488N and 192N respectively. The confidence interval was determined at 95%.

8 SUMMARY OF RESULTS

8.1 Lessons learnt

8.1.1 Literature

Although the literature contains much information on burden and spacing design for blasting practices, it reveals much less on the design of the stemming region and very little on stemming material specifically. It is generally assumed that the stemming will hold until the collar breaks. The experience of many professionals in the field of blasting shows that this is not a correct assumption unless care is taken in selecting the stemming material. The majority of the evaluations on stemming have been carried out in surface mines. Until this study, no stemming evaluation testing rig existed for underground blasting designs.

8.1.2 Low pressure

At low pressures (0 – 600kPa) the stemming materials could be separated into categories that behaved differently during pressure testing. The first category that was identified was characterised by the stemming capsule being ejected without any pressure build up. The majority of the test runs could be grouped into this category. Figure 8.1 below indicates the arithmetic mean of this category for each product.

It should be noted that the final horizontal line after each graph has reached maximum pressure only indicates the resistance to airflow in the system. Hence, what figure 8.1 indicates, is an index of the amount of residue that was left behind in the blast hole after ejection of the stemming plug occurred. This gives no indication as to the actual performance of the product.

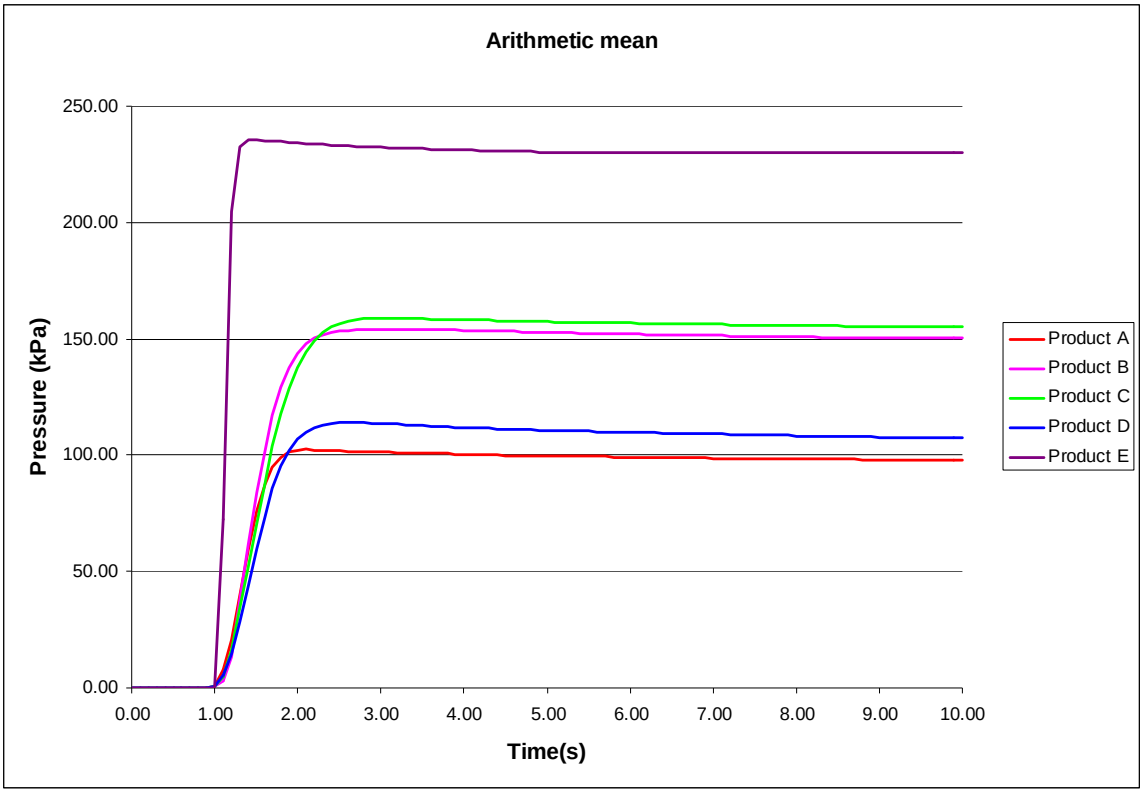

Figure 8.1: The arithmetic mean of each of the products where a number or all of the stemming capsules were ejected during the pressure testing.

The test results reveal that product E left substantially more residue in the blast hole than any of the other products, whereas product A produced almost no residue after ejection (figure 8.1).

The second category identified included those tests where the stemming product was ejected after a pressure build-up. During these test runs the stemming capsule was retained in the hole after the pressure reached the system's maximum. One to two seconds passed and then the stemming capsule was ejected at high velocity. This pattern is clearly shown in figure 8.2 below.

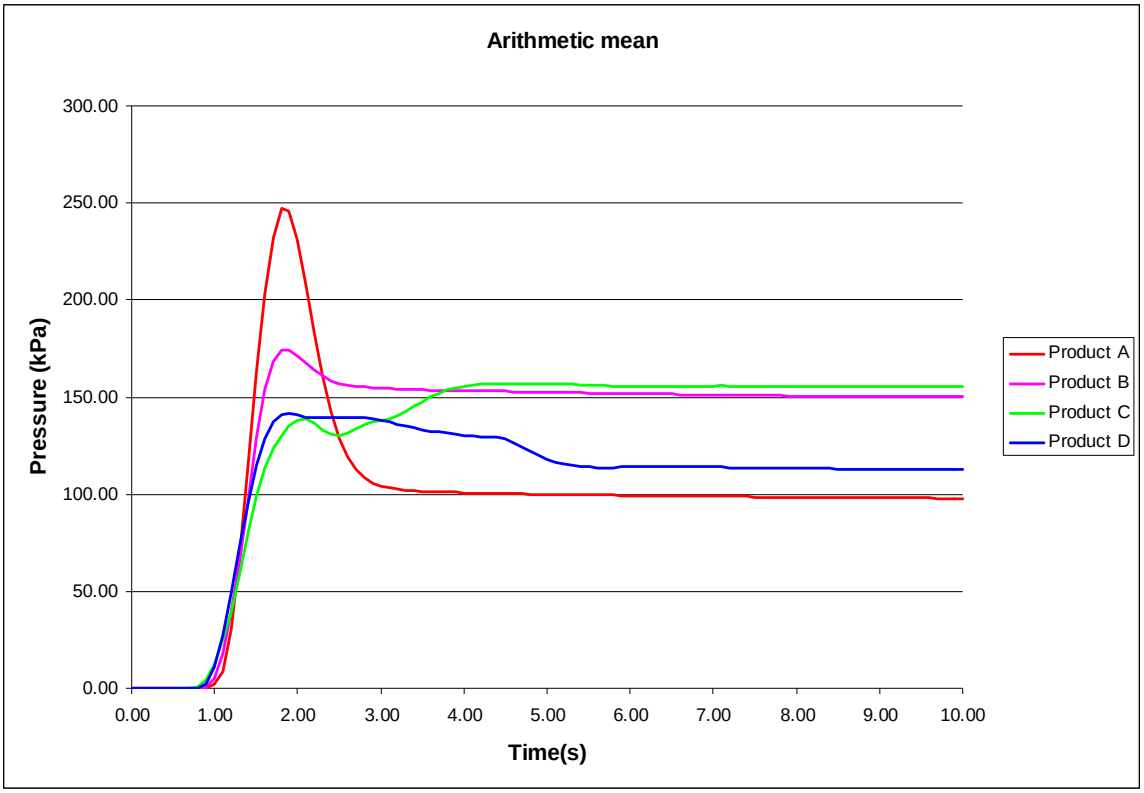

Figure 8.2: The arithmetic mean of each of the products where a number or all of the stemming capsules were ejected after a pressure build up.

Figure 8.2 indicates that product A was able to withstand substantially higher pressures before ejection than any other product. Product B behaved similarly to product A but reached a lower maximum pressure. In contrast to this, product C indicated a local maximum and then, after a local minimum, showed a gradual increase to reach maximum pressure. This could be ascribed to the fact that product C is a porous foam with a high level of adhesiveness. As pressure is applied, the inner core of the stemming plugs moves towards the opening of the hole. At the time that this inner core reached a 'fresh' area, the adhesiveness comes into play again and increases the pressure yet again. Another more likely explanation for the behaviour of product C is the escaping of gasses through the middle or core while leaving foam behind against the sidewalls of the hole. Product D firstly indicted a maximum pressure, then movement occurred, but it managed to maintain a pressure similar to that of its maximum. The product was able to

maintain this pressure for 2.5 seconds. This was followed by another drop in pressure when the product was finally ejected. Product E did not show any pressure build-up before ejection.

The third category that was identified contained those test runs where the stemming capsules were not ejected. Only two of the products, products A and D , were able to resist all the air pressure that was applied to it until the system reached its maximum pressure.

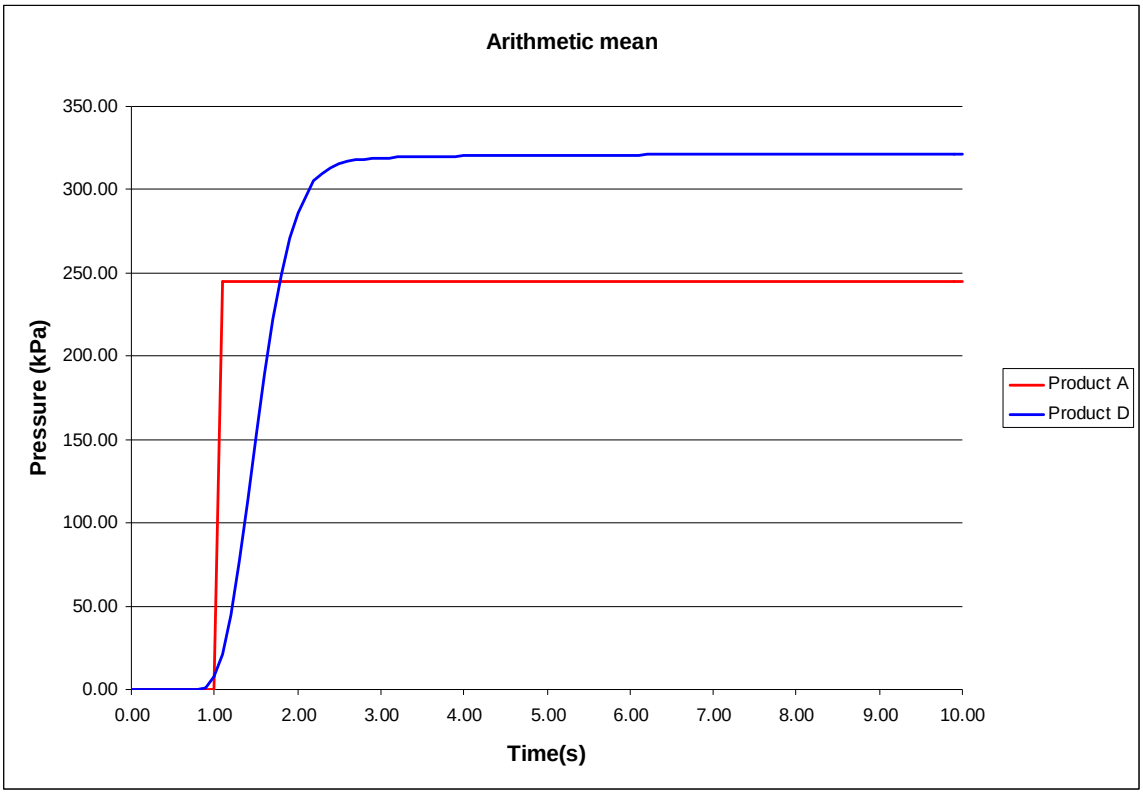

Figure 8.3: The arithmetic mean for products A and D where a number or all of the stemming capsules were not ejected during the pressure testing.

Figure 8.3 indicates that product D was, on average, able to maintain pressure better than product A. Product D has been designed with a wedge-cone configuration. This causes the forces applied to the one end of the plug to be directly proportional to the normal forces applied by the plug on the sidewall. The stemming plug must therefore disintegrate before it will be ejected from the hole.

This would be so if the plug was able to make a tight seal with the inner walls of the hole.

Box plots were used to statistically analyse the low pressure test results further. Although the use of box plots constitutes a simpler, descriptive statistical method, compared to the use of histograms or quantitative probability density functions, they do have some advantages. They provide a quick, graphic approach for examining one or more sets of data, without the need to test the assumption of the statistical distribution of the data. The assumption that data are normally distributed can be a hindrance in statistical analyses because binning techniques can heavily influence the histogram by assuming the position of the median. Incorrect variance calculations will heavily affect the probability density function.

The relevance of the application of the statistical tools such as the arithmetic mean and standard deviation, in this context, could be irrelevant to assist in an improved understanding of the behaviour of the stemming. Other less sophisticated analyses would be recommended.

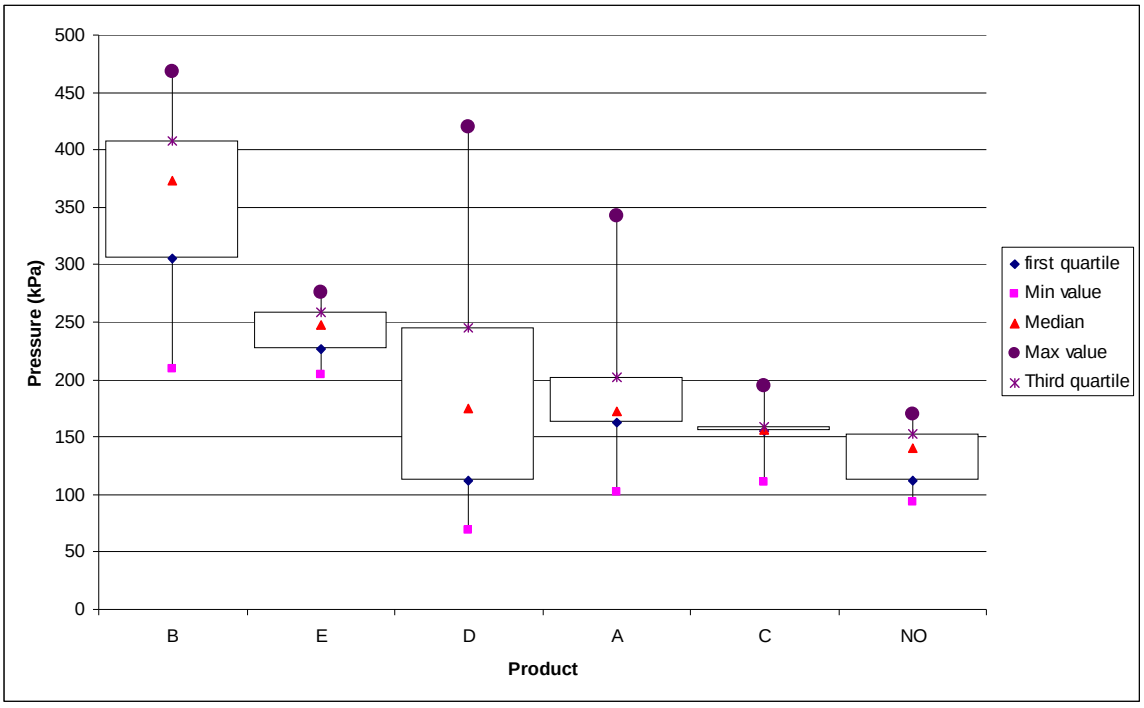

Figure 8.4: Box plot distribution for the low pressure tests of all the products.

The box plots graphed in figure 8.4 indicate the distributions of the peak pressures for all the products tested. The products have been arranged from the highest median value on the left to the lowest on the right. This figure clearly shows that product B performed better than all the other products in terms of the value of the median, as well as the distribution of the second and third quartile. An inter-quartile range of 240kPa was indicated for product B. Product E displayed the narrowest distribution when compared to all the other products. The difference between the minimum and maximum values for product E was only 71kPa. A median value of 248kPa was calculated for this product. Product D indicated the largest inter-quartile range of 132kPa as well as the largest difference between the maximum and minimum values. This difference was calculated at 351kPa. Product A displayed a relatively small inter-quartile range of 40kPa; however, a large difference between the maximum and minimum values is noted. The median value of this product was very similar to the value of the first quartile.

Product C displayed the smallest inter-quartile range at only 4kPa. This was expected for the control test run where no stemming was used. This phenomenon has been observed because for all the other test results, the variance caused by the system was excluded from the data. The lowest median was observed for the control test . This was an expected outcome. The product ranking was therefore as follows: B, E, D, A followed by C.

8.1.3 High pressures

At higher pressures the standard deviation of the products became larger and it became increasingly difficult to make clear distinctions between the individual products.

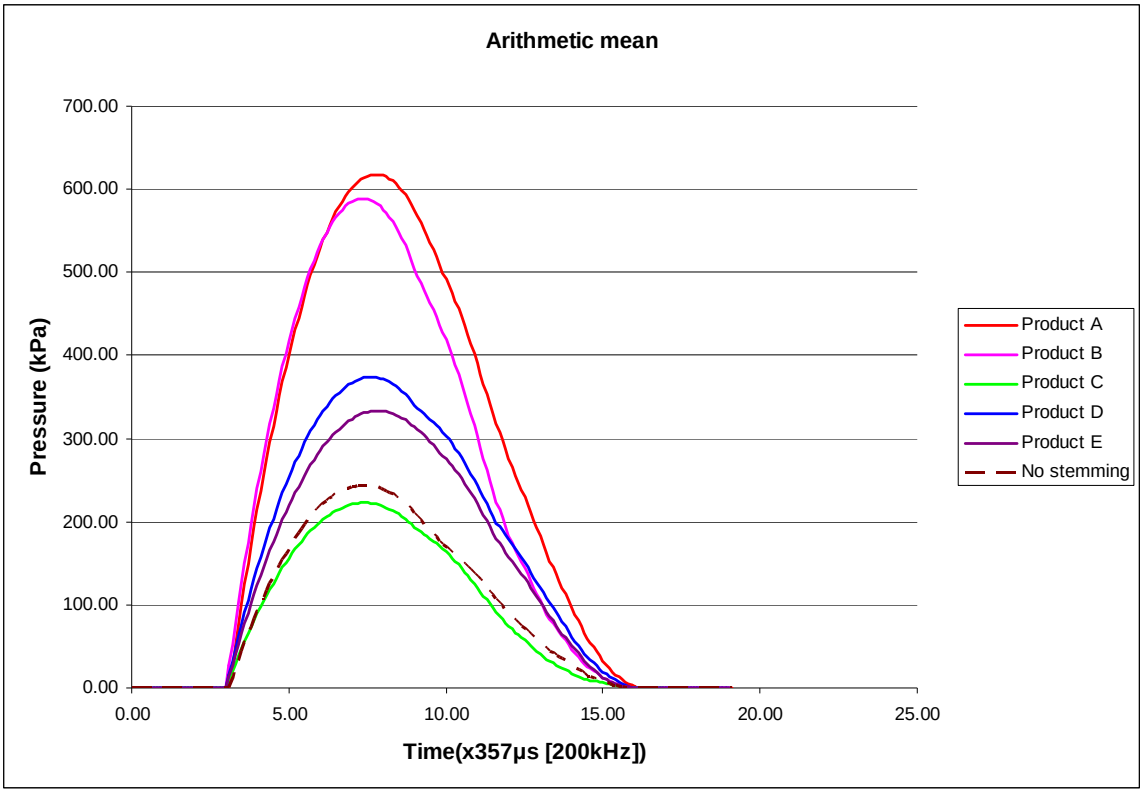

Figure 8.5: The arithmetic mean of all the products.

Figure 8.5 indicates that under the conditions specific to this study, it is more efficient to use product A, B, D or E, than no stemming at all. Figure 8.6 provides the box plot distributions for each of the products. The control test runs where no stemming was used have also been indicated.

The box and whisker plots indicating the lower, middle and upper quartile distributions are provided in figure 8.5. The red triangles indicate the median of each of these distributions. The products have been arranged in decreasing median value. The extreme outliers have been excluded from the data analysis. The limiting value of the extreme outliers was taken to be three times the inter-quartile range.

Maximum values of more than 1200 kPa have been reached by product B but product A produced a higher mean value. The inter-quartile ranges of product A and product B were very similar at 595 kPa and 607 kPa respectively. Product E

reached a larger maximum value than product D but with an inter-quartile range of 328kPa and 443kPa respectively.

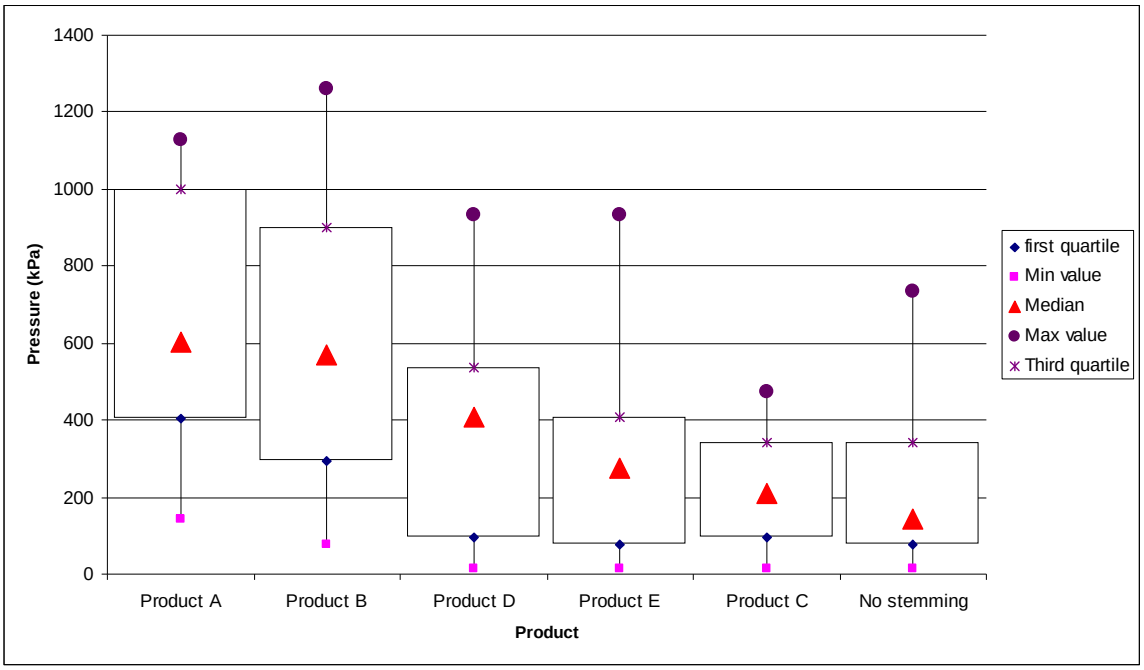

Figure 8.6: The quartile distribution for each of the products and the control test run (indicated as 'no stemming').

The median of product D was, however, higher than that of product E. A difference of 131 kPa was observed between the medians of product D and E. One extreme outlier from product E was excluded from the calculations. Figure 8.6 shows that both the median and inter-quartile range of product C were lower than that of the control run. The inter-quartile ranges were 246 kPa and 263 kPa for product C and the control run respectively.

A similar ranking of the products was observed when the median was used as a measure of performance. The product ranking was as follows: A, B, D, E followed by C and then the control run.

8.2 Testing the hypothesis

Classic hypotheses testing methods involve assumptions about the distribution of data. The most common assumption is that the data are normally distributed random variables. However, the data generated in this study are not normally distributed. The alternative to the classic parametric hypotheses tests are non-parametric hypothesis tests. In the latter, no assumptions are made regarding the distribution of the data. Non-parametric methods are often referred to as distribution free methods as they do not rely on assumptions that the data are drawn from a given probability distribution. The median of one data bundle is compared to the median of another by making use of a binomial distribution.

The significance of the difference in the median of the peak pressures of the separate test runs needed to be determined. The aim of the first hypothesis test was to determine whether there was a significant difference in the median value of the high and low pressure tests when no stemming was used.

The proposed hypothesis as stated in chapter 5, is as follows:

H_0: The median value of the high pressure tests when no stemming was used is not significantly higher than the median value when low pressure was used.

H_1: The median value of the high pressure tests when no stemming was used is significantly higher than the median value when low pressure was used.

The median value of the low pressure tests with no stemming has been calculated at: 140.5 kPa

Thus:

$H_0 = 140.5$ kPa

$H_1 > 140.5$ kPa

Let X denote the number of values of the high pressure tests that exceeded 140.5 kPa. The number of times that the peak pressure of the high pressure tests exceeded 140.5kPa was 14.

Thus:

$X \approx B(22, 0.5)$ with the observed value of X =14

Now:

$P(X \geq 14) = 1 - P(X \leq 13) = 0.143 > 0.05$

The null hypothesis is therefore accepted and it hence, it can be stated that: there is evidence, at a 5% level of significance, that there is no difference between the median values of the pressures obtained during the low pressure test when compared to the high pressure tests.

The above hypothesis was tested to determine if the pressure of the testing system for the 2nd phase was significantly higher than that of the 1st phase, when no stemming was used. If there is no significant difference in the pressure of the system alone, then the differences observed in the pressures in the 1st and 2nd phase was due to the change in the way that the stemming products reacted to the pressure that was applied.

The proposed hypothesis for the other tests is as follows:

H_0: The median value of the high pressure tests when a stemming product was used is not significantly higher than the median value when low pressure was used.

H_1: The median value of the high pressure tests when a stemming product was used is significantly higher than the median value when low pressure was used.

The above hypothesis test was conducted on each of the stemming materials and the results are displayed in table 8.1 below.

Table 8.1 Results of hypothesis testing

Product	P(x)	H_0
A	0.001	Reject
B	0.008	Reject
C	0.143	Accept
D	0.143	Accept
E	0.416	Accept
Control	0.143	Accept

The probability of the null hypothesis being true is represented by the column titled P(x) where x is the number of successes in the trail. A success is represented by an occurrence where no evidence exists (at a level of significance of 5%) that the median of the low pressure tests is lower than a specific high pressure test run.

In four of the six hypothesis tests that were conducted the null hypothesis was accepted. Hence, only two products displayed a positive difference between the high and low pressures measured, with a level of significance of 5%. Product A and product B displayed a significantly higher pressure during the high pressure tests when compared to the low pressure tests. A positive difference between the medians of the pressure for the low and high pressure tests was observed for product A and B and was 431kPa and 198kPa respectively.

9 CONCLUSIONS AND RECOMMENDATIONS

9.1 Conclusions

The purpose built high pressure test rig has not proved to be a capable tool to test stemming products under high pressure conditions. High and low pressure allow some performance differentiation to be made but in terms of performance prediction the low pressure test did not prove to be sufficient, with the relevant level of significance, to predict the performance ranking of the products under high pressure conditions.

If the assumption is made that an equivalent increase in pressure, from the low pressure tests to the high pressure tests, would have a similar effect on the deformation characteristics of each of the stemming products, it could be deduced that the product that indicated the highest resistance to movement at low pressures will also have the same ranking at high pressures. This will lead to the conclusion that the products reacted differently, in terms of deformation mechanics, during the low pressure tests when compared to the high pressure tests. The lack of a good correlation between the high and the low pressure test results will counter the facilitation of an accurate prediction of a stemming product's pressure performance at explosion reaction pressures.

Two products that displayed significantly higher pressure results than all the other products tested in the high pressure tests are of similar design. These designs are tried and tested and evaluated in numerous others studies, including those by Brinkman (1990).

The products have been ranked in table 9.1 according to the median value of their pressure test results. The ranking order has been determined according to these specific results and according to the specific conditions under which these tests were performed.

Table 9.1: Ranking of products

	High pressure		Low pressure	
Product	Median (kPa)	Rank	Median (kPa)	Rank
A	603.95	1	172.90	4
B	571.15	2	373.25	1
C	210.20	5	155.86	5
D	407.10	3	174.78	3
E	275.80	4	247.89	2
Control	144.60	NA	140.53	NA

Two of the five product categories seem to indicate loosely at low pressure what could be expected at high pressures. These are the homogeneous gravel ampoules (product B) as well as the mechanical plug categories (product C). Product B was ranked second during the low pressure tests and first during the low pressure tests. Product D was ranked fourth during the low pressure tests and third during the high pressure tests.

This study proved that there is a perceptible difference in the ability of stemming products, with different physical designs, to resist pressure in a blasthole. The test results indicated that the tried and tested designs perform better than the newer designs. It must also be noted that all the stemming products performed better than the control tests. This leads to the conclusion that any stemming is better than no stemming at all. What is still unclear is however, what would be the specific requirements from an ideal stemming product in terms of the material type, length diameter and exact design.

Temperature measurements at or close to the collar of the blasthole could indicate what temperatures a stemming product could be exposed to. This will help designers of stemming products to determine what type of material would be ideal for manufacturing a stemming product.

The primary focus of end users of stemming products should be to implement the application of stemming materials in small diameter blast holes and to closely monitor the use thereof. The secondary focus should be to determine the type of stemming product most suitable for the specific mining conditions.

Manufacturers of stemming products must take the following factors into account when designing their particular product:

- Stemming products should follow a simple design.
- Correct application of stemming products should be easy and require minimum care and supervision.
- Granular capsule products have indicated pressure performance superior to the newer designs.
- Correct product design for a particular hole diameter plays an important role in stemming product performance.
- The type of explosive used plays a role in stemming application

9.2 Recommendations for further work

The understanding of the performance of stemming material as well as the correct specifications and optimum use of stemming material will be difficult to achieve with the use of a theoretical modeling system. The number of parameters and assumptions that would be involved in the exercise would make any theoretical calculation extremely complex and the calculations impractical.

The parameters that need to be included in any stemming evaluation process should include at least the following: the rock type, the explosive type, length of stemming, stemming material properties, hole diameter, length of blasthole and fragmentation requirements. Since the focus is on the amount of explosive energy that is supposed to be transferred to the rock for good fragmentation, one needs to be able to determine what type of stemming material will perform best for specific rocks conditions. This will be extremely difficult to achieve with a theoretical model.

A more practical approach would be to persevere with the empirical route and develop a better experiment that will involve field tests. These field tests could include the testing of stemming in the current stemming test rig but should also include tests with small quantities of high explosives used in small blast holes in a homogeneous material (rock or concrete).

ACKNOWLEDGEMENTS

1. Dr RCW Webber-Youngman at the University of Pretoria (South Africa) for support and advice during masters studies

2. Prof Roger Thompson at the Curtin University of Technology (Australia) for guidance and couching during research

3. Dr J Steynberg at the University of Pretoria (South Africa) for statistical analysis of the test results

4. Barry Prout at African Explosives Limited for making funds and facilities available for the research

5. Dr Tom Szendrei who advised on the types of explosives that could be useful in this type of application

6. Hilton Dart for assistance and advice during the field testing

REFERENCES

1 Agnew W.G., Johnson J.A., and Mosier M., Stemming in metal mines. Progress report 4. BuMines RI 3646, 1942, 4pp.

2 Armstrong L.W and Moxon N.T. 1993. The effects of confinement on fragmentation and movement. BHP Research, Newcastle Laboratories, Shortland, N.S.W Australia

3 Brent G.F. and Smith G.E. 1999. The detection of blast damage by borehole pressure measurement. Published at SAIMM Sixth International Conference for rock fragmentation by blasting, 8-12 Aug. 1999

4 Britton and Gozon (1984) in the International Journal of Mining Engineering of 1984

5 Brinkmann J.R. 1990. An experimental study of the effects of shock and gas penetration in blasting, Chamber of mines research organisation, Auckland Park, South Africa.

6 Cancec, I.A., Gallardo, G.N. and Gutierrez, S.M. 2001. The importance of explosive confinement. Proc. Annual Conf. Explosives and Blasting Techniques, Vol. II, pp107-120.

7 Cook, P.M.A. Raimondi, R, and Lambert C.J, 1996. Phase-coherent transport in hybrid superconducting structures: The case of *d*-wave superconductors School of Physics and Chemistry, Lancaster University, Lancaster LA1 4YB, United Kingdom

8 Cowan, B.W., Otuonye, O.F. and Ligon, J.B. 1986. Analysis of stress waves induced from single hole stemmed blasts. Michigan Technological University, Houghton, Michigan, USA

9 De la rey M, e-mail correspondence.

10 Eloranta J.W., 1994. Stemming selection for large diameter blastholes. Proceedings of the twentieth annual conference of explosives and blasting technique, San Diego, California January 30 – February 3, 1994. International society of explosive engineers, Cleveland, Ohio, pp 255-272

11 Esen S. 2003. A Statistical Approach to Predict the Effect of Confinement on the Detonation Velocity of Commercial Explosives. Julius Kruttschnitt Mineral Research Centre, The University of Queensland, Brisbane, Australia

12 Evmenov V. F. and Romashov A. N. Influence of the type of stemming on the seismic-wave parameters in explosive on a slope. Vol. 17. Issue 6. 1981.

13 Explosives Today, Series 2. No. 46, June 1987.

14 Jensen, R.P. and Preece, D.S. 2000. Modelling explosive/rock interaction during presplitting using ALE computational methods. Jnl. S. African Inst. Min. Met. Vol. 100, No.1, pp23-26

15 Kerhavarz M. H. 2005 A simple approach for determining detonation velocity of high explosive at any loading density. Department of Chemistry, Malek-ashtar University of Technology, Iran

16 Kopp J. W. 1987. Stemming ejection and burden movements from small borehole blasts. United States Department of the Interior, Bureau of Mines. USA

17 Lee R.A., Rogers J.A. and Whitaker K.C.1995 The origins and effects of inter-deck pressure in decked blasts. Advanced systems group, The Ensign-Bickford Company, Simsbury, Connecticut, USA

18 Lagasse P., 2005, Encyclopaedia of Columbia University Press, University of Columbia, New York, USA

19 Long L. Blast control plugs Proceedings of the twentieth annual conference of explosives and blasting technique, San Diego, California January 30 – February 3, 1994. International society of explosive engineers, Cleveland, Ohio

20 Lownds, C. 1995, Prediction of Fragmentation Based on Energy Distribution of Explosives. Proceedings of the twenty-first conference of Explosives and Blasting Technique, Nashville, Tennessee, February 5-9, 1995. International Society of Explosives Engineers, Cleveland, Ohio, pp 286-297

21 Persson, P.A., Holmberg, R. and Lee, J. 1994. Rock blasting and explosives engineering. Boca Raton, CRC Press, USA, p242

22 Olofsson S.O. Applied explosives technology for construction and mining, second edition. Ljungforetagen tryckeriab Orebro, Sweden

23 Otuonye F.O. Effective Blasthole Stemming. Presented in Partial Fulfilment of the Requirements for The Degree Doctor of Philosophy in The Graduate School of The Ohio State University. 1981

24 Sarma K.S. Explosive energy ratings- implications in assessing blast performance pp198 – 204. Journal of mines, metals and fuels. Volume 43. Issue 8. 1995

25 Sen. G. C and Silitonga M. Effect of confinement on ground vibrations due to blasting. The AIMM bulletin and proceedings. Vol. 289. Issue 6. pp 213 – 215. University of Houston 2000

26 Singh, M.M., Singh, R.B., Pal-Roy, P., Bagchi, P. and Dhar, B.B. 1994. An approach to improve blasting efficiency in an iron-ore mine. Intl. Jnl. Surf. Min. Recl. Engn, Vol 8, No. 3, pp87-93

27 Sontagg, R.E., Borgnakke, C., Van Wylen, G.J. 1998. Fundamentals of thermodynamics. 5th edition, pg 99 – 200.

28 Snelling W.O. and Hall C. 1912 The effect of stemming on the efficiency of explosives, Department of the interior, Bureau of Mines, USA

29 Stimpson B. and Yablonski J.J. 2000. Improving powder factor and cap-rock fragmentation in limestone quarrying. CIM bulletin, Vol. 93, No. 1041, pp 138-144.

30 Szendrei T. 2007. The use of ballistite to generate rapid in test equipment. Dynamic Physic Consultants.

31 Wilson A.H., Jermy C.A., Ridgeway M. Rock-strength and physical properties of Norites of the Merensky and Bastard Units, western Bushveld Complex, School of Geological Sciences, University of KwaZulu-Natal, Durban, South Africa, 4041